A Heterogeneous Model of Packed Bed Catalytic Converter for SI Engines and Its Validation

by

Shadab Firoz

DEPARTMENT OF MECHANICAL ENGINEERING

INDIAN INSTITUTE OF TECHNOLOGY, KANPUR

February, 2001

A Heterogeneous Model of Packed Bed Catalytic Converter for SI Engines and Its Validation

A Thesis Submitted

in Partial Fulfillment of the Requirements

for the degree of

Master of Technology

by

Shadab Firoz

Department of Mechanical Engineering
Indian Institute of Technology
Kanpur – India
February, 2001

CERTIFICATE

It is certified that the work contained in this thesis entitled **"A Heterogeneous Model of Packed Bed Catalytic Converter for SI Engines and Its Validation"** by **Mr. Shadab Firoz** has been carried out under the supervision of the undersigned. This work has not been submitted elsewhere for the award of a degree.

Dr. B. P. Pundir

Professor
Department of Mechanical Engineering
Indian Institute of Technology
Kanpur, India.
Date: February 23, 2001.

To

My Grandparents

CONTENTS

Chapter 2 Mathematical Model

ABSTRACT

A one dimensional, plug flow, non-adiabatic, heterogeneous steady state mathematical model is developed for tubular packed bed type exhaust catalytic converters for small spark ignition engine application. The proposed model incorporates a two step oxidation of propane and single step oxidation of carbon monoxide present in the exhaust stream with simultaneous diffusion and reactions on catalyst solid surface and in fluid phase. The mass and energy balance equations are coupled for solid phase and fluid phase reactions. The model predictions on conversion efficiency for carbon monoxide and hydrocarbon, temperatures and pressure drop are compared with a homogenous model and experimental results.

Flow pattern in the muffler of a moped fitted with conical catalytic converter developed by M/s Indian Oil Corporation Limited, R&D Centre, Faridabad is studied using a CFD software. The catalytic converter model is applied to this conical shaped converter. Predictions of model for the conical catalytic converter are compared with cylindrical catalytic converter of equal catalyst volume.

ACKNOWLEDMENT

I take this opportunity to express my indebtedness and deep sense of gratitude to my thesis supervisor Dr. B. P. Pundir for introducing me into the exciting field of Vehicular Emission Control. His inspiring guidance, systemic approach, stimulating discussions and extensive care helped to shape my thesis as well as my personal attitude towards academics. It is my immense good fortune to be under his tutelage and I am profoundly grateful to him.

I also wish to express my gratitude to Dr. V. Eswaran who helped me from the very beginning of my thesis, in other words he laid down the foundation of my work. Whenever I approached, he took keen interest in my thesis problem. I wish to thank all the teachers who taught me and were a source of constant encouragement.

I am grateful to my colleagues in this laboratory, namely Mr. B. Lachhi Ram and Mr. Manoj Sharma for help I received from them on various occasion. I also thanks all the people who have directly or indirectly helped in the completion if the thesis. I extend my profound thanks to my friends Bijendra, Sanjai Yadav, Manish Kumar, Abdul Razzaq, V.D. Saxena, Prashant and all of my friend at hall-5 who have made my stay here a most memorable one.

It is difficult to find words to express my gratitude to my sisters, Nishat, Sufia and Sana for their infallible support and inspiration throughout my stay her. This work could not have been completed without the blessings of my parents. Even to think of thanking them is to trivialize all that they have done for me. My profoundest debts to them therefore, remain silent and unacknowledged.

List of Figures

List of tables

Nomenclature:

A_{CS}	Area of cross section of the packed bed	m^2
a_v	Ratio of particle surface area to volume	m^{-1}
BET	BET surface area	m^2/kg
Bi_H	Biot number for heat transfer	*****
Bi_M	Biot number for mass transfer	*****
$\dddot{C}$	Constant	*****
$C_{b,i}$	Bulk concentration of specie i	$kmol/m^3$
C	Concentration	$kmol/m^3$
C_P	Specific heat	joule/kmol·K
C_S	Surface concentration of specie i	$kmol/m^3$
$\overline{D}$	Applicable diffusion coefficient	m^2/s
D_{AB}	Molecular diffusion coefficient of A in a mixture of A and B	m^2/s
$D_{k,i}$	Knudsen diffusion coefficient of specie i	m^2/s
D_{in}	Inlet inner diameter of conical converter	m
D_O	Outside diameter of the cylindrical reactor	m
D_p	Diameter of a single catalyst pellet	m
D_T	Inside diameter of the cylindrical reactor	m
$\overline{E}$	Total energy of the system	joule
E_a	Activation energy	joule/kmol
E	Energy	joule
F	Molar flow rate	kmol/s

G	Mass Flux	$kg/m^2 \cdot s$
H	Enthalpy	joule/kmol
ΔH°_{298}	Standard heat of reaction	joule/kmol
ΔH_R	Heat of reaction	joule/kmol
h	Cone height of the conical converter	m
h_b	Heat transfer coefficient in a packed bed	$W/m^2 \cdot K$
h_{fs}	Heat transfer coefficient between fluid and catalyst surface	$W/m^2 \cdot K$
h_O	Outside heat transfer coefficient in packed bed	$W/m^2 \cdot K$
h_{wf}	Fluid-Wall heat transfer coefficient in packed bed	$W/m^2 \cdot K$
$h_{w,eff}$	Effective wall heat transfer coefficient in packed bed	$W/m^2 \cdot K$
J	Diffusive mole flux	$kmol/m^2 \cdot s$
K_i	Adsorption equilibrium constant	$m^3/kmol$
k'	Kinetic rate constant	various units
k_{af}	Axial fluid thermal conductivity in a packed bed	W/m·K
$k_{a,eff}$	Effective axial thermal conductivity in packed bed	W/m·K
k_{as}	Axial solid thermal conductivity in a packed bed	W/m·K
k_f	Thermal conductivity of the fluid	W/m·K
k_m	Mass transfer coefficient	m/s
$k_{r,eff}$	Effective radial thermal conductivity in a packed bed	W/m·K
k_{rf}	Radial fluid thermal conductivity in a packed bed	W/m·K
k_{rs}	Radial solid thermal conductivity in a packed bed	W/m·K
k_w	Thermal conductivity of wall in a packed bed	W/m·K
L	Length of the cylindrical catalytic converter	m
L_{eq}	Equivalent length	m
M	Molar mass	kg/kmol
m	Mass	kg
$\dot{m}$	Exhaust mass flow rate	Kg/s

N_i	Number of moles of specie i	kmol
Nu_b	Nusselt number for a packed bed	*****
Nu_b'	Nusselt number for a single catalyst pellet	*****
Nu_{fw}	Nusselt number at the wall in a packed bed	*****
P	Absolute pressure	Pa
$Pe_{H,af}$	Radial Peclet number for heat transfer in packed bed	*****
$Pe_{H,rf}$	Radial Peclet number for heat transfer in packed bed	*****
Pr	Prandtl number	*****
$\dot{Q}$	Volumetric flow rate	m^3/s
$\dot{Q}_H$	Total heat flow rate	joule/s
$\dot{q}'''$	Heat flow rate per unit volume	$joule/m^3$
Re_b	Reynolds number in a packed bed	*****
R_g	Universal gas constant	joule/kmol·K
R	Rate of reaction	kmol/kg·s
r_{eq}	Equivalent radius of the pore	m
r_p	Outer radius of pellet	m
r_w	Outer radius of pellet substrate	m
Sc	Schmidt number	*****
Sh_b	Sherwood number for a packed bed	*****
Sh_b'	Sherwood number for a single catalyst pellet	*****
T_f	Fluid phase temperature	K
T_s	Solid phase temperature	K
t	Time	s
U	Overall heat transfer coefficient	$watt/m^2 \cdot K$
v	Volume	m^3
v^*	Interstitial velocity within the catalyst	m/s

v_s	Mass average superficial velocity	m/s
$\dot{W}_s$	Rate of shaft work done	J/s
$\dot{W}_T$	Total rate of work done	J/s
x_i	Stoichiometric coefficient of specie i	*****
Y	Mole fraction	*****
Z	Compressibility factor	*****
z	linear distance along the converter axis	m

Greek symbols:

α	Reaction order	*****
α_C	Half cone angle of the conical converter	*****
α_T	Thermal diffusivity	m^2/s
β	Reaction order	*****
γ	Reaction order	*****
η	Effectiveness factor of the catalyst pellet	*****
κ	Permeability of porous medium	m^2
ρ	Mass density	kg/m^3
ρ_C	Mass density of the catalyst pellet	kg/m^3
ρ_p	Solid mass density of the pellet	kg/m^3-
ϑ_i	Specific volume of specie i	
μ	Dynamic viscosity	Pa·s
ξ_i	Diffusional volume	*****
σ	Pore constriction factor	*****
$\tilde{\tau}$	Pore tortuosity factor	*****
υ	Kinematic viscosity	m^2/s
Φ	Thiele Modulus	*****
ϕ_p	Pellet porosity	*****

ϕ	Bed void fraction	*****

Subscripts:

i	Specie	*****
in	Inlet	*****
out	Outlet	*****
T	Total	*****
∞	Ambient	*****

Superscripts:

c	Catalytic	*****
f	Fluid phase	*****
h	Homogeneous	*****
s	Solid phase	*****

CHAPTER 1

INTRODUCTION

1.1 MOTIVATION:

Many industrial activities, and particularly energy generation, industrial production and vehicular traffic have brought about a significant increase in environmental pollution. The rise in civilization is closely related to improvement in transportation of men and material. In the development of transport, the internal combustion engines, both petrol and diesel engines occupy a very important position. The petrol engine has provided reliable small power units for personalized transport. The internal combustion engine is now known to be the major source of emissions of unburned hydrocarbons, carbon monoxide and oxides of nitrogen into atmosphere.. These pollutants affect not only human health but also animal, plant and materials.

In the developing countries like India, importance of two-wheelers can not be neglected. The sale of new two-wheelers is approximately 10 times that of passenger cars and together they consume about 60% or more of the total gasoline in country [Pundir et. al. 1994]. The two-wheelers are highly polluting vehicles as most of these use two-stroke engine due to its simplicity, low cost and higher power to weight ratio compared to a four-stroke engine. The two-stroke engines produce a large amount of unburned hydrocarbon and have poor efficiency due to its nature of operation in which short-circuiting of fresh mixture during scavenging and higher incidence of misfired combustion particularly at light load occur. The CO emissions are also high for the size of vehicle [O' Sullivan, 1999]. But, NO_x emissions are very low as a result of high residual gas fraction, thereby lowering the combustion temperature [Heywood, 1989]. Two wheelers are the main contributors to urban air pollution in India particularly to CO and HC. In order to handle this problem, the Govt. of India has legislated for lower emission limits for all the mobile sources.

In India emission levels were lowered in April 1996 and again in April 2000. Now, still tougher standards are being proposed for this decade [Pundir, 1997].

Research and development efforts have already started in order to meet the stricter norms in future. Various means have been suggested to control emissions for two-wheelers e.g. tuning of intake and exhaust system, use of lean mixtures etc. But these have only given a marginal reduction in hydrocarbon and CO emissions. However, substantial emission reductions are possible only by elimination of scavenged through fuel loses or by after burning of unburned hydrocarbon and CO in the exhaust system [Xiaobo et. al., 1996]. Since employing in-cylinder fuel injection is still on a laboratory

active catalyst surface area are sufficient to allow close to 100 percent conversion with high catalytic activity.

1.2.1 Monolith Reactor System:

This employs a ceramic or metallic monolith of honeycomb structure held in a metal can in the exhaust stream. The active catalyst material is impregnated into a highly porous alumina washcoat about 20 μm thick that is applied to the channel walls. The typical monolith has square-cross-section channel with inside dimension of ~ 1 mm separated by thin (0.15 to 0.3 mm) porous walls. The number of channels per square cm varies between about 30 and 60. The washcoat, 5 to 15 percent of the weight of the monolith, has a surface area of 100 to 200 m^2/g.

1.2.2 Packed Bed Reactor System:

This system uses a bed of spherical ceramic pellets to provide a large surface area in contact with the flow. With pellet catalyst, the noble metal catalyst is impregnated onto the highly porous surface of the spherical alumina pellets to a depth of about 250 μm. The pellet material is chosen to have good crush and abrasion resistance after exposure to temperature of the order of 1000 ^0C. The gas flow is directed down through the bed to provide a large flow area and low pressure drop.

The comparison of the packed beds and monolith structures shows,

- In packed beds, attrition is a problem as a result of pellet motion during use. This problem may be reduced by using hard pellets.

- The use of low-density pellets to improve light-off characteristic may aggravate the problem of attrition. Also, as pellet loss occurs, voids are formed in the bed and bypassing of exhaust gases may occur.
- In packed beds, the gas flow is turbulent which results in high mass transfer rate while in monolith structures, the gas flow is laminar which results in lower mass transfer rate.
- Pressure drops are generally lower in monolith structures.

In the present work, hard pellets i.e. of cordierite instead of alumina have been used.

1.2.3 Oxidation Catalyst:

The function of an oxidation catalyst is to oxidize CO and hydrocarbons to CO_2 and water in exhaust gas stream. About half the hydrocarbons emitted by the SI engine are unburned fuel components. The saturated hydrocarbons (which comprise 20 to 30 percent) are most difficult to oxidize. The ease of oxidation increases with increasing molecular weight. Sufficient oxygen must be present to oxidize the CO and HC. This may be supplied by the engine itself running lean of stoichiometric or by injection of secondary air upstream of the converter. Because of their high intrinsic activity, noble metals are most suitable as the catalytic material. They show higher specific activity for HC oxidation, are more thermally resistant to loss of low-temperature activity, and are much less deactivated by the sulphur in the fuel than base metal oxides. A mixture of platinum (Pt) and palladium (Pd) is most commonly used. Pure noble metals sinter rapidly in the 500 to 900 ^{0}C temperature range experienced by exhaust catalyst.

Indian Oil Corporation Limited with The Associated Cement Cos. Ltd. (ACC) has developed an alternate material for pellet beads, which has good properties over conventional alumina pellet beads.

1.2.4 NO Catalyst:

NO is removed by reduction reactions using the CO, hydrocarbons, and H_2 in the exhaust. Alumina-supported noble metal catalysts reduce NO with CO-H_2 mixtures. The NO-reduction activity of noble metals is in the order Ru>Rh>Pd>Pt. Ruthenium (Ru) and Rhodium (Rh) produce considerably less NH_3 than Pd or Pt under slightly rich conditions. While these properties make Ruthenium a desirable NO catalyst, it forms volatile oxides under oxidizing conditions which result in loss of Ruthenium from alumina support. Therefore Rh is generally used for reduction of NO.

1.2.5 Three-way Catalyst:

If an engine is operated at all times with an air/fuel ratio at or close to stoichiometric, then both NO reduction and CO and HC oxidation can be done in a single catalyst bed. Enough reducing gases CO and H_2 will be present to reduce NO and enough O_2 to oxidize the CO and hydrocarbons. Such a catalyst is called 'Three-way Catalyst' since it removes all three pollutants simultaneously. There is a narrow range of air/fuel ratio near stoichiometric in which high conversion efficiency for all three pollutants are achieved. The width of this window is narrow, about 0.1 air/fuel ratio for catalyst with high mileage use, and depends on catalyst formulation and engine operating conditions. Because of cyclic variations in exhaust gas composition about a set point close to

stoichiometric, it is desirable that catalyst be able to reduce NO when a slight excess of oxygen is present (on the lean side) and remove CO and HC when there is a slight deficiency of oxygen (on the rich side). To remove NO under slightly lean-of-stoichiometric condition, the catalyst must react the CO, H_2, or HC with NO rather than O_2, as the exhaust gas passes through the catalyst bed. Rhodium is the principle ingredient used in commercial catalysts to remove NO. It is very active for NO reduction, is much inhibited by CO and sulfur compounds, and produces less NH_3 than Pt.

1.2.6 Catalytic Converter Design Considerations:

The requirements of catalytic systems, in addition of the main task of achieving legislative emission requirements, are:

- Minimal space requirement,
- Minimal additional weight,
- Limited complexity,
- Minimal pressure drop,
- Minimal additional cost ,
- Suitable production technology for mass production and
- High durability.

Catalytic oxidation reactions being highly exothermic in nature, catalytic reaction steps giving rise to temperature gradients. The released energy is first transported by conduction within the catalyst and then by convective heat transfer to the bulk fluid. If sufficiently high temperatures are encountered within the reactor, homogeneous gas phase reactions also contribute to the overall energy balance. As the gases flow past the

converter, depending on its geometry, substantial pressure drop may be encountered which may severely affect the engine performance. The catalyst support system should permit successful completion of the above processes and achieve the desired results.

1.3 MODELING OF CATALYTIC CONVERTERS:

A mathematical model is a system of equations, which describes the relationship among the various physical and chemical variables governing the process.

Mathematical models are classified into several types. One extreme is the empirical model, in which experimental data are described by an arbitrary set of functions, the only criterion being the 'goodness of fit' determined by statistical means. An experimental model may describe a set of experimental data and be able to predict new values of a dependent variable within the range of experimentally measured parameters. The danger in using such a model is tendency to extrapolate to regions outside of the original experimental parameters. On the other hand, a purely empirical model should not necessarily be discarded simply because it has little or no mechanistic base.

The other type is phenomenological model, which is based on the fundamental physio-chemical process encountered. If it is possible to derive a theoretical model, which describes all such processes, then the model can be used directly for design without the need for experiments. This is invariably an impossible task for real systems, usually because some physical constants must be measured experimentally. The phenomenological model can be divided into 'Lumped Parameter Model' and 'Distributed Parameter Model'. A lumped parameter model ignores some or all of the spatial variations, which may exist for one or more of the properties of the system and

uses an average value. A distributed parameter model accounts for all spatial property variations.

A practical and useful approach may be to derive as scientifically meaningful a model as possible with a few constants as necessary, and then to determine each constant in a separate experiment. The final model should be tested for its ability to predict the behaviour of the full process.

Factors, which affect the selection of the type of model, include the following:

- The precision to which the model parameters are known,
- The desired accuracy and precision of the solution,
- The importance of various phenomena,
- The power of the computer.

Enhanced computational capabilities have changed the method of design and development so contribution of mathematical modeling gained importance while earlier works were based on experiments.

There are four distinct areas for the modeling of catalytic converter:

- Chemical Reaction Kinetics,
- Heat Transfer & Thermodynamics,
- Gas Dynamics,
- Diffusion and Adsorption.

Though the theories have been developed but their successful applications as an usable engine design tool is rather sporadic in nature. While mathematical modeling of a complete engine is now a standard tool for the engine designer, modeling of the catalytic converter systems has not evolved at a comparative pace.

1.4 LITERATURE SURVEY:

A number of studies on mathematical modeling of the catalytic converter have been carried out since early 1970's both on packed bed and monolith catalytic converters.

1.4.1 Packed Bed Catalytic Converters:

Kuo et. al. [1971], four years before the implementation of the first emissions reduction legislation in the USA requiring the use of catalytic converters, developed mathematical model that predicts the performance of catalytic converter system. The model contains all the important system parameters and process variables e.g. catalyst density and heat capacity, catalyst activity, initial bed temperature, inlet exhaust gas composition and converter location.

Se et. al. [1980] developed a detailed mathematical model of a single catalyst pellet to describe its behavior under transient conditions encountered during the warm-up period of automobile exhaust catalytic converters. This model is capable of describing the time behavior of a composite catalyst pellet, and thus provides a convenient means of examining the effects of poisoning penetration and various noble metal impregnation strategies. They found that catalyst light-off was delayed with increasing carbon monoxide or propylene concentration in the exhaust gas, whereas increasing the oxygen concentration improves both light-off and steady state activity and faster light-off occurs when a catalyst pellet exposed to a higher exhaust gas flow rate.

Oh et. al. [1985] developed a transient mathematical model which described the dynamic behaviour of packed bed catalytic converter during warm up. They found that the model prediction agreed very well with the results of engine dynamometer

experiments for three Pt-alumina catalyst of different properties and can be used to predict the warm-up performance of packed bed catalytic converter from specified system parameters and inlet exhaust gas conditions. Oh et. al.[1985] further found that the model could also be applied to dual bed converter because the latter converter normally operates in the oxidizing mode during warm-up.

Khandekar S. [2000] developed a steady state mathematical model of packed bed catalytic converters for two-stroke petrol engines. He used homogeneous model in which it was assumed that concentrations and temperatures of species at pellet surface and in gas phase are same. The model predictions were compared with experimental results. A new catalytic rate of reaction for carbon monoxide and propane was proposed which is being described in section 1.4.3. He further concluded that a heterogeneous model is needed for improvement in prediction ability of the model.

1.4.2 Monolith Catalytic Converters:

Larry et. al. [1976] applied orthogonal collection method to solve the mathematical model of monolithic catalytic converter. The orthogonal collection method was developed for application to problems having irregular geometeries. Most of the previous works were on rectangular region. They also included transient heat and mass transfer in three dimensions. They found that more accurate results were obtained for the asymptotic Nusselt number for the geometeries like square, rectangles with aspect ratio of 0.5 and 0.25.

Heck et. al. [1976] developed mathematical model which account for simultaneous heat transfer, mass transfer and chemical reaction in the oxidation of carbon

monoxide over platinum containing monoliths. A two-dimensional model was used to predict unusual behavior of the Nusselt number in the presence of rapid reaction. It was found that monolithic reactor behavior was dominated by the position of the light-off point, where the catalytic walk temperature took an upward leap, the wall concentration fallen to zero, and the reaction becomes mass transport limited.

Naoki et. al. [1996] analyzed numerically the conversion characteristics of monolith exhaust catalyst under warming-up conditions and verified it with experimental results. They found that there is large maldistribution of species concentration inside the catalytic converter during warm-up. In the outer region of monolith, CO and HC pass through the channel without being converted. They also found that during warm-up, about 50% of the total HC mass in catalyst out-gas are exhausted from the channels in the outer 25% of the cross-sectional area of the converter. Conversion performance of the exhaust monolith during warm-up is greatly improved by both heat insulation and high noble metal loading on the outer region of the upstream part of the monolith. It was seen that decreasing metal loading on the downstream part of the monolith did not reduce the conversion and high noble metal loading on the inner region of the upstream part of the monolith accelerated the conversion rates at an early stage of warming-up process.

1.4.3 Chemical Kinetics:

For modeling of the catalytic converters, reaction rate constants for oxidation of carbon monoxide and unburned hydrocarbons are required.

Sterling et. al. [1973] studied kinetics of carbon monoxide and propylene oxidation on a platinum- alumina catalyst with synthetic gas mixture between 205 ^{0}C and

372 ^{0}C. The rates of oxidation of carbon monoxide and propylene increase with increasing concentration and are inhibited by carbon monoxide, propylene and nitric oxide. They formulated complex kinetic equations are of the form,

$$r_{CO} = -\frac{k_{r1}(CO)(O_2)}{R(\theta)}$$

$$r_{C_3H_8} = -\frac{k_{r2}(C_3H_8)(O_2)}{R(\theta)}$$

where k_{r1} and k_{r2} are rate constants and $R(\theta)$ is a resistance term which includes the inhibition effect of carbon monoxide , propylene and NO on reaction rate.

Hegedus et. al. [1977] used an integral reactor to study the CO-O_2 reaction over Pt-coated beads. They presented a rate expression in the same form as Voltz et. al. [1973] without the inhibition terms for propene (C_3H_6) and NO. They obtained a different activation energy (about 40% lower) and CO adsorption equilibrium constant (5% higher) than Voltz et. al. [1973] and attributed the difference to the influences of C_3H_6 and NO. Also, stable isothermal multiplicity was observed which was investigated in the conversion-temperature-mass flow domain.

Cant et. al. [1978] studied steady state oxidation of carbon monoxide over supported noble metals with particular reference to platinum. Activation energy, kinetic orders and relative activities had been determined for the oxidation of CO by O_2 over five supported noble metals. The results were compared with the prediction of a model, which used parameters derived from measurements made with only reactant present in the gas

phase. The results showed much lower activation energy and only a slight negative order dependence on CO.

Herkowitz et. al. [1983] studied CO oxidation on platinum supported catalysts. The conversion of carbon monoxide to carbon dioxide was measured in a recycle reactor automatically controlled by a computer. Two platinum/SiO_2 catalyst of different dispersion were employed. The rate data were correlated by three LHHW kinetic models. Which are listed in table 1.1 .

Table 1.1

Model	*I*		*II*		*III*	
Mechanism	$CO+s \Leftrightarrow CO_s$ $O_2+2s \Leftrightarrow 2O_s$ $CO_s+O_s \rightarrow CO_2+2s$		$CO+s \Leftrightarrow CO_s$ $O_2+s \Leftrightarrow O_2s$ $COs+O_2s \rightarrow CO_2+O_s+s$		$CO+s \Leftrightarrow COs$ $O_2+s \Leftrightarrow O_2s$ $COs+O_2s \rightarrow CO_3s_2$ $CO_3s_2+CO_s \rightarrow 2CO_2+3s$	
Kinetic Expression, r	$\frac{k_r \cdot K_{CO} \cdot K_{O_2}^{1/2} \cdot C_{CO} \cdot C_{O_2}^{1/2}}{\left(1+K_{CO} \cdot C_{CO}+K_{O_2}^{1/2} \cdot C_{O_2}^{1/2}\right)^2}$		$\frac{k_r \cdot K_{CO} \cdot K_{O_2} \cdot C_{CO} \cdot C_{O_2}}{\left(1+K_{CO} \cdot C_{CO}+K_{O_2} \cdot C_{O_2}\right)^2}$		$\frac{k_r \cdot K_{CO}^2 \cdot K_{O_2} \cdot C_{CO}^2 \cdot C_{O_2}}{\left(1+K_{CO} \cdot C_{CO}+K_{O_2} \cdot C_{O_2}\right)^2}$	
Paramters	1	2	1	2	1	2
$A_1, Kg\,mol/(kg.surf.Pt)$	2.8×10^{8}	9.1×10^{8}	8.1×10^{4}	4.8×10^{4}	1.3×10^{5}	7.9×10^{4}
$A_2, m^3/Kg\,mol$	39	37	16	13	23	17
$A_3, m^3/Kgmol$	1.8×10^{-4}	3.0×10^{-6}	2.4×10^{3}	1.3×10^{3}	2.0×10^{3}	1.1×10^{3}
α_1, K	7680	8000	7980			
α_2, K	−2210	−3230	−3330			
α_3, K	1120	−230	−310			

a. s indicate an active site.

b. $k_r = A_1 \cdot \exp\left(-\frac{\alpha_1}{T}\right)$; $K_{CO} = A_2 \cdot \exp\left(-\frac{\alpha_2}{T}\right)$; $K_{O_2} = A_3 \cdot \exp\left(-\frac{\alpha_3}{T}\right)$

Khandekar S. [2000] used LHHW model with modified catalytic rate of reactions for carbon monoxide and also propane. For catalytic rate of reaction for carbon monoxide, he modified activation energy term as proposed by Hekowitz et. al. [1983] from 7980 to 8300. Thus,

$$-R_{CO}^{C} = \frac{k' \cdot k_{CO} \cdot k_{O_2} \cdot C_{CO}^{\alpha} \cdot C_{O_2}^{\beta}}{\left(1 + k_{CO} \cdot C_{CO} + k_{O_2} \cdot C_{O_2}\right)^{r}}$$

where

$$k' = A_1 \cdot \exp\left(\frac{-8300}{T}\right)$$

$$k_{CO} = A_2 \cdot \exp\left(\frac{-3330}{T}\right)$$

$$k_{O_2} = A_3 \cdot \exp\left(\frac{-310}{T}\right)$$

where A_1, A_2 *and* A_3 *are cons* tan *ts.*

For propane oxidation the pre-exponential constants in the catalytic rate of reaction as proposed by Wanke[1973] was modified from $3.15*10^4$ to $12.8*10^4$.

Thus

$$-R_{C_3H_8}^{c} = 12.8 \times 10^4 \cdot \exp\left(-\frac{89126}{R_g \cdot T}\right) \cdot C_{C_3H_8}$$

where R_g is universal gas constant.

A brief summary of the various forms of the rate of reaction for carbon monoxide is given below in Table 2.2:

Table 2.2

Rate Law Form	*Proposed By*	*Reference*
$-R_{CO}^{C} = \frac{k \cdot Y_{O_2}}{Y_{CO}^{0.5}}$	Shishu (1972)	(Boehman et.al.1993)
$-R_{CO}^{C} = \frac{k_1 \cdot Y_{O_2} Y_{CO}}{\left(Y_{O_2} + k_2 Y_{CO}^2\right)}$	Young (1974)	
$-R_{CO} = \frac{k \cdot Y_{O_2} Y_{CO}}{\left(1 + K_{O_2} Y_{O_2} + K_{CO} Y_{CO}\right)^2}$	Shishu (1972)	
$-R_{CO}^{C} = \frac{k \cdot Y_{O_2} Y_{CO}}{\left(1 + K_{CO} Y_{CO}\right)^2}$	Hegedus et.al. (1977)	
$-R_{CO}^{C} = \frac{k \cdot K_{CO} K_{O_2} C_{CO} C_{O_2}}{\left(1 + K_{CO} C_{CO} + K_{O_2} C_{O_2}\right)^2}$	Herkowitz et.al. (1983)	
$-R_{CO}^{C} = \frac{k \cdot Y_{CO} Y_{O_2}^2}{\left(1 + K_{CO} Y_{CO}\right)^2}$	Montreuil et.al. (1992)	

1.5 STATREMENT OF THE PROBLEM:

For the purpose of present study, the overall domain of the problem has been subdivided into the following parts:

I. To develop a one-dimensional, plug flow, non-adiabatic, heterogeneous, steady state mathematical model for tubular packed bed exhaust catalytic .The model should predict the steady state conversion, temperature and pressure profiles along the axial direction.

III. The model should incorporate simultaneous diffusion and reaction phenomenon occurring in the catalyst washcoated cordorite pellets.

IV. To compare the model with homogenous model and experimental values.

V. To validate the model with experimental data.

VI. To study flow field in the exhaust muffler of a converter designed for a moped using CFD software.

VII. To carry out parametric analysis with the mathematical model for above moped catalytic converter.

CHAPTER 2

MATHEMATICAL MODEL

2.1 INTRODUCTION:

The heterogeneous mathematical modeling of the packed bed catalytic converter, involves the formulation of mathematical equations describing the following:

(a) The Basic Governing Equations:

- The Solid Phase Mole Balance Equation.
- The Fluid Phase Mole Balance Equation.
- The Momentum Balance Equation.
- The Solid Phase Energy Balance Equation.
- The Fluid Phase Energy Balance Equation.

(b) The Chemical Kinetics:

- The Rate of Homogeneous Reaction for Carbon Monoxide.
- The Rate of Homogeneous Reaction for hydrocarbons, in this case, Propane.
- The Rate of Catalytic Reaction for Carbon Monoxide.

- The Rate of Catalytic Reaction for Propane.

(c) The Physical Properties:

- Gas Viscosity Data.
- Specific Heats for all the species involved.
- Heat of Reaction for Propane and Carbon Monoxide oxidation.
- Effective Diffusivity of the Catalyst Pellet.

(d) The Heat and Mass Transfer:

- The Thermal Conductivity of the Pellet.
- The Thermal Conductivity of the Fluid.
- Solid Surface to Fluid Heat Transfer Coefficient.
- Bed to Wall Heat Transfer Coefficient.
- Overall Heat Transfer Coefficient for the Packed Bed.
- Fluid to Solid Surface Mass Transfer Coefficient for all the species involved.

(e) The Pellet Diffusion and Effectiveness Factor:

- The Catalyst Pellet Effectiveness Factor for Carbon Monoxide.
- The Catalyst Pellet Effectiveness Factor for Propane.

2.2 THE BASIC GOVERNING EQUATION:

In this section, the fundamental governing equations in the present study are derived. Control volume as shown in Fig. 2.1 is chosen for which mole, momentum and energy balance equations are applied for solid and fluid phase. Fig. 2.2 shows the process of mass transfer from bulk flow to the solid surface of the pellet and heat transfer from solid surface of the pellet to the bulk flow.

2.2.1 The Solid Phase Mole Balance Equation:

The rate of disappearance of species '*i*' in the solid catalyst is:

$$\begin{bmatrix} Moles \\ transported\ to \\ catalyst\ surface \end{bmatrix} = \begin{bmatrix} Moles \\ reacted\ in \\ catalytic\ reaction \end{bmatrix}$$

which can be expressed in terms of the incremental surface area as:

$$k_{m,i} \cdot \Delta S \cdot C_f \cdot \left(Y_i^f - Y_i^s\right) = \eta \cdot \left(-R_i^c\right) \cdot \Delta V \cdot \rho_C \cdot (1-\phi) \tag{2.1}$$

where $k_{m,i}$ is the fluid to solid mass transfer coefficient for the '*i*'th species, C_f is the molar density (concentration), Y_i^f and Y_i^s are mole fractions of '*i*'th component at fluid and solid phase respectively, η is the effectiveness factor, $(R_i)_c$ is the catalytic rate of formation of '*i*'th species, ρ_C is the mass density of catalyst pallet, ϕ is the porosity of the catalyst bed.

Noting that,

$$a_v = \frac{\Delta S}{\Delta V} \tag{2.2}$$

The equation can be simplified to:

$$k_{m,i} \cdot a_v \cdot C_f \cdot \left(Y_i^f - Y_i^s\right) - \eta \cdot \left(-R_i^c\right) \cdot \rho_C \cdot (1-\phi) = 0. \tag{2.3}$$

where, a_v is the solid particle surface area per unit bed volume.

2.2.2 The Fluid Phase Mole Balance Equation:

The mole balance for the fluid phase is,

$$[Moles\ in]-[Moles\ out]-\begin{bmatrix} Moles\ reacted\ in \\ \text{hom}\,ogeneous \\ reaction \end{bmatrix}-\begin{bmatrix} Moles\ transported \\ to\ catalyst\ surface \end{bmatrix}=0\,. \qquad (2.4)$$

Which is,

$$-\Delta F_i-(-R_i)_h\cdot\Delta V\cdot\phi-k_{m,i}\cdot\Delta S\cdot C_f\cdot\left(Y_i^f-Y_i^s\right)=0$$

Noting that $F_i = v_s \cdot A_C \cdot C_i = v_s \cdot A_C \cdot C_f \cdot Y_i$ and dividing by $\Delta V = A_C \,.\, \Delta z$, introducing and as the volume element, final mole balance equation is,

$$-\frac{d\left(C_f\cdot v_s\cdot Y_i^f\right)}{dz}-\left(-R_i^h\right)\cdot\phi-k_{m,i}\cdot a_v\cdot C_f\cdot\left(Y_i^f-Y_i^s\right)=0 \qquad (2.5)$$

where F_i is the molar flow rate, v_s is the superficial velocity and R_i^h is homogenous rate of formation of species *'i'* , A_C is the cross sectional area of packed bed.

(a) Multiple Reactions:

In the present study, multiple reactions are modeled. A two step oxidation reaction of propane, which is first oxidized, to carbon monoxide and then the carbon monoxide later, gets converted to carbon dioxide. Detailed explanation of this two-step model is presented in section 2.3.

Necessary modifications, as described below, have to be incorporated into the governing equations for accounting for the multiple reactions. The general hydrocarbon reaction for two step oxidation is given by:

$$C_nH_m(g)+\left(\frac{n}{2}+\frac{m}{4}\right)O_2(g)\rightarrow nCO(g)+\frac{m}{2}H_2O(g) \qquad \textit{Step I} \qquad (2.6\text{-a})$$

$$nCO(g)+\frac{n}{2}O_2(g) \rightarrow nCO_2(g) \qquad \textit{Step II} \qquad (2.6\text{-b})$$

Taking n=3 and m=8, we get,

$$C_3H_8(g)+3.5O_2(g)\rightarrow 3CO(g)+4H_2O(g) \qquad \textit{Step I} \qquad (2.6\text{-c})$$

$$CO(g)+\frac{1}{2}O_2(g) \rightarrow CO_2(g) \qquad \textit{Step II} \qquad (2.6\text{-d})$$

Since we explicitly know the intrinsic rates of reaction for propane (C_3H_8) and carbon monoxide (CO), we can apply the stoichiometric relationship between the reacting species to get the following relationship for the rate of reactions for both catalytic reaction and homogeneous reaction, from Equation 2.6-c,

$$-r'_{C_3H_8}=1.0(-r'_{C_3H_8}) \qquad (2.7\text{-a})$$

$$-r'_{O_2}=3.5(-r'_{C_3H_8}) \qquad (2.7\text{-b})$$

$$+r'_{CO}=3.0(-r'_{C_3H_8}) \qquad (2.7\text{-c})$$

$$+r'_{H_2O}=4.0(-r'_{C_3H_8}) \qquad (2.7\text{-d})$$

and from Equation 2.6-d, we get:

$$-r''_{CO}=1.0(-r''_{CO}) \qquad (2.8\text{-a})$$

$$-r''_{O_2}=0.5(-r''_{CO}) \qquad (2.8\text{-b})$$

$$-r''_{CO_2}=1.0(-r''_{CO}) \ . \qquad (2.8\text{-c})$$

The subscripts *I* and *II* refers to the reaction steps. Thus applying the solid phase mole balance Equation 2. 3, we get,

$$C_f \cdot k_m \cdot a_v \cdot \left(Y^f_{C_3H_8} - Y^s_{C_3H_8}\right) = -\eta \cdot 1.0\left(r'^c_{C_3H_8}\right) \cdot \rho_C \cdot (1-\phi) \tag{2.9-a}$$

$$C_f \cdot k_m \cdot a_v \cdot \left(Y^f_{O_2} - Y^s_{O_2}\right) = -\eta \cdot \left\{3.5\left(r'^c_{C_3H_8}\right) + 0.5\left(r''^c_{CO}\right)\right\} \cdot \rho_C \cdot (1-\phi) \tag{2.9-b}$$

$$C_f \cdot k_m \cdot a_v \cdot \left(Y^f_{CO} - Y^s_{CO}\right) = -\eta \cdot \left\{-3.0\left(r'^c_{C_3H_8}\right) + 1.0\left(r''^c_{CO}\right)\right\} \cdot \rho_C \cdot (1-\phi) \tag{2.9-c}$$

$$C_f \cdot k_m \cdot a_v \cdot \left(Y^f_{H_2O} - Y^s_{H_2O}\right) = -\eta \cdot \left\{-4.0\left(r'^c_{C_3H_8}\right)\right\} \cdot \rho_C \cdot (1-\phi) \tag{2.9-d}$$

$$C_f \cdot k_m \cdot a_v \cdot \left(Y^f_{CO_2} - Y^s_{CO_2}\right) = -\eta \cdot \left\{-1.0\left(r''^c_{CO}\right)\right\} \cdot \rho_C \cdot (1-\phi) \tag{2.9-e}$$

and applying the fluid phase mole balance equation 2.5, we get,

In general, for catalytic combustion, the molar flow rate will be changing as the reaction progresses. As only equal number of moles occupy equal volumes in the gas phase, the volumetric flow rate will also change. Thus, we get,

$$\frac{d\left(C_f \cdot v_s \cdot Y^f_{C_3H_8}\right)}{dz} = 1.0\left(r'^h_{C_3H_8}\right) \cdot \phi - k_m \cdot a_v \cdot C_f\left(Y^f_{C_3H_8} - Y^s_{C_3H_8}\right) \tag{2.10-a}$$

$$\frac{d\left(C_f \cdot v_s \cdot Y^f_{O_2}\right)}{dz} = \left\{3.5\left(r'^h_{C_3H_8}\right) + 0.5\left(r''^h_{CO}\right)\right\} \cdot \phi - k_m \cdot a_v \cdot C_f\left(Y^f_{O_2} - Y^s_{O_2}\right) \tag{2.10-b}$$

$$\frac{d\left(C_f \cdot v_s \cdot Y^f_{CO}\right)}{dz} = \left\{-3.0\left(r'^h_{C_3H_8}\right) + 1.0\left(r''^h_{CO}\right)\right\} \cdot \phi - k_m \cdot a_v \cdot C_f\left(Y^f_{CO} - Y^s_{CO}\right) \tag{2.10-c}$$

$$\frac{d\left(C_f \cdot v_s \cdot Y^f_{H_2O}\right)}{dz} = -4.0\left(r'^h_{C_3H_8}\right) \cdot \phi - k_m \cdot a_v \cdot C_f\left(Y^f_{H_2O} - Y^s_{H_2O}\right) \tag{2.10-d}$$

$$\frac{d\left(C_f \cdot v_s \cdot Y^f_{CO_2}\right)}{dz} = -1.0\left(r''^h_{CO}\right) \cdot \phi - k_m \cdot a_v \cdot C_f\left(Y^f_{CO_2} - Y^s_{CO_2}\right) \tag{2.10-e}$$

$$F_{TOTAL} = F_{C_3H_8} + F_{O_2} + F_{CO} + F_{H_2O} + F_{CO_2} + F_{N_2} \quad (2.11\text{-a})$$

$$F^{\circ}_{TOTAL} = F^{\circ}_{C_3H_8} + F^{\circ}_{O_2} + F^{\circ}_{CO} + F^{\circ}_{H_2O} + F^{\circ}_{CO_2} + F^{\circ}_{N_2} \quad (2.11\text{-b})$$

where,

F_{TOTAL} = Total molar flow rate at a point, and F°_{TOTAL} = Entering total molar flow rate of the species.

The next step is to replace all the concentrations terms in the rate laws in terms of molar flow-rates. For a flow system, the concentration of species at a given point can be determined from the molar flow rate and the volumetric flow rate of the specie. We know that,

$$C_T = \frac{F_T}{\dot{Q}} = \frac{P}{R_g \cdot T_f} \quad (2.12\text{-a})$$

$$C_{Tin} = \frac{F_{Tin}}{\dot{Q}_0} = \frac{P_{in}}{R_g \cdot T_{in}} \quad (2.12\text{-b})$$

where,

C_T = Total concentration, P= Absolute pressure, R_g=Universal Gas Constant, T=Absolute temperature and $\dot{Q}$= Volumetric Flow Rate of species, T_f is fluid phase temperature. The subscript *in* refers to the inlet conditions.

From Equation 2.12-a, b, we get,

$$\dot{Q} = \dot{Q}_{in}\left(\frac{F_T}{F_{Tin}}\right)\left(\frac{P_{in}}{P}\right)\left(\frac{T_f}{T_{in}}\right). \quad (2.13)$$

Thus, in general,

$$C_j = C_{Tin}\left(\frac{F_j}{F_T}\right)\left(\frac{P}{P_{in}}\right)\left(\frac{T_{in}}{T_f}\right), \tag{2.14}$$

where C_j refers to the concentration of species j.

2.2.3 The Momentum Balance Equation:

For Newtonian fluids, the one-dimensional form of the Darcy's law for flow through porous media, giving the linear relationship between velocity and pressure drop is given by [Bear, 1972]:

$$-\frac{dP}{dz} = \frac{\mu}{\kappa}\cdot v_S \tag{2.15}$$

$$v_s = \frac{\dot{Q}}{A_{CS}} = \phi \cdot v \tag{2.16}$$

The above law is valid at low flow rates. At higher flow rates fluid inertial effects become important. Therefore, an extension to Darcy's law, known as the Forchheimer equation [Hayes and Kolaczkowski, 1997] was proposed to account for those effects. The general form is given by,

$$-\frac{dP}{dz} = \left(\frac{\mu}{\kappa} + \frac{\ddot{C}\cdot\rho\cdot v_S}{\sqrt{\kappa}}\right) \tag{2.17}$$

The constant $\ddot{C}$ may assume various values as per the actual working situation. A commonly used permeability for packed beds of uniformly sized smooth particles is obtained from the Black-Kozeny friction factor analysis, supplemented with experimental results [Bird et. al., 1960], which gives,

$$\kappa = \frac{D_P^2\cdot\phi^3}{150\cdot(1-\phi)^2} \tag{2.18}$$

The equivalent particle diameter, D_p is defined as,

$$D_P = \frac{6}{a_v} \quad where,$$
$$a_v = \frac{particle\ surface\ area\ to\ volume}{particle\ volume} \tag{2.19}$$

For the case of spherical pellet D_p = actual diameter of the pellet. A commonly expressed form of the constant $\ddot{C}$ is given by,

$$\ddot{C} = \frac{0.143}{\phi^{1.5}} \tag{2.20}$$

Substituting Equations 2.18 and 2.20 in 2.17 we get,

$$\frac{dP}{dz} = -\frac{v_s \cdot (1-\phi)}{D_p \cdot \phi^3} \cdot \left[\frac{150 \cdot \mu \cdot (1-\phi)}{D_p} + (1.75 \cdot \rho \cdot v_s) \right]. \tag{2.21}$$

The above equation is called the Ergun Equation [Ergun, 1952] widely used for predicting pressure drops in packed beds. The value of the constants appearing in Equation 2.21, viz. 150 and 1.75 was originally proposed. The values depend on the particle surface roughness, particle size distribution, particle shape and packing homogeneity.

In catalytic combustion reaction the fluid is a compressible gas. Thus the fluid density depends on the temperature and the pressure. The equation of continuity can be applied to one-dimensional flow in a packed tube of constant cross-sectional area to get:

$$\frac{d(\rho \cdot v_s)}{dz} = 0 \quad \text{or} \quad \rho \cdot v_s = \rho_{in} v_{\sin} = G = cons\tan t \tag{2.22}$$

which modifies Equation 2.21 to,

$$\frac{dP}{dz} = -\frac{G \cdot (1-\phi)}{\rho \cdot D_p \cdot \phi^3} \cdot \left[\frac{150 \cdot \mu \cdot (1-\phi)}{D_p} + (1.75 \cdot G) \right]. \tag{2.23}$$

Equation 2.23 can be further modified by using,

$$C_T = \frac{F_T}{\dot{Q}} = \frac{P}{RT_f Z} \quad , \tag{2.24-a}$$

where, Z and Z_{in} are the compressibility factors,

$$C_{Tin} = \frac{F_{Tin}}{\dot{Q}_{in}} = \frac{P_{in}}{RT_{in} Z_{in}} \quad , \tag{2.24-b}$$

$$\dot{Q} = \dot{Q}_{in}\left(\frac{F_T}{F_{To}}\right)\left(\frac{P_{in}}{P}\right)\left(\frac{T_f}{T_{in}}\right) \text{ (neglecting the ratio of compressibility factor).} \tag{2.25}$$

and

$$\rho_{in} = \rho\left(\frac{F_T}{F_{Tin}}\right)\left(\frac{P_{in}}{P}\right)\left(\frac{T_f}{T_{in}}\right). \tag{2.26}$$

to obtain,

$$\frac{dP}{dz} = -\frac{G\cdot(1-\phi)}{\rho_{in}\cdot D_p\cdot\phi^3}\cdot\left[\frac{150\cdot\mu\cdot(1-\phi)}{D_p} + (1.75\cdot G)\right]\left(\frac{F_T}{F_{Tin}}\right)\left(\frac{P_{in}}{P}\right)\left(\frac{T_f}{T_{in}}\right). \tag{2.27}$$

This is the final form of the momentum equation for the plug flow tubular reactor.

2.2.4 The Solid Phase Energy Balance Equation:

The solid phase consists of the catalysts, which is not flowing, and the gas, which fills the pore volume of the catalyst. We can consider the solid as an open system with diffusion of mass in and out. The gas reacts and heat is released. At steady state this must be balanced by heat that is transferred from the solid. In other words,

[Heat *released by reaction]* = [*Heat transfer from solid*]

In this analysis heat is transferred from the solid by convection. Heat transfer by conduction and radiation are neglected and the whole pellet is assumed as having the uniform temperature.

The heat released by reaction is,

$$[Heat\ releaed\ by\ reaction] = -(1-\phi)\cdot \rho_C \cdot \eta \cdot \left(-R_i^s\right)\cdot \Delta H_R^s$$

where ΔH_R^s is the heat of reaction at solid phase temperature and h_{fs} is the heat transfer coefficient between fluid and catalyst surface.

The solid phase energy balance equation is therefore,

$$(1-\phi)\cdot \rho_C \cdot \eta \cdot \left(-R_i^s\right)\cdot \Delta H_R^s + h_{fs}\cdot a_v \cdot \left(T_s - T_f\right) = 0 \qquad (2.28)$$

2.2.5 The Fluid Phase Energy Balance Equation:

The steady state fluid phase energy balance equation is,

$$\begin{bmatrix} Enthalpy\ increase \\ as\ a\ result\ of \\ temperature\ rise \end{bmatrix} = \begin{bmatrix} Heat\ added \\ to\ gas \\ from\ surface \end{bmatrix} + \begin{bmatrix} Heat\ generated \\ in\ gas\ phase \\ reaction \end{bmatrix} + \begin{bmatrix} Heat\ added \\ from \\ surrounding \end{bmatrix}$$

The left-hand side is,

$$[LHS] = Q_v \cdot \rho \cdot C_P \cdot \Delta T_f \qquad (2.29)$$

where Q_v is volumetric flow rate, $\rho$is mass density, C_p is constant pressure heat capacity.

The area of heat transfer in the elemental volume is the circumference of the channel multiplied by the length, that is,

$$\Delta A_T = \pi \cdot D_T \cdot \Delta z \tag{2.30}$$

where D_T is the reactor diameter. The heat exchange with surroundings depends on an overall heat transfer coefficient, which includes the heat transfer at the inside reactor wall, the outside reactor surface and conduction through the wall, and the driving force, which is the temperature difference between the fluid in the reactor and the surroundings. The heat loss from the elemental volume element is then,

$$\begin{bmatrix} \textit{Heat added} \\ \textit{from surroundings} \end{bmatrix} = q_{conv} = \pi \cdot D_T \cdot \Delta z \cdot U \cdot \left(T_{3,\infty} - T_f\right) \tag{2.31}$$

where $T_{3,\infty}$ is the temperature of the heat transfer fluid surrounding the reactor.

The right hand side is,

$$[RHS] = h_{fs} \cdot \Delta S \cdot \left(T_s - T_f\right) - \Delta V \cdot \phi \cdot \left(-R_i^h\right) \cdot \Delta H_R^h + \pi \cdot D_T \cdot \Delta z \cdot U \cdot \left(T_{3,\infty} - T_f\right) \tag{2.32}$$

where ΔH_R^f is heat of reaction at fluid phase temperature and h_{fs} is the pellet to fluid heat transfer coefficient.

Therefore energy balance over ΔV is,

$$-Q_v \cdot \rho \cdot C_P \cdot \Delta T_f - \Delta V \cdot \phi \cdot \left(-R_i^h\right) \cdot \Delta H_R^h + \Delta S \cdot h_{fs} \cdot \left(T_s - T_f\right) + \pi \cdot D_T \cdot \Delta z \cdot U \cdot \left(T_{3,\infty} - T_f\right) = 0 \tag{2.33}$$

Dividing through by $\Delta V = A_c \cdot \Delta z$, noting again that,

$$a_v = \frac{\Delta S}{\Delta V} \quad , \quad v_s = \frac{Q_v}{A_C} \quad and \quad \Delta V = \frac{\pi}{4} \cdot {D_T}^2 \cdot \Delta z \tag{2.34}$$

gives,

$$-v_s \cdot \rho \cdot C_P \cdot \frac{\Delta T_f}{\Delta z} - \Delta H_R \cdot \left(-R_i^h\right) \phi + h_{fs} \cdot a_v \cdot \left(T_s - T_f\right) + \frac{4}{D_T} \cdot U \cdot \left(T_{3,\infty} - T_f\right) = 0 \tag{2.35}$$

Taking the limit as $\Delta V \longrightarrow dv$, we obtain the ordinary differential equation,

$$-v_s \cdot \rho \cdot C_P \cdot \frac{dT_f}{dz} - \Delta H_R \cdot \left(-R_i^h\right) \cdot \phi + h_{fs} \cdot a_v \cdot \left(T_s - T_f\right) + \frac{4}{D_T} \cdot U \cdot \left(T_{3,\infty} - T_f\right) = 0 \tag{2.36}$$

The temperature at the reactor inlet must be known to solve this IVP.

2.3 THE CHEMICAL KINETICS:

The rate expression, essentially a mathematical model of the reaction, relates the rate of reaction to the local temperature, concentration of the reactants and two or more empirical constants. When expressed in terms of a local value of temperature and concentration, it is termed as the intrinsic rate expression. The global rate is a rate that is observed in a reactor, and may include much heat and mass transfer effects combined together. The reaction mechanism is a description of all the steps, which occur before the reactants are turned into final products. The development of reaction rate expressions is often quite difficult, drawing upon empirical evidence as well as theory.

The rate expressions for elementary reactions of the form, $aA + bB \xrightarrow{k_1} cC + dD$ are almost always expressed in the Arrhenius type model,

$$-R_A = k_1 \exp\left(-\frac{E_a}{R_g T}\right) C_A^{\alpha} C_B^{\beta} \qquad (2.37)$$

where k_1 is called the pre-exponential constant, E_a = activation energy, R_g is the universal gas constant and α and β are real numbers. It is difficult, if not impossible, to predict the pre-exponential factor and the activation energy theoretically and these values are usually determined from experimental data.

§ 2.3.1 Homogeneous Oxidation of Carbon Monoxide:

Apart from its presence in the exhaust gas, carbon monoxide appears as an intermediate chemical species in the combustion of hydrocarbons. When hydrocarbons are oxidized, CO appears first and is later converted to CO_2 in a slow secondary reaction. The overall reaction may be represented as:

$$Step\ \text{I}: HC + O_2 \rightarrow CO + H_2O \qquad (2.38\text{-a})$$

$$Step\ \text{II}: CO + \frac{1}{2}O_2 \rightarrow CO_2 \qquad (2.38\text{-b})$$

While there have been many studies of the oxidation of CO, a frequently used rate expression for homogeneous CO combustion is [Hayes et. al. 1997],

$$-R_{CO}^{h} = 1.26e^{10} \exp\left(-\frac{20131}{T_f}\right) C_{CO}\, C_{O_2}^{0.25}\, C_{H_2O}^{0.5} \qquad \text{mol/m}^3\text{·s.} \qquad (2.39)$$

where concentrations are in mol/m^3 and temperature is in Kelvin.

2.3.2 Homogeneous Oxidation of Propane:

Much of the work done in determining rate equations for the homogeneous combustion of hydrocarbons has been based on the study of laminar flame propagation. The actual mechanism of hydrocarbon combustion is very complex and the inclusion of

this mechanism in a reactor model will yield a very expensive computational problem. Furthermore, for most catalytic combustion applications it is probably not necessary to go into such details.

The simplest model has a single step. This model contains only four species and no intermediate concentration is included.

$$C_nH_m(g)+\left(\tfrac{n}{2}+\tfrac{m}{4}\right)O_2(g)\rightarrow nCO(g)+\tfrac{m}{2}H_2O(g) \qquad (2.40)$$

Some success at predicting flame speeds has been shown using one step models, but they obviously have some drawbacks. One of these is that they predict the immediate formation of CO_2 in one step, whereas it is known that CO is produced first, and then reacts relatively slowly to form CO_2. To account for these shortcomings various multi-steps models have been proposed. However it must be realized that for every new species introduced in the homogeneous reaction scheme, a corresponding catalytic rate expression must be available. Keeping this in mind it is probably best to limit the model choice to at the most a two step model for the homogeneous oxidation of propane.

Therefore for the present study, a two step model introduced by Dryer, Hautman et. al. [1981] and Westbrook [1984] has been incorporated. The overall reaction is summarized as,

$$C_3H_8+3.5O_2\rightarrow 3CO+4H_2O \qquad (2.41\text{-a})$$

$$CO+\frac{1}{2}O_2\rightarrow CO_2 \qquad (2.41\text{-b})$$

The CO oxidation step is same as given in the previous section. The rate expression for homogeneous combustion of propane gas as given by [Hayes, 1997] used in present study is,

$$-R^{h}_{C_3H_8} = 3.2e^{7} \exp\left(-\frac{15100}{T_f}\right) C^{0.1}_{C_3H_8}\, C^{1.65}_{O_2} \qquad (2.42)$$

where all concentrations are in mol/m^3 , temperature is in Kelvin and the rate is expressed in mol/m^3·s.

2.3.3 Catalytic Oxidation of Carbon Monoxide:

The Langmuir Hinshelwood Hougen Watson (LHHW) reaction model is frequently used to model the catalytic oxidation of carbon monoxide. This model assumes that the rate determining step (i.e. that step which is intrinsically slow) in the overall mechanism of CO oxidation is the reaction between adsorbed CO and adsorbed oxygen atoms or molecules [Scott Fogler, 1994]. The common feature of all LHHW models is that the rate equation is expressed as a ratio. The numerator is referred to as the kinetic driving force. The denominator represents the inhibition force due to adsorption of the species on the surface. The general form of LHHW models for catalytic oxidation of CO is represented as,

$$-R^{c}_{CO} = \frac{k' K_{CO} K_{O_2} C^{\alpha}_{CO} C^{\beta}_{O_2}}{\left(1 + K_{CO} C_{CO} + K_{O_2} C_{O_2}\right)^{\gamma}} \qquad (2.43)$$

It can be seen that, at any given temperature, an increase in reactant concentration will result in an increase in the kinetic driving force, which has the tendency to increase the rate of reaction. However, this will also increase the value of the adsorption inhibition

term that will tend to decrease the rate of reaction. Thus, the net result solely depends on the local conditions.

LHHW rate equations are also well known to give rise to multiple steady states [Nauman, 1987]. From mathematical point of view this means that for any given set of inlet conditions to the reactor, there exists more than one set of solution variables that satisfies the set of governing equations. The steady state at which the reactor will actually function depends on how operating conditions were varied, or in other words the history of the reactor. Plug flow reactors lack any internal mechanism for memory. There is no axial dispersion of heat or mass. What has happened previously has no effect on what is happening now. This fact prevents steady state multiplicity in plug flow reactors, unless there is some form of external feedback. Given a set of operating conditions, only one output is possible.

Various forms of the above model, as reported in the literature have been incorporated and tested.

2.3.4 Catalytic Oxidation of Propane:

Propane is a typical compound frequently used as a representative to model the fast burning components of an automobile exhaust, as reaction rate constants for typical gasoline are not available.

Typical rate expressions encountered in the literature are presented in the form of power law models. Wanke [1973] proposed the intrinsic rate model used in the present study. The study was based on oxidation of propane in air at atmospheric pressure over a commercial catalyst. The spherical beads have the active catalyst deposited in the

washcoat near the surface of the pellets. The rate expression was reported to be linear having the form,

$$-R^{c}_{C_3H_8} = 3.15e^{4} \exp\left(-\frac{89126}{R_g T_s}\right) C_{C_3H_8} \qquad (2.44\text{-a})$$

The rate has the units of mol/kg·s, the mass being the total mass of the entire pellets including the weight of the substrate. The above model does not take into account the inhibition effects, if any, by other chemical species present.

Khandekar [2000] modified it with new value of pre-exponential coefficient, which has been used in the present problem. This is following,

$$-R^{c}_{C_3H_8} = 12.85\times10^{4} \exp\left(-\frac{89126}{R_g T_s}\right) C_{C_3H_8} \qquad (2.44\text{-b})$$

2.4 PHYSICAL PROPERTIES:

The physical property models, required for the overall model development are as follows:

2.4.1 Gas Viscosity:

The viscosity of the gases is approximated to the viscosity data for air given in Holman [1997] and is modeled as,

$$\mu = 3.1227e^{-6} + 5.47613e^{-8}T - 1.93284e^{-11}T^{2} + 3.65582e^{-15}T^{3} \qquad (2.45)$$

where T is in Kelvin and μ is in Pa.s.

2.4.2 Specific Heat of Species:

The specific heat of the species, involved in the chemical reaction, as a function of temperature are modeled as [Hayes, 1997]

$$C_p(C_3H_8) = -4.04 + 30.43e^{-2}T - 15.70e^{-5}T^2 + 31.68e^{-9}T^3 \quad (2.46\text{-a})$$

$$C_p(CO_2) = 22.22 + 5.971e^{-2}T - 3.495e^{-5}T^2 + 7.457e^{-9}T^3 \quad (2.46\text{-b})$$

$$C_p(CO) = 28.11 + 0.067e^{-2}T + 0.536e^{-5}T^2 - 2.218e^{-9}T^3 \quad (2.46\text{-c})$$

$$C_p(O_2) = 25.44 + 1.518e^{-2}T - 0.715e^{-5}T^2 + 1.310e^{-9}T^3 \quad (2.46\text{-d})$$

$$C_p(N_2) = 28.85 - 0.157e^{-2}T + 0.807e^{-5}T^2 - 2.868e^{-9}T^3 \quad (2.46\text{-d})$$

where T is in Kelvin to give C_p in Joule/mol.K.

2.4.3 Heat of Reaction:

For the two step reaction represented as,

$$C_3H_8 + 3.5\,O_2 \rightarrow 3CO + 4H_2O \quad (2.47\text{-a})$$

$$CO + 0.5\,O_2 \rightarrow CO_2 \quad (2.47\text{-b})$$

by definition, we know that,

$$\Delta H_R = \Delta H^{\circ}_{298.15} + \int_{298.15}^{T} \Delta C_p \cdot dT \quad \text{and} \quad \Delta C_p = \sum_{products} x_i C_p - \sum_{reactants} x_i C_p \quad (2.48)$$

substituting the values from Equation 2.44, we get,

$$(\Delta C_p)_{C_3H_8} = 128.09 - 0.344734T + 24.0253e^{-5}T^2 + 56.2985e^{-9}T^3 \quad (2.49\text{-a})$$

$$(\Delta C_p)_{CO} = -18.61 + 0.05045T - 3.6741e^{-5}T^2 + 9.02e^{-9}T^3 \quad (2.49\text{-b})$$

and Equation 2.45-a transforms as,

$$\Delta H_{R,C_3H_8}(T) = -1220779. - 128.1T + 0.172T^2 - 8.008e^{-5}T^3 + 14.07e^{-9}T^4 \quad (2.50\text{-a})$$

$$\Delta H_{R,CO}(T) = -279380. - 18.61T + 0.025T^2 - 1.225e^{-5}T^3 + 2.255e^{-9}T^4 \quad (2.50\text{-b})$$

where T is in Kelvin and ΔH in Joule/mol.

2.4.4 Effective Diffusivity of the Pellet:

The overall mathematical model of the reactor requires the value of the effective diffusivity of the catalyst pellet. The effective diffusivity is the combined effect of the Bulk diffusivity and the Knudsen diffusivity. These quantities are modeled as follows:

(a) Bulk Diffusion:

The diffusive flux of a component 'A' in a mixture of 'A' and 'B' is represented in terms of concentration gradient and according to Fick's Law is given by:

$$J_A = -C_T \cdot D_{AB} \frac{dY_A}{dz} \tag{2.51}$$

Here D_{AB} is the bulk molecular diffusion coefficient for component 'A' diffusing in a mixture of 'A' and 'B', C_T is the total concentration, Y_A is the mole fraction of specie 'A' and dz is the axial distance along the reactor. Considerable attention has been given in the literature to predict the mass diffusion coefficient D_{AB}. Assuming ideal gas behavior, kinetic theory may be used to show that:

$$D_{AB} \approx P^{-1} T^{\frac{3}{2}} \tag{2.52}$$

This relation applies to restricted pressure and temperature ranges only. Bird et. al. [1960] Provide detailed discussions of the available theoretical treatments and comparisons with experiments. Skelland [1974] and Ried and Sherwood [1966] provide more detailed treatments of this subject. Reid et. al. [1987] and Fuller et. al. [1966] also discuss the calculation of D_{AB}. A method developed by Fuller et. al. [1966] gives the following formula for D_{AB},

$$D_{AB} = \frac{1.013e^{-2} \cdot T^{1.25}\left(\frac{1}{M_A} + \frac{1}{M_B}\right)^{0.5}}{P \cdot \left(\left(\sum \xi_i\right)_A^{\frac{1}{3}} + \left(\sum \xi_i\right)_B^{\frac{1}{3}}\right)^2} \qquad (2.53)$$

D_{AB} has the units m^2/s, P is the pressure in Pa and ξ_i are diffusional volumes. Values of the latter for simple atoms and molecules are given in the table below [Fuller, 1966]:

Table 2.1 Atomic and Structural Diffusion Volume Increments

C	H	O	N	Cl	S	Aromatic Rings
16.5	1.98	5.48	5.69	19.5	17.0	-20.2

Table 2.2 Diffusion Volumes of Common Simple Molecules

H_2	N_2	O_2	Air	CO	CO_2	N_2O	H_2O	NH_3
7.07	17.90	16.60	20.10	18.90	26.90	35.90	12.70	14.90

Note: For systems involving more than two components, the diffusion of each species can be treated as if it were diffusing through another single species rather than through a mixture by applying a correction factor to D_{AB} [Hill, 1977].

(b) Knudsen Diffusion:

The pores of the catalyst pellet are usually quite small and there are a significant number of collisions between the gas molecules and the pore walls. If the pores are sufficiently large so that collision between molecules are much more frequent than those between molecule and the wall, the mechanism of diffusion is the same as the bulk phase. When the mean free path of the diffusing molecules is larger than the mean pore

diameter, then the molecules "rattles" down each pore by successive collisions with the pore walls. For a single straight cylindrical pore [Hirschfelder et. al. 1954]:

$$D_{K,A} = \frac{2}{3} \cdot (\text{Pore Radius}) \cdot (\text{Mean Thermal Speed of Molecule 'A'}) \qquad (2.54)$$

By kinetic theory of gases it can be shown that:

$$D_{K,A} = 97 \cdot r_{eq} \left(\frac{T}{M_A} \right)^{0.5} \qquad (2.55)$$

Where r_{eq} is the equivalent pore radius in m, T is in $^{\circ}K$ and the molar mass of the diffusion species, M_A is in kg/kmol or g/mol. Frequently the equivalent pore radius is taken as the average radius of the pores in the pellet. Alternatively, it may be computed from the expression by Satterfield [1963]:

$$r_{eq} = \frac{2 \cdot \phi_p}{(BET) \cdot \rho_p} \quad , \qquad (2.56)$$

where BET= Brunauer-Emmet-Teller surface area of the catalyst, ϕ_P is the pellet porosity and ρ_p is the pellet density.

(c) Effective Diffusivity:

When the Knudsen and bulk diffusivities are significantly different, applicable diffusivity is determined by smaller of the two.

$$\overline{D} = \mathrm{D_{AB}} \text{ or } \mathrm{D_{K,A}} \quad (\text{smaller of the two}) \qquad (2.57)$$

When the two diffusivities are commensurate, the combined effect is actually worse than either acting alone. The following equation is adequate for most purposes for calculating the applicable diffusivity $\overline{D}$,

$$\frac{1}{\overline{D}} = \frac{1}{D_{AB}} + \frac{1}{D_{K,A}} \tag{2.58}$$

The pores in the pellet are not straight and cylindrical; rather, they are a series of tortuous, interconnecting paths of varying cross-sectional areas. It would not be feasible to describe diffusion within each and every one of the tortuous pathways individually. This requires that we modify the diffusion coefficient of the gas in the pores to account for:

(a) The void fraction of the catalyst.

(b) The tortuosity of the pores. Tortuosity can be defined as the ratio of the distance that a molecule travels along the pore(s) and pore interconnections to get between two points, to the shortest distance between those points.

(c) The variation in the cross sectional area of the pores.

The effective diffusivity of the catalyst pellet can be measured experimentally. In the absence of experimental data, its value may be estimated from the pore size distribution and catalyst porosity data given by [Scott Fogler, 1992],

$$D_{eff} = \frac{\phi_p \cdot \sigma}{\tilde{\tau}} \cdot \overline{D} \tag{2.59}$$

where,

ϕ_P is the pellet porosity, σ is the pore constriction factor which accounts for the variation in cross-sectional area that is normal to the diffusion and $\tilde{\tau}$ is pore tortuosity factor.

2.5 THE HEAT TRANSFER:

The heat transfer between a fluid flowing through a packed bed and the wall is interpreted according to a one-dimensional model characterized by an overall transfer coefficient, h_{fs} and by two-dimensional model with one parameter, the coefficient of coefficient, h_{fs} and by two-dimensional model with one parameter, the coefficient of thermal conductivity k_P or two parameters, the effective thermal conductivity λ_P and wall heat transfer coefficient, α_P.

The mathematical model of the packed bed requires relationships for heat transfer processes occurring within the bed. These processes are modeled as described below.

2.5.1 Thermal Conductivity of Packed Beds:

The heat transfer Wasch [1971] et. al. studied on heat transfer in packed beds. The experimental results for overall heat transfer coefficient h_w, effective thermal conductivity k_p and wall heat transfer coefficient α_w were correlated as a function of Reynolds number, flow rates, particle and tube diameter. All correlations of the parameters in function of Reynolds number lead to straight lines, which intersect the heat transfer coefficient axis. Correlations were also setup between the parameters of the various models.

The energy balance equations for the model require the effective thermal conductivity for the packed bed. The equations are, [Dixon and Cresswell, 1979],

$$k_{r,eff} = k_{rf} + k_{rs}\left[\frac{1+\dfrac{8k_{rf}}{h_{wf}D_T}}{1+\left(\dfrac{\dfrac{16}{3}k_{rs}\left(\dfrac{1}{h_{fs}D_P}+\dfrac{0.1}{k_P}\right)}{(1-\phi)\left(\dfrac{D_T}{D_P}\right)^2}\right)}\right] \tag{2.60}$$

and

$$k_{a,eff} = k_{af} + k_{as}\left[\frac{1}{1+\dfrac{\dfrac{16}{3}k_{as}\left(\dfrac{1}{h_{fs}D_P}+\dfrac{0.1}{k_p}\right)}{(1-\phi)\left(\dfrac{D_T}{D_P}\right)^2}}\right] \tag{2.61}$$

where the subscripts *'a'* and *'r'* refer to axial and radial respectively, *'f'* and *'s'* refers to fluid and solid phase respectively, *'w'* refers to the wall and *'p'* refers to the single pellet. For R_b greater than 50 and D_T / D_P greater than 10, it is reasonable to approximate the above equation as,

$$k_{r,eff} = k_{rf} + k_{rs} \tag{2.62-a}$$

$$k_{a,eff} = k_{af} + k_{as} \tag{2.62-b}$$

The radial and axial conductivity of the solid, k_{rs} and k_{as}, respectively are given by, [Wakao and Kaguei, 1982]

$$k_{rs} = k_{as} = \frac{2k_f(1-\phi)^{0.5}}{1-\frac{k_f\overline{B}}{k_p}}\left[\frac{\left(1-\frac{k_f}{k_P}\right)\overline{B}}{\left(1-\frac{k_f\overline{B}}{k_P}\right)^2}\ln\left(\frac{k_P}{\overline{B}k_f}\right)-\left(\frac{\overline{B}-1}{2}\right)-\left(\frac{\overline{B}-1}{\left(1-\frac{k_f\overline{B}}{k_P}\right)}\right)\right] \qquad (2.63)$$

where,

$$\overline{B} = \overline{C}\left[\frac{1-\phi}{\phi}\right]^{\frac{10}{9}}, \qquad (2.64)$$

and $\overline{C} = 1.25$ for spheres and 1.4 for crushed particles [Hayes, 1997].

The conductivities, k_{rf} and k_{af} are correlated using the Peclet numbers for heat transfer, given by, [Wakao and Kaguei, 1982]

$$(Pe_H)_{rf} = \frac{GC_PD_P}{k_{rf}} = \left(0.1+\frac{0.66\phi}{\mathrm{Re}_b\,\mathrm{Pr}}\right)^{-1} \qquad (2.65)$$

$$(Pe_H)_{af} = \frac{GC_PD_P}{k_{af}} = \left(\frac{0.73\phi}{\mathrm{Re}_b\,\mathrm{Pr}}+\frac{0.5}{\left(1+\frac{9.7\phi}{\mathrm{Re}_b\,\mathrm{Pr}}\right)}\right)^{-1} \qquad (2.66)$$

where,

$$\mathrm{Re}_b = \frac{D_P\rho v_s}{\mu} = \frac{D_PG}{\mu} \qquad \text{Bed Reynolds Number} \qquad (2.67)$$

$$\mathrm{Pr} = \frac{\mu C_P}{k_f} \qquad \text{Prandtl Number} \qquad (2.68)$$

Thus, provided the thermal conductivities of the fluid and the catalyst particles, the bed porosity, equivalent particle diameter and the reactor diameter are known, the thermal conductivities required for the reactor model can be computed.

2.5.2 Bed to Wall Heat Transfer Coefficients:

In the pseudo-homogeneous model, the combined effective heat transfer coefficient at the wall, $h_{w,eff}$, is used. Defining a Nusselt number at the wall,

$$Nu_{fw} = \frac{h_{wf} D_P}{k_f} \tag{2.69}$$

where, from [Yagi and Wakao, 1959]

$$Nu_{fw} = 0.6 \mathrm{Pr}^{0.33} \mathrm{Re}_b^{0.5} \qquad 1 < \mathrm{Re}_b < 40 \tag{2.70-a}$$

$$Nu_{fw} = 0.2 \mathrm{Pr}^{0.33} \mathrm{Re}_b^{0.8} \qquad 40 < \mathrm{Re}_b < 2000 \tag{2.70-b}$$

Also, from [Dixon A.G. and Cresswell,1979], we note that,

$$\frac{h_{w,eff}}{k_{r,eff}} = \frac{h_{wf}}{k_{rf}} \tag{2.71}$$

Thus we can find the effective bed to wall convective heat transfer coefficient.

2.5.3 Overall Heat Transfer Coefficients:

The heat transfer between the reactor side fluid and the heat transfer fluid surrounding the reactor can be divided into three components.

(a) Convective heat transfer between the reactor fluid and the inside wall, which is governed by the inner convective heat transfer coefficient, $h_{w,eff}$.

(b) Conduction through the reactor wall which is proportional to the thermal conductivity of the wall, k_w,.

(c) Finally, there is heat transfer between the outside reactor wall and the heat transfer fluid, governed by the outer heat transfer coefficient, h_o.

The overall heat transfer coefficient, U, combines these three parameters. For a reactor tube of outside diameter D_o the relation is,

$$\left(\frac{1}{U}\right)=\left(\frac{1}{h_{w,eff}}\right)+\left(\frac{D_T}{2k_w}\right)\ln\left(\frac{D_{in}}{D_T}\right)+\frac{D_T}{D_{in}}\frac{1}{h_{in}} \qquad (2.72)$$

The outside heat transfer coefficient may be estimated from standard heat transfer correlations. The best value for U is still a matter of debate and various correlations have been proposed as given in De Wasch and Froment [1972], Froment and Bischoff [1990] and Dixon A.G. and Cresswell [1979].

2.6 PELLET DEFFUSION EFFECTIVENESS FACTOR:

In heterogeneous reaction sequence, mass transfer of reactants first takes place from the bulk fluid to the external surface of the pellet. The reactants then diffuse from the external surface into and through the pores within the pellet washcoat, with the reactions taking place only on the catalytic surface of the pores. A schematic representation of this two-step diffusion process is shown in Figure 2.2.Thus we observe that there are two types of diffusion resistance in the heterogeneous catalytic reaction:

(a) <u>External Resistance</u>: This is encountered for diffusion of the reactants or products between the bulk fluid and the external surface of the catalyst. The main cause of this external resistance is the formation of a concentration boundary layer as the flow takes place along the catalyst pellets. This has a tendency to either increase or decrease the concentration at the surface relatively to the bulk or the free stream concentration. The resulting concentration difference is the driving force for mass transfer.

The rate of mass transfer of a component 'A' present in the bulk stream can be expressed using the mass transfer coefficient [Incropera and DeWitt, 1996],

$$J_A = k_{m,A}\left(C_{b,A} - C_{S,A}\right) \tag{2.73}$$

Various ways of estimation of the mass transfer coefficient have been proposed. Generally, it can be safely calculated from the heat and mass transfer analogy. For heat and mass transfer of a single sphere, under forced convection, the following Ranz and Marshall [Wakao and Kaguei, 1982] equation is popularly recognized,

$$Nu'_b = 2 + 0.6\,\mathrm{Re}_b^{0.5}\,\mathrm{Pr}^{0.33} \tag{2.74-a}$$

$$Sh'_b = 2 + 0.6\,\mathrm{Re}_b^{0.5}\,Sc^{0.33} \tag{2.74-b}$$

$$Nu'_b = \frac{h'_b D_P}{k_f} \quad \Leftrightarrow \quad Sh'_b = \frac{k'_{m,A} D_P}{D_{AB}} \tag{2.75-a}$$

$$\mathrm{Pr} = \frac{\upsilon}{\alpha_T} \quad \Leftrightarrow \quad Sc = \frac{\upsilon}{D_{AB}} \tag{2.75-b}$$

The Nusselt and Sherwood numbers for packed beds are generally higher than those predicted from the above equation. This difference reduces as the Reynolds number is reduced. For higher Reynolds number Wakao and Kaguei [1982] analyzed a large amount of packed bed data and proposed the following correlations,

$$Nu_b = 2 + 1.1 \mathrm{Re}_b^{0.6}\, \mathrm{Pr}^{0.33} \tag{2.76-a}$$

$$Sh_b = 2 + 1.1 \mathrm{Re}_b^{0.6}\, Sc^{0.33} \tag{2.76-b}$$

$$Nu_b = \frac{h_b D_P}{k_f} \quad \Leftrightarrow \quad Sh_b = \frac{k_{m,A} D_P}{D_{AB}} \tag{2.77-a}$$

$$\mathrm{Pr} = \frac{\upsilon}{\alpha_T} \quad \Leftrightarrow \quad Sc = \frac{\upsilon}{D_{AB}} \tag{2.77-b}$$

From the above equations, it is concluded that, in general, to increase the mass transfer coefficient and hence the rate of reaction one may either decrease the particle size or increase the bulk fluid velocity.

The relative magnitude of the external mass transfer resistance, as compared to the internal pore diffusion resistance may be calculated by the Biot Number for mass transfer, defined as,

$$Bi_M = \frac{k_{m,A} L_{eq}}{D_{eff}} = \frac{\text{Internal mass transfer resistance to diffusion in solid}}{\text{external mass transfer resistance to convection in a fluid}} \tag{2.78}$$

For the present modeling, the external resistance to mass transfer was neglected as the Bi_M value was calculated to be well above 100.

(b) <u>Internal Resistance</u>: This is encountered for diffusion of the reactants from the external pellet surface (pore mouth) to the interior of the pellet and vice versa for the products. In a porous catalyst pellet, for the reaction to occur inside the pores, the reactants must diffuse into it. As the reactants diffuse into the pellet washcoat, they

encounter active sites and some of the reactants react. The reactant concentration decreases as the distance into the catalyst pellet increases, giving rise to a concentration gradient into the pellet as shown in Figure 2.3. Thus the entire washcoat is not accessible to the same reactant concentration. If the diffusion velocity is much lower than the intrinsic reaction rate, the concentration gradient can be quite large. When using the intrinsic reaction rates it is necessary to know the gas phase concentration at the active sites. Therefore it is necessary to have a means of calculating the effective rate of reaction in a catalyst with a variable concentration profile. This is achieved by defining effectiveness factor, a parameter that accounts for variations in concentration throughout the pellet washcoat resulting in the variation in the rate of reaction.

$$\eta = \frac{\text{Average Rate of Reaction for a catalyst pellet}}{\text{Rate of Reaction evaluated at surface conditions}}$$

The governing equation for simultaneous diffusion and reaction within the catalyst pellet will provide the functional relationship for effectiveness factor.

Performing the one dimensional, steady state mole balance in spherical co-ordinates for isothermal conditions within the pellet and assuming that the diffusive flux based on effective diffusivity within the pellet follows Fick's law, we get,

$$[\text{Flow in}] - [\text{Flow out}] = [\text{Disappearence by reaction}]$$

or

$$-\frac{d\left(J_A r^2\right)}{dr} = \left(\rho_C R_A^C\right) \qquad (2.79\text{-a})$$

$$\eta = \frac{3}{\Phi}\left[\frac{1}{\tanh(\Phi)} - \frac{1}{\Phi}\right] \tag{2.81}$$

where Φ is called the Thiele modulus defined as,

$$\Phi = \frac{D_P}{2}\sqrt{\frac{(\rho_C k')}{D_{eff}}} \tag{2.82}$$

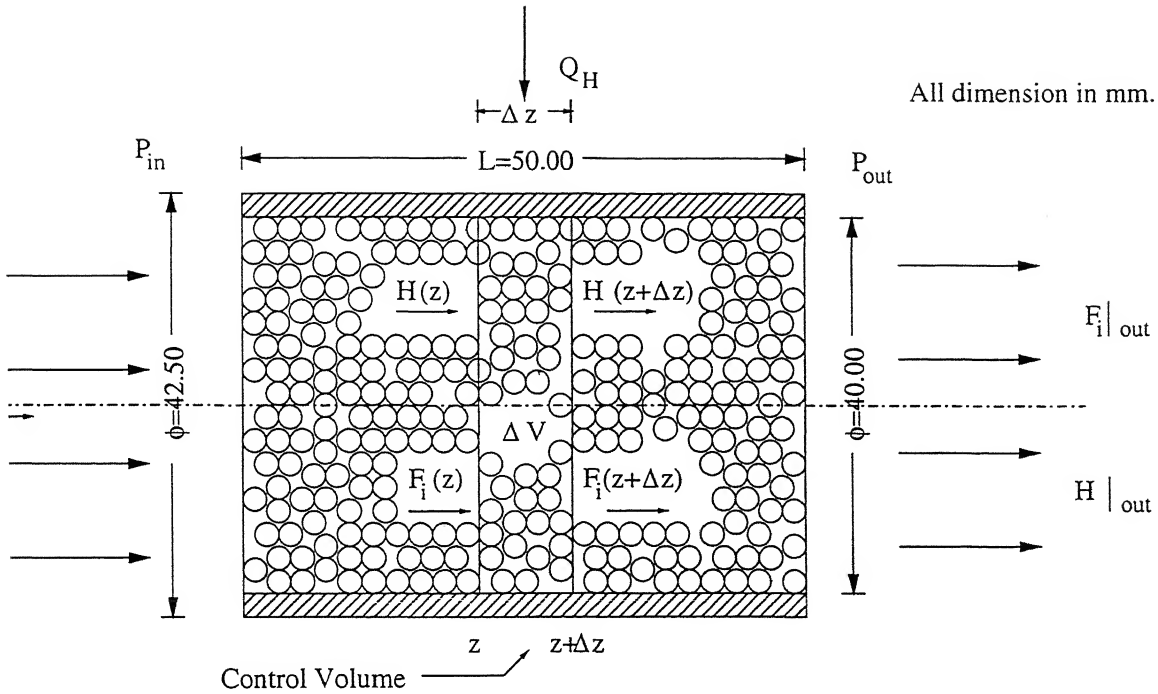

Figure 2.1 : Differential volume element used in developing shell balance for the 1D packed bed model, non-adaiabtic case.

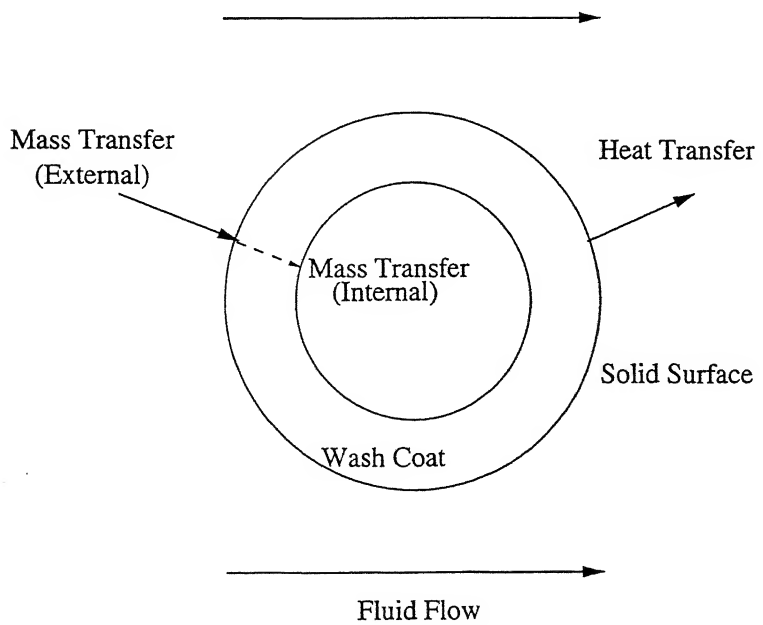

Figure2.2: Heat and mass transfer between fluid and solid surface of the pellet.

CHAPTER 3

THE SOLUTION STRETAGY

The final sets of governing equations for one dimensional, plug flow, non-adiabatic, heterogeneous, steady state catalytic reactor have been described in the chapter 2. These form a set of coupled ordinary differential equations in fluid and solid phase. The inlet data on gas temperature and composition and mass flow rate is known. The transport properties of the packed bed along with the stoichiometric and constitutive constraints complete the set of equations. The problem although non-linear, is well posed and is solved as follows:

- The basic governing equations in solid phase are solved.
- Once the solid phase values are known, new values at $z=z_0+\Delta z$ in fluid phase are solved by Runge-kutta Gill algorithm for solving simultaneous ordinary differential equations.
- The transport properties are handled as a separate subroutine providing the results to the main solver.

CHAPTER 3

THE SOLUTION STRETAGY

The final sets of governing equations for one dimensional, plug flow, non-adiabatic, heterogeneous, steady state catalytic reactor have been described in the chapter 2. These form a set of coupled ordinary differential equations in fluid and solid phase. The inlet data on gas temperature and composition and mass flow rate is known. The transport properties of the packed bed along with the stoichiometric and constitutive constraints complete the set of equations. The problem although non-linear, is well posed and is solved as follows:

- The basic governing equations in solid phase are solved.
- Once the solid phase values are known, new values at $z=z_0+\Delta z$ in fluid phase are solved by Runge-kutta Gill algorithm for solving simultaneous ordinary differential equations.
- The transport properties are handled as a separate subroutine providing the results to the main solver.

CHAPTER 3

THE SOLUTION STRETAGY

The final sets of governing equations for one dimensional, plug flow, non-adiabatic, heterogeneous, steady state catalytic reactor have been described in the chapter 2. These form a set of coupled ordinary differential equations in fluid and solid phase. The inlet data on gas temperature and composition and mass flow rate is known. The transport properties of the packed bed along with the stoichiometric and constitutive constraints complete the set of equations. The problem although non-linear, is well posed and is solved as follows:

- The basic governing equations in solid phase are solved.
- Once the solid phase values are known, new values at $z=z_0+\Delta z$ in fluid phase are solved by Runge-kutta Gill algorithm for solving simultaneous ordinary differential equations.
- The transport properties are handled as a separate subroutine providing the results to the main solver.

- An implicit Thomas algorithm solves the pellet diffusion equation and effectiveness factors are then computed in separate subroutines.

3.1 THE MAIN SOLVER:

The final set of governing equations may be summarized as follows:

3.1.1 The Solid Phase Mole Balance Equation:

$$Y^s_{C_3H_8} = Y^f_{C_3H_8} + \left[\frac{1.0\times r'^c_{C_3H_8}\times\eta_{C_3H_8}\times\rho_C(1-\phi)}{C_f\times k_m\times a_v}\right] \tag{3.1-a}$$

$$Y^s_{O_2} = Y^f_{O_2} + \left[\frac{\left\{\left(3.5\times r'^c_{C_3H_8}\times\eta_{C_3H_8}\right)+\left(0.5\times r''^c_{CO}\times\eta_{CO}\right)\right\}\times\rho_C\times(1-\phi)}{C_f\times k_m\times a_v}\right] \tag{3.1-b}$$

$$Y^s_{CO} = Y^f_{CO} + \left[\frac{\left\{\left(-3.0\times r'^c_{C_3H_8}\times\eta_{C_3H_8}\right)+\left(1.0\times r''^c_{CO}\times\eta_{CO}\right)\right\}\times\rho_C\times(1-\phi)}{C_f\times k_m\times a_v}\right] \tag{3.1-c}$$

$$Y^s_{H_2O} = Y^f_{H_2O} + \left[\frac{-4.0\times r'^c_{C_3H_8}\times\eta_{C_3H_8}\times\rho_C\times(1-\phi)}{C_f\times k_m\times a_v}\right] \tag{3.1-d}$$

$$Y^s_{CO_2} = Y^f_{CO_2} + \left[\frac{-1.0\times r''^c_{CO}\times\eta_{CO}\times\rho_C\times(1-\phi)}{C_f\times k_m\times a_v}\right] \tag{3.1-e}$$

3.1.2 The Fluid Phase Mole balance Equation:

$$\frac{dY^f_{C_3H_8}}{dz} = \frac{\left\{1.0\times r'^h_{C_3H_8}\times\phi - k_m\times a_v\times C_f\times\left(Y^f_{C_3H_8}-Y^C_{C_3H_8}\right)\right\}}{\left(C_f\times v_s\right)} \tag{3.2-a}$$

$$\frac{dY^f_{O_2}}{dz} = \frac{\left\{\left(3.5\times r'^h_{C_3H_8}+0.5\times r''^h_{CO}\right)\times\phi - k_m\times a_v\times C_f\times\left(Y^f_{O_2}-Y^s_{O_2}\right)\right\}}{\left(C_f\times v_s\right)} \tag{3.2-b}$$

$$\frac{dY_{CO}^{f}}{dz}=\frac{\left\{\left(-3.0\times r_{C_3H_8}^{'th}+1.0\times r_{CO}^{''h}\right)\times\phi-k_m\times a_v\times C_f\times\left(Y_{CO}^{f}-Y_{CO}^{s}\right)\right\}}{\left(C_f\times v_s\right)} \tag{3.2-c}$$

$$\frac{dY_{H_2O}^{f}}{dz}=\frac{\left\{-4.0\times r_{C_3H_8}^{'th}\times\phi-k_m\times a_v\times C_f\times\left(Y_{H_2O}^{f}-Y_{H_2O}^{s}\right)\right\}}{\left(C_f\times v_s\right)} \tag{3.2-d}$$

$$\frac{dY_{CO_2}^{f}}{dz}=\frac{\left\{-1.0\times r_{CO}^{''h}\times\phi-k_m\times a_v\times C_f\times\left(Y_{CO_2}^{f}-Y_{CO_2}^{s}\right)\right\}}{\left(C_f\times v_s\right)} \tag{3.2-e}$$

3.1.3 The Momentum Balance Equation:

$$\left(\frac{dP}{dz}\right)=-\frac{G\cdot(1-\phi)}{\rho_0\cdot D_p\cdot\phi^3}\cdot\left[\frac{150\cdot\mu\cdot(1-\phi)}{D_p}+(1.75\cdot G)\right]\left(\frac{F_T}{F_{T0}}\right)\left(\frac{P_0}{P}\right)\left(\frac{T_f}{T_0}\right) \tag{3.3}$$

3.1.4 Solid Phase Energy Balance Equation:

$$T_s=T_f-\frac{\left\{(1-\phi)\times\rho_C\times\left(r_{C_3H_8}^{'c}\times\Delta H_{R_{C_3H_8}}\times\eta_{C_3H_8}+r_{CO}^{''c}\times\Delta H_{R_{CO}}\times\eta_{CO}\right)\right\}}{h_{fs}\times a_v} \tag{3.4}$$

3.1.5 Fluid Phase Energy Balance Equation:

$$\frac{dT_f}{dz}=\frac{\left\{\Delta H_{R_{C_3H_8}}\times\left(r_{C_3H_8}^{'h}\right)-\Delta H_{R_{CO}}\times\left(-r_{CO}^{''h}\right)\right\}\times\phi+h_{fs}\times a_v\times\left(T_s-T_f\right)+\frac{4\times U}{D_T}\times\left(T_\infty-T_f\right)}{v_s\times\rho\times C_P} \tag{3.5}$$

We know the initial condition of fluid phase i.e.

$$Y_i^f(0) = Y_i^f\,\|_{inlet} \quad \vdots \quad P(0) = P\,\|_{inlet} \quad \vdots \quad T_f(0) = T_f\,\|_{inlet}$$

Using these initial conditions, solid phase equations are solved. So now all the solid and fluid phase parameters are known before going to next step.

By applying Runge-Kutta Gill Simultaneous Solver in fluid phase, values at $z=z_0+\Delta z$ are obtained. Again repeating the above process we obtain these values at different sections along z direction.

3.2 THE PELLET DEFFUSION EQUATION:

The one dimensional diffusion reaction equation for the catalyst pellet is given by

$$\frac{\partial^2 C_i}{\partial r^2} + \frac{2}{r}\frac{\partial C_i}{\partial r} - \frac{f(C_i)}{D_{eff}} = 0$$
$$@\ r = r_P \Rightarrow C_i\,| = C_{iS} \vdots @\ \ r = r_w \Rightarrow \left.\frac{\partial C_i}{\partial r}\right| = 0 \qquad (3.6)$$

After incorporating a fictitious cell at the inside boundary ($r = r_w$) and discretizing the above equation along with the boundary conditions, using N nodes between r_P and r_w we get,

$$\frac{C_i^{j-1} - 2C_i^j + C_i^{j+1}}{\Delta r^2} + \frac{1}{r_j}\left(\frac{C_i^{j+1} - C_i^{j-1}}{\Delta r}\right) - \left(\frac{f(C_i^j)}{D_{eff}}\right) = 0 \qquad (3.7)$$

and

$$@\ j = 1 \Rightarrow C_i = C_S \quad @\ \ j = N \Rightarrow \frac{C_{N+1} - C_{N-1}}{2\Delta r} = 0$$

Rearranging equation 3.7, We get,

$$\bar{b}C_i^{j-1} + \bar{d}C_i^{j} + \bar{a}C_i^{j+1} - \frac{f\left(C_i^{j}\right)}{D_{eff}} = 0 \qquad (3.8)$$

Where,

$$f\left(C_i^{j}\right) = \rho_C\left(-R_i^{c}\right)$$

and

$$\bar{b} = \left(\frac{1}{\Delta r^2} - \frac{1}{r_j \Delta r}\right) \vdots\ \bar{d} = -\frac{2}{\Delta r^2} \vdots\ \bar{a} = \left(\frac{1}{\Delta r^2} + \frac{1}{r_r \Delta r}\right)$$

and

$$\Delta r = \frac{r_P - r_w}{(N-1)} \quad \vdots\ r_j = r_w + (j-1)\Delta r$$

To solve the above set of equations the following steps are followed,

1. Guess C_i at all nodes form $j=2$ to N by linear interpolation between the limits $C_s<C<0$. Apply the boundary condition at $j=1$ and $j=N+1$ (fictitious node).
2. Solve the resulting tridiagonal matrix by Thomas Algorithm.
3. Update the value of C_j and go to step 1 until a converged concentration field is obtained.
4. Find the effectiveness factor of the pellet for CO oxidation using equation 2.80.

3.3 COMPARISON OF COMPUTATIONAL STEP SIZE:

Initially, computational step size of 3 mm was chosen because pellet diameter is 3 mm and Khandekar S.[2000] used 3mm step size for computations in the homogeneous

model. Figures 3.3-3.5 show comparison of computational step size of 3 mm, 1mm and 0.5 mm at T_{in}=450^{0}C with same mass flow rate on CO and HC conversion efficiency and, solid and fluid phase temperatures.

It can be seen that use of smaller step size results in more precise calculations as it updates solid phase parameters at each small step resulting in higher predicted conversion rates and temperatures. Comparing values of the parameters on these step sizes, one can see that there is a significant difference between calculations for 3mm step size and 1 mm step size. But there is very little difference between 1mm and 0.5 mm step size. Therefore, further computations are done using 1mm step size as it yields more precise results and is computationally more efficient.

3.4 COMPUTATION FOR CONICAL CATALYTIC CONVERTER:

Conical catalytic converter is subdivided into five equal parts as shown in figure 3.6. Inlet velocity is computed from 'Fluent' software by giving mass flow rate at a particular temperature. Computations are performed in these subsections separately as shown in Figure 3.7. For each subsection area is calculated and then inlet velocity for subsequent computational steps are calculated conservation of mass. The values of mole fractions and gas temperatures are averaged at the outlet of catalyst bed.

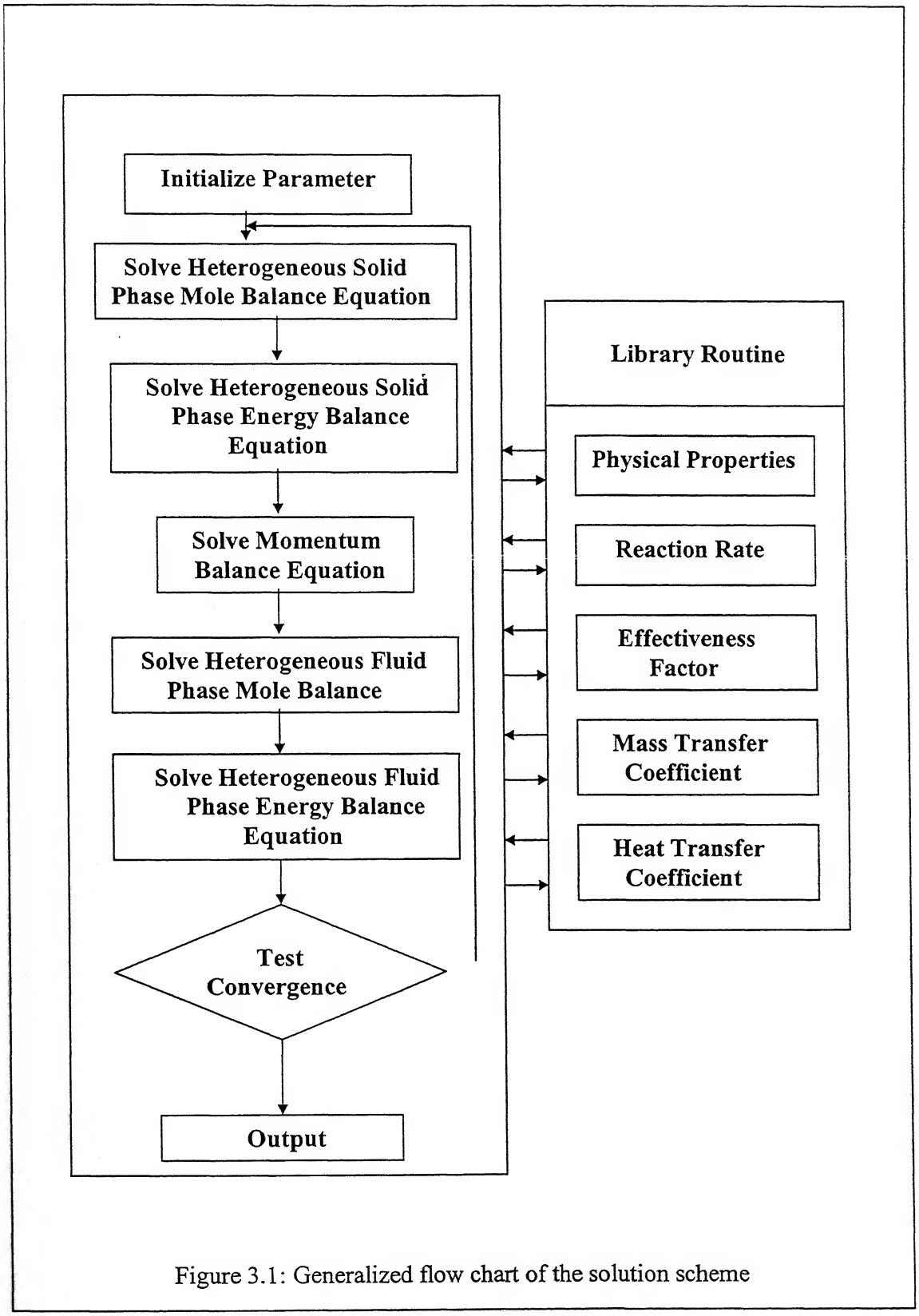

Figure 3.1: Generalized flow chart of the solution scheme

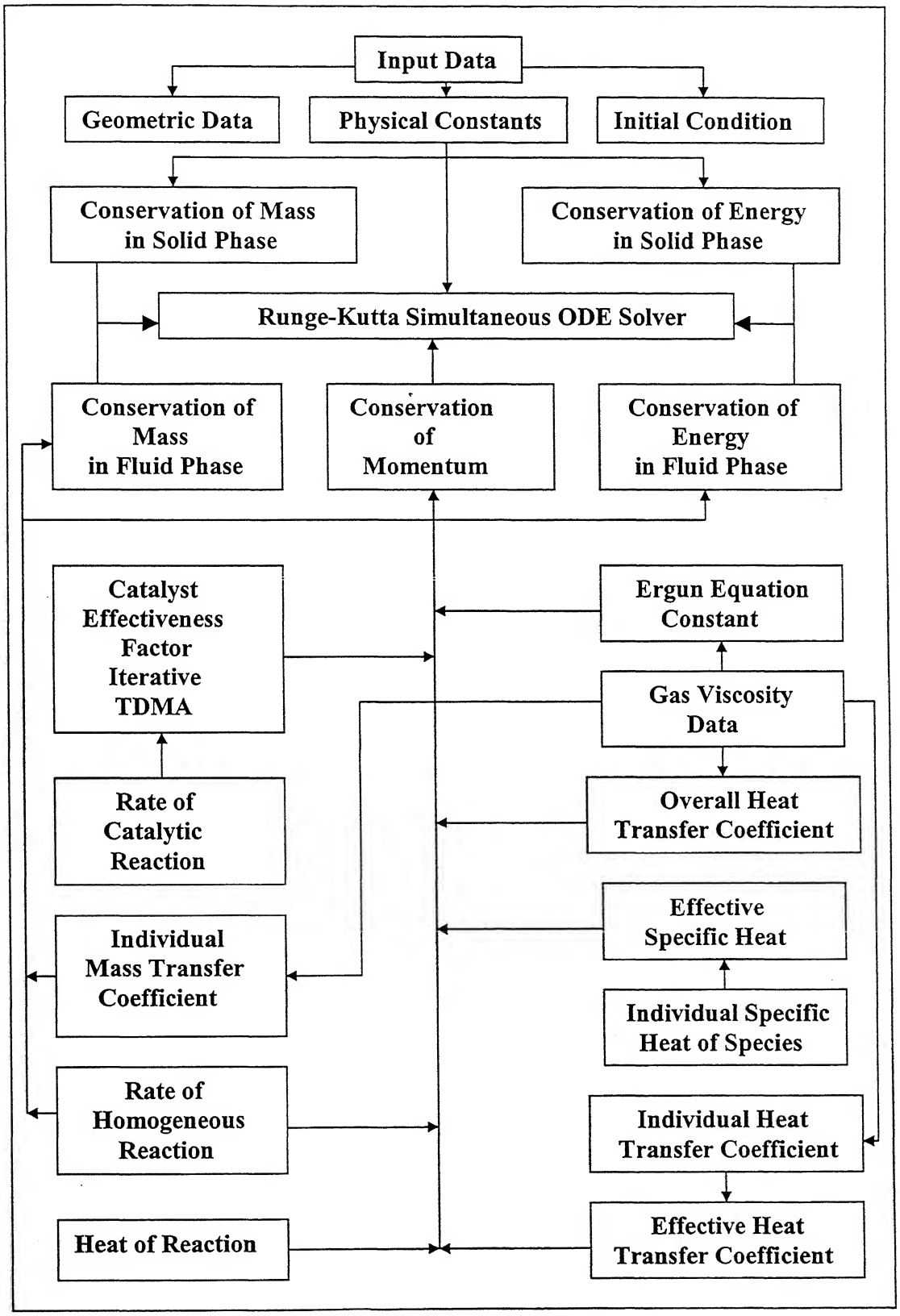

Figure3.2: Flow chart of the solver

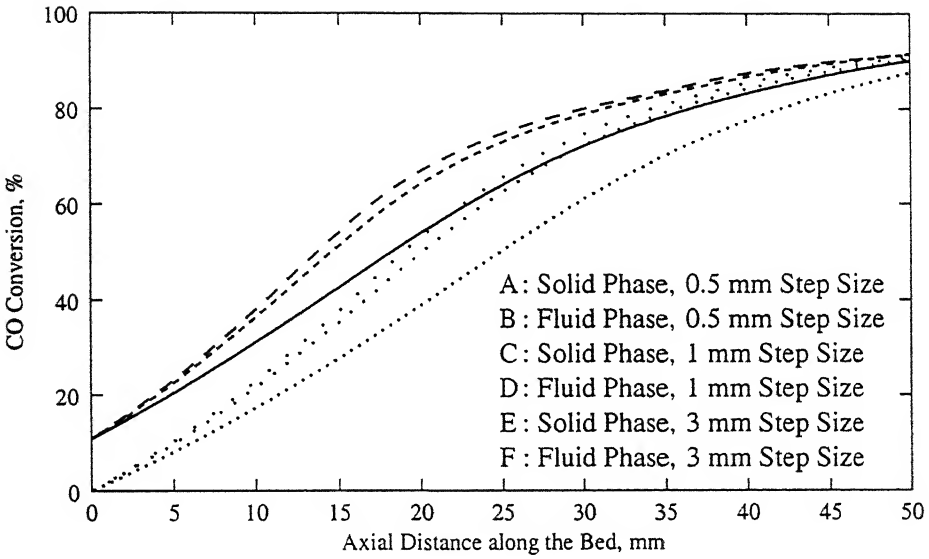

Figure 3.3: Effect of computational step size in axial direction along catalyst bed on CO conversion, adiabatic heterogeneous model $T_{in} = 450\ ^{o}C$, $\dot{m}_{in} = 1.362$ g/s

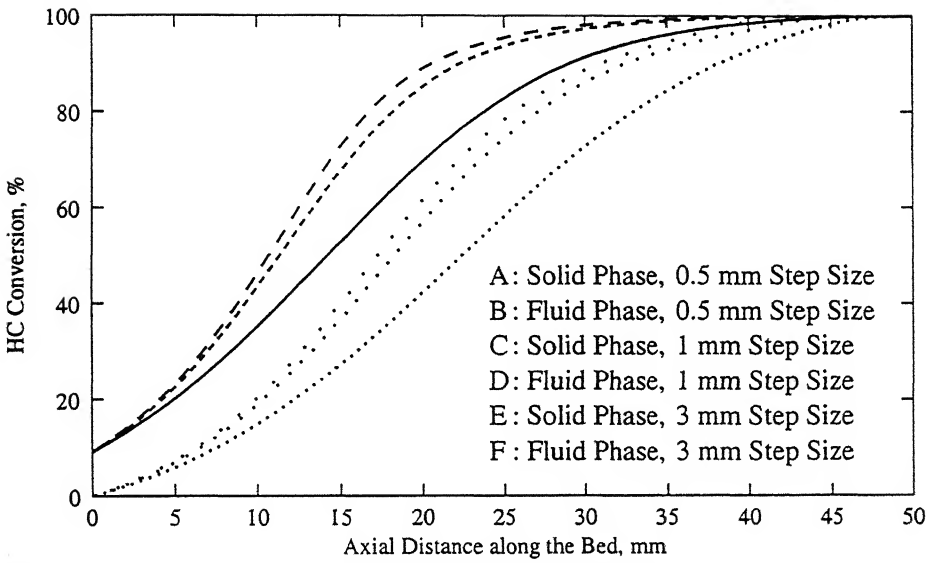

Figure 3.4: Effect of computational step size in axial direction along catalyst bed on HC conversion, adiabatic heterogeneous model, T_{in}= 450 °C, $\dot{m}_{in}$= 1.362 g/s

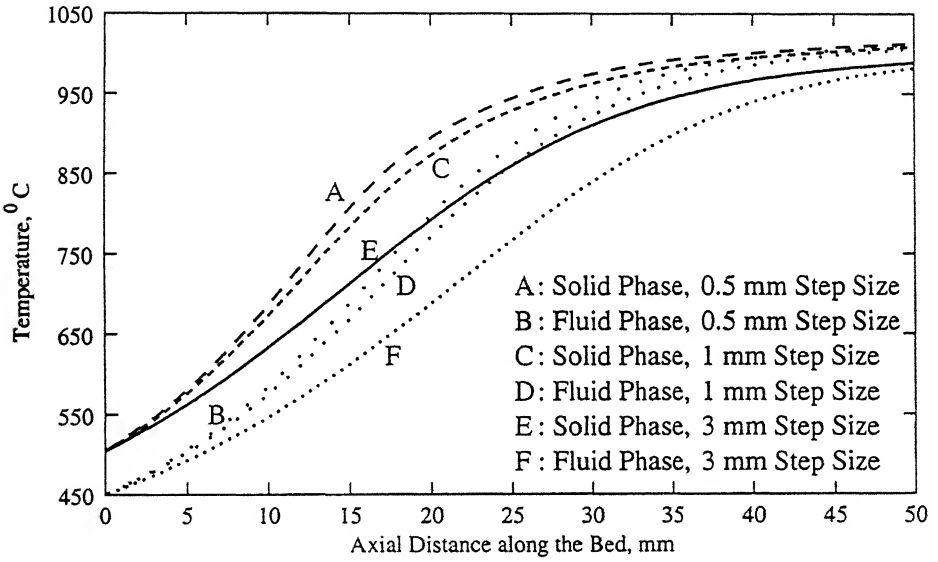

re 3.5: Effect of computational step size in axial direction along catalyst bed on solid and fluid phase temperatures, adiabatic heterogeneous model, T_{in}= 450 °C, $\dot{m}_{in}$= 1.362 g/s

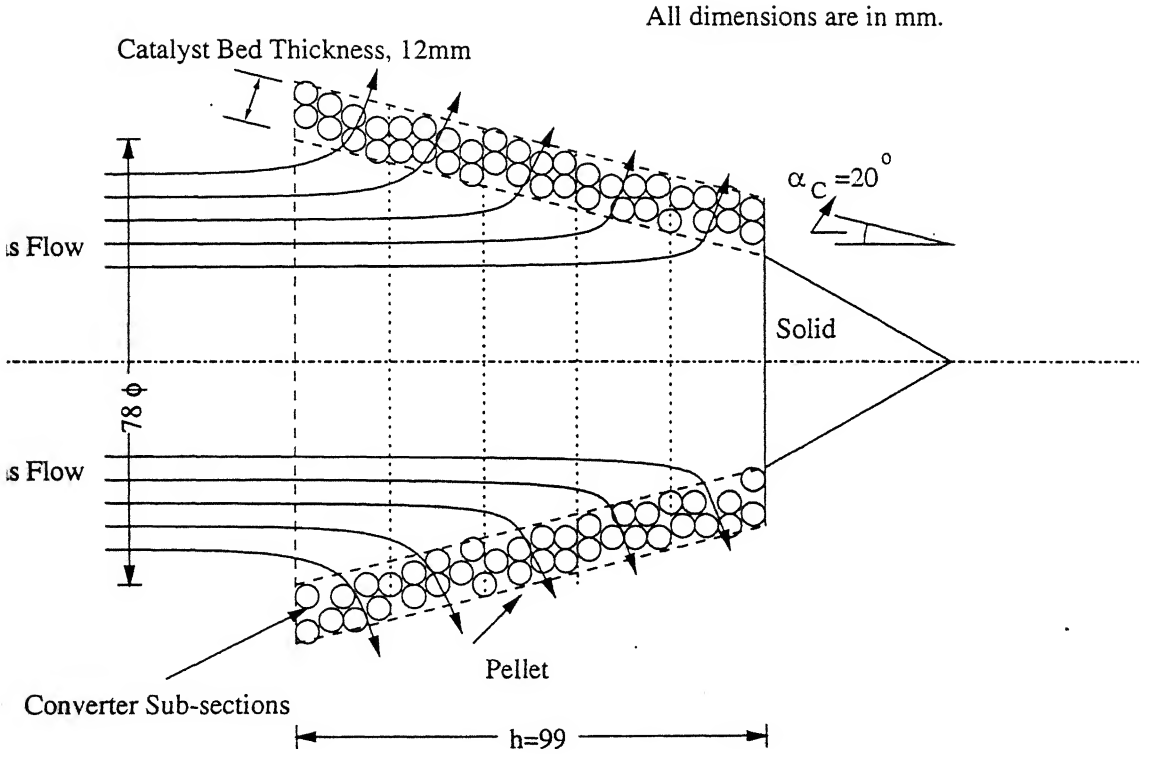

Figure 3.6: Schematic representation of a conical catalytic converter.

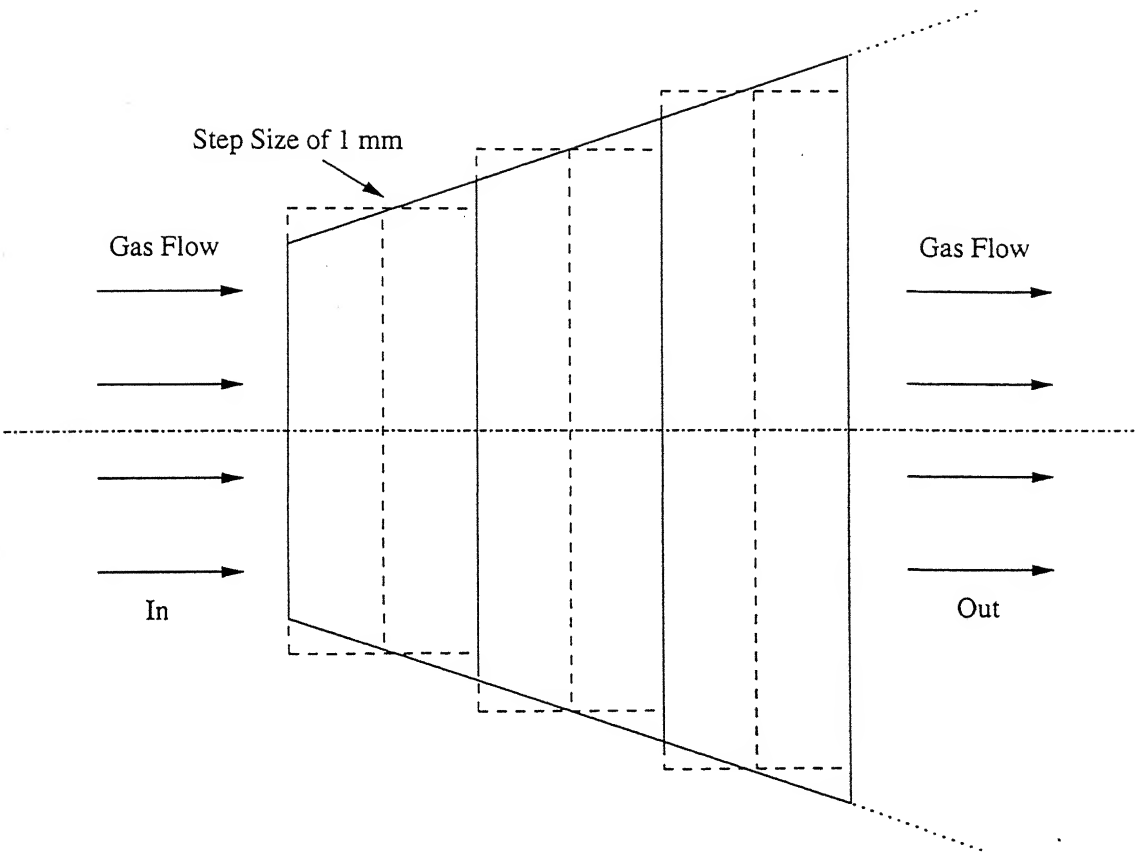

Figure 3.7: Schematic representation of one of the sub-sections of figure 3.6 along catalyst bed.

CHAPTER 4

RESULTS

The results obtained from the present study are presented in this chapter. The results are presented into the following sequence:

- CO and HC conversion and catalyst bed temperatures with adiabatic heterogeneous model,
- Effect of adiabatic and non-adiabatic conditions on heterogeneous model predictions,
- Comparison of non-adiabatic heterogeneous and homogeneous models,
- Comparison of heterogeneous and homogeneous models with the experimental results on a portable generator,
- Flow field and pressure variation along flow for a moped the exhaust muffler equipped with conical catalytic converter using Fluent 5.3,CFD software,
- Conversion efficiency, temperature and pressure drop for a moped catalytic converter with different catalyst bed thickness,

- Comparison of performance of conical and cylindrical catalytic converters of equal catalyst volume.
- Comparison of performance of cylindrical converter with two different catalyst volume.

For computation of results input data used are given in Table 4.1. These data were obtained experimentally by Khandekar S. [2000] on a two-stroke gasoline engine portable generator set. Two different mass flow rates corresponding to 100W and 600W generator output and the corresponding measured exhaust gas composition as shown in Table 4.2 are used. Computations are also done for two different arbitrary inlet gas temperatures of 300 and 450^{0}C are used to study response of the model to the inlet gas temperature. These temperatures are also typical of genset operation as observed experimentally.

4.1 CO and HC Conversion and Catalyst Bed Temperatures with Adiabatic Heterogeneous Model:

Computations are done for solid and fluid phase conversion of CO and HC and outlet temperature with two different mass flow rates corresponding 100W and 600W output. CO conversion is presented on Figs. 4.1 and 4.2, HC on Figs. 4.3 and 4.4. Figs. 4.5 and 4.6 show temperatures along the catalyst bed of the converter. It is seen from Figs. 4.1-4.4 that for the same inlet temperature, higher conversion of CO and HC are obtained at the lower mass flow rates and vise versa. For example, at 300 ^{0}C inlet temperature, at 1.362 and 1.750 g/s mass flow rates space velocities are 33.53 s^{-1} and 42.33 s^{-1} respectively. Lower space velocity at 1.362 g/s mass flow rate results in higher

residence time of gases in the converter and hence higher rates of reaction and conversion. These results are further supported by the higher solid and fluid phase temperatures compared to those for 1.750 g/s at mass flow rate of 1.362 g/s (Figs. 4.5 and 4.6). At inlet temperature of 300 ^{0}C, solid phase temperature at the converter outlet increased from 429 to 513 ^{0}C and fluid phase temperature from 405 to 472^{0}C when mass flow rate is decreased from 1.750 to 1.362 g/s. At 450 ^{0}C inlet temperature, corresponding increase in solid phase and fluid phase temperatures are smaller with reduction in only 28 and 18 ^{0}C respectively.

Comparing Figs. 4.1 and 4.2 it is seen that for 1.362 g/s mass flow rate when inlet temperature is increased from 300 to 450 ^{0}C, CO conversion increases from 46.3% to 92.6%, doubling the conversion. For these computations, inlet composition of the exhaust gas was kept the same. HC conversion increases from 21.6 to 100%, which is more than four times for the same conditions. HC conversion appears to be more sensitive to temperature than CO conversion. For same mass flow rate, catalyst outgas almost doubled increases from 513^{0}C to 1011^{0}C when inlet temperature increases from 300 to 450 ^{0}C(Figs. 4.5 and 4.6).

Figs. 4.1 and 4.3 further show that CO and HC conversion both for solid and fluid phase increase gradually along the catalyst bed at 300 ^{0}C inlet temperature. However, at higher inlet temperature of 450 ^{0}C, CO and HC conversion increase sharply in the first half of the catalyst bed and then tapers off in the second half. At high inlet temperature, reaction rates are significantly higher and hence higher conversion rates and heat release. Subsequently, as the concentration of reacting species reduce the conversion rates and heat release also reduce in the second half of the catalyst bed. On the other hand, space

velocity increases from 33.5 to 42.3s^{-1} when temperature is increased from 300 to 450 ^{0}C for the same mass flow rate of 1.362g/s. hence, residence time decreases accordingly its effect being reduction in conversion and temperature rise. However, the effect of inlet gas temperature on rates of reaction being of exponential form far outweighs negative influence of reduced residence time which results in very high increase in CO and HC conversion as well as solid and fluid temperatures.

Figs. 4.1 and 4.2 show that at the lower inlet gas temperature the difference between solid and fluid phase CO and HC conversion increases along the catalyst bed. However, the higher inlet temperature of 450 ^{0}C, this difference first increases slightly up to middle of the catalyst bed and then decreases gradually in the second half of the bed. The same behavior is seen solid and fluid phase temperatures in Figs. 4.5 and 4.6. This also could be attributed to significantly higher rates of reaction in the first half of the catalyst bed at T_{in} = 450 ^{0}Ccompared to 300 ^{0}C on the solid catalyst. The conversion and temperature increase at a faster rate at solid surface of the catalyst than in fluid when inlet temperature is increased. One may conclude that for higher inlet temperatures, catalytic converter of smaller volume could be used. But for practical applications, an engine warm-up and inlet temperature at light loads are also to be catered for and hence has to be arrived at a compromise between conversion efficiency and catalyst volume

4.2 Effect of Adiabatic and Non-Adiabatic Conditions on Heterogeneous Model:

Figs. 4.7-4.12 show the effect of heat transfer from catalytic converter to the surroundings on CO and HC conversion and catalyst bed temperatures predicted by the heterogeneous model. Again, the data are shown for two mass flow rates and two inlet

gas temperatures as earlier. As expected, CO and HC conversion (Figs. 4.7-4.10) and solid and fluid phase temperatures (Figs. 4.11 and 4.12) are higher for adiabatic condition than non-adiabatic condition. Fig. 4.7 and 4.8 show that heat transfer from the converter reduces CO conversion by 1 to 4% in solid phase and 0.8 to 3% in fluid phase. Higher differences are obtained at lower mass flow rates and lower inlet temperatures. For example, at 1.362 g/s mass flow rate and 300 ^{0}C inlet temperature, reduction in CO conversion obtained are 4 and 3% in solid and fluid phase respectively (Fig. 4.7-a). Corresponding reduction for 1.750 g/s mass flow rate and 450 ^{0}C inlet temperature are 1 and 0.8% only (Fig. 4.8-b). Similar trends are observed for HC conversion as well. The heat transfer from the converter reduces HC conversion by 0 to 5% in solid phase and 0 to 2.75% in fluid phase. For 1.362 g/s mass flow rate and T_{in} = 450^{0}C, 100% HC conversion is obtained both in solid and fluid phases.

Similarly, Fig. 4.11 and 4.12 show that heat transfer from the converter reduces solid phase temperature by 35 to 18^{0}C and fluid phase temperature by 30 to 15 ^{0}C. Higher differences are obtained at lower mass flow rates and lower inlet temperatures. At 1.362 g/s mass flow rate and 300 ^{0}C inlet temperature, reduction in solid and fluid phase temperatures obtained are 35 and 28 ^{0}C, respectively (Fig. 4.11-a). Corresponding reduction for 1.750 g/s mass flow rate and 450 ^{0}C inlet temperature are 26 and 23 ^{0}C (Fig. 4.12-b).

.3 Comparison of Non-Adiabatic Heterogeneous and Homogeneous Models:

Predictions of non-adiabatic heterogeneous and homogenous models are compared for two mass flow rates and two inlet temperatures as mentioned above. Figs. 13 and 4.14 compares CO conversion, Figs. 4.15 and 4.16 HC conversion and Figs.

4.17 and 4.18 the fluid phase temperatures. CO and HC conversion, and fluid phase temperature predicted by heterogeneous model are higher than the homogenous model. Difference in CO conversion is higher for lower mass flow rate (1.362 g/s) than the higher mass flow rate (1.750 g/s) for same inlet temperature (Fig. 4.13 and 4.14). For example, at inlet temperature equal to 300 ^{0}C, heterogeneous model gives 7.54 and 9.72% higher CO conversion at 1.750 to 1.362 g/s mass flow respectively. At T_{in} = 450^{0}C,corresponding difference was 8.62 and 12.4%.

Similar trends are seen for HC conversion (Figs. 4.15 and 4.16) in which at inlet temperature equal to 300 ^{0}C, HC conversion for heterogeneous model is 2.00 compared to 4.38% by homogeneous model for 1.750 and 4 compared to 10.46% for 1.362 g/s mass flow rate. At inlet temperature equal of 450 ^{0}C and mass flow fate equal to 1.362 g/s, 100% HC conversion occurs in heterogeneous model. But heterogeneous model gives 92% HC conversion. At mass flow rate of 1.750 g/s conversion in heterogeneous model goes up to 93% compared to 79.4% conversion for homogeneous model.

Figs. 4.17 and 4.18 compares fluid phase temperature for the two models. At T_{in} = 300^{0}C, heterogeneous model gives higher fluid phase temperature by 66 and 530C for 1.750 to 1.362 g/s mass flow rate at converter outlet. At T_{in} = 450^{0}C, fluid phase temperature at catalyst outlet is higher by 51 and 67^{0}C for 1.750 and 1.362g/s mass flow rates respectively.

4 Comparison of Heterogeneous and Homogeneous Models with the Experimental Results on a Portable Generator:

The predictions of heterogeneous model are compared with homogeneous model and experimental results (Khandekar S. [2000]) on a two-stroke 2-kVA gasoline fueled

portable genset. Experimental data on CO and HC conversion at different genset output and mass flow rates are given in Table 4.2 and gas temperature in Table 4.3. Computed data are given in Table 4.4 and are compared with experimental data in Figs. 4.19-4.24. CO conversion predicted by heterogeneous model is compared with those of homogeneous model and experimental data in Fig. 4.19. Heterogeneous model predicts 5 to 10% higher conversion (Table 4.4) than the homogeneous model. Up to 400W output of the engine, there is a good correlation with experimental data. CO Conversion efficiency at outputs higher than 400W is under-predicted by both the models.

Fig. 4.20 compares HC conversion efficiency. At lower loads, heterogeneous model slightly under-predicts conversion efficiency but at higher loads, it over predicts. Homogenous model under predicts throughout the operational range.

In Figs. 4.21-4.24, catalyst bed temperatures with heterogeneous and homogenous models are compared with experimental data at no load, 200W, 400W and 700W outputs, respectively. Heterogeneous model predicts higher bed temperature than homogenous model, although these are still significantly lower than the experimental data. Further the experimental data show that catalyst bed temperature rise sharply to near maximum at just about 17mm downstream of the inlet. Such behavior of heterogeneous model is observed at 450 ^{0}C inlet temperature. However, even at 700W output, the measured inlet temperature is only 385 ^{0}C and using this temperature model predicts only a gradual increase in gas temperature along the catalyst bed. Experimental exhaust gas outlet temperatures at 500W and 700W are 772 and 866 ^{0}C respectively.

It is known that significant oxidation of CO in bulk gas results for temperature above 700^{0}C and oxidation of HC above 600^{0}C. As the gas-sampling probe is not exactly

it the converter outlet but in the mixing volume at the converter outlet, post catalytic eaction might have occurred showing higher CO conversion and gas temperatures. As egards, HC conversion rates of reaction for propane have been used observed in lifferential (micro) reactors. The reaction rates for typical gasoline in integral reactors ould be different which may account for the difference observed between experimental nd predicted values. However, the predicted in CO and HC conversion and gas emperatures show good correlation with the experimental data. Heterogeneous model as shown significant improvement over homogeneous model in correlation with xperimental observations.

4.5 Flow Field and Pressure Variation for the Exhaust Muffler Equipped with Conical Catalytic Converter using Fluent 5.3,CFD Software:

4.5.1 Procedure:

For application of the model to complicated catalytic converter geometry, inlet xhaust mass flow rate, gas condition and gas velocity to different converter sections are equired. Pressure drop across the converter is another important data for ensuring inimum adverse effect of the converter fitment in the engine muffler.

There are many CFD softwares like Fluent, Flow3D, Phoenix etc which offer a latively quicker engineering solution to a variety of flow and heat transfer related roblems. These softwares may be effectively used for optimization of design and duction of time for prototype development. It is important to note that at this stage, the ea of specific chemical kinetic modeling as required for the catalytic converter system, not within the domain of these commercial. The softwares are effective and quick tools get valuable flow information especially in systems involving complicated geometry.

These softwares numerically solve the governing partial differential equations that lescribe the transport processes. The partial differential equations are reduced to ılgebraic expressions either by integrating the governing equations (in control volume nethod) or discretizing by 'Taylor aeries approximations' (in the finite volume method) ›ver the discrete sub-domains of the overall physical domain describing the problem. Therefore, a set of grid lines must be specified in order to discretize and create sub-lomains. The process of creating this sub-domain is called grid generation.

In this study grids are generated and boundary conditions are applied using Gambit' and for solving the equations, 'Fluent 5.3' is used.

Following steps are followed in 'Gambit',

. Create geometry of the problem concerned.

. Create the faces so that it can draw grid.

. Choose the size and type of grid for the geometry.

. Define the boundary conditions i.e. inlet velocity, outlet velocity, wall, symmetry etc.

. Define the continuum whether it is solid or fluid.

. Export it to 'Fluent'.

Following steps are followed in 'Fluent',

Scale the geometry.

Input the material and its physical parameters like density, specific heat, viscosity ıd thermal conductivity.

Choose the model for the flow.

Define the operating condition i.e. value of pressure at any cross-section.

Input the values of boundary condition.

6. If the material is porous like in present case, give the porosity for the domain comprising porous material.

7. Define the velocity vector i.e. direction if the domain of the porous material is not perpendicular to flow as in the present case.

8. Iterate the equation, results are obtained once the convergence criteria is satisfied.

4.5.2 Geometry of Catalytic Converter and Flow Field (Asymmetric Muffler):

Fig. 4.26 shows the drawing of the exhaust muffler of a typical moped designed by M/s IOCL, R&D Centre, Faridabad. This muffler is fitted with the packed bed catalytic converter of the conical configuration with its apex in the down stream direction. The muffler has asymmetric exhaust gas inlet. To solve the flow problem on this physical domain, rectangular grids of 3 mm size are generated (Fig. 4.27). Fig. 4.28 and 4.29 show the velocity contours and velocity vectors respectively. It is seen that the velocity of gas through the converter increases as one moves from periphery towards apex. Fig. 4.30 shows contours of stream function in the muffler. There are also several recirculation zones on expansion in the different part of the muffler.

It may be concluded from this figure that being higher near apex of the cone, the part of converter away from cone is relatively underutilized. It is seen that velocity inlet to the converter is 2.9 to 2.93m/s in the lower portion of the converter when one moves towards apex of the converter. Inlet velocity in upper portion of the converter is 0.76 to 0.78, higher being towards the apex. Fig. 4.31 shows the pressure variation. A pressure difference of 1.46 KPa is seen across the muffler. Outlet pressure is atmospheric in all cases.

Next it is studied whether flow field becomes more uniform if the apex of the cone is located towards upstream. Fig. 4.32 shows the schematic of asymmetric exhaust muffler with apex of the conical converter in the up-stream direction. Fig. 4.33 is for grid. These grids are rectangular with each side is of 3mm. Figs. 4.34 and 4.35 are for velocity in contour and vector form respectively. There is higher velocity in the narrow passages between the obstruction plates but smaller velocity is in the corners of the inlet portion where recirculation of flow occurs. Velocity through the catalyst bed is smaller because of obstruction by the pellets. Similarly, Fig. 4.36 and 4.38 are for stream function and pressure respectively. Unlike muffler of Fig. 4.30, there is less recirculation of flow in the inlet section (4.36), which gives better result. Inlet velocity to the converter is 0.98-1.1m/s in the lower portion while in upper portion, it is 0.65-0.67m/s. higher velocity is towards apex. There is a pressure difference of 1.63KPa across muffler.

4.5.2 Geometry of Catalytic Converter and Flow Field (Symmetric Muffler):

To study the effect of location of exhaust gas inlet on flow field, symmetric inlet geometry to the muffler was created as shown in Figs. 4.38 and 4.44. Both versions of apex towards downstream as well as upstream were studied.

Fig. 4.38 gives the drawing of muffler with symmetric inlet and with apex of the converter towards downstream direction. Fig. 4.39 shows rectangular grid of 3mm size. Figs. 4.40-4.43 show velocity contours, velocity vectors, stream function and pressure respectively. Here recirculation of flow in the both corners of the inlet section is observed (Figs. 4.40-4.42). It is seen that higher portion of the flow takes place near the converging section. This may result in poor conversion as volume of the catalyst near the apex is less and also overheating of the pellets in the converging section may take place. So geometry

should be modified to avoid this phenomena. Inlet velocity to catalyst bed varies between 0.78 to 0.81m/s. higher velocity occurs near apex. 2.12 KPa pressure drop occurs across the muffler.

In the same way, Fig. 4.44 shows schematic of exhaust muffler with apex of the converter towards upstream direction. Grid is shown in Fig. 4.45 and Figs. 4.46-4.49 are for velocity contours, velocity vectors, stream function and pressure drop, respectively. As expected, same pattern is seen here. Velocity varies from 0.77 to 0.80m/s higher being near apex of the converter. Here pressure drop of 1.73 KPa is seen which is lower than the previous arrangement in which apex of the cone was towards downstream direction.

For further computations for catalytic conversion, inlet velocity of exhaust gas to the converter is taken as uniform as observed in muffler with symmetric inlet velocity condition. for example, for mass flow rate of 1.5525g/s, inlet velocity to e converter section is taken equal to 0.8m/s for T_{in}=300^{0}C.

4.6 Conversion Efficiency, Temperature and Pressure Drop for Conical Catalytic Converter of a Moped with Different Catalyst Bed Thickness:

The computations are done for these exhaust mass flow rates at different inlet temperatures for a fixed exhaust gas composition given in Table 4.6.

At first, conical catalytic converter of 12mm catalyst bed thickness as designed by M/s Indian Oil Corporation Limited, R&D Centre, Faridabad is studied. Five different inlet temperature e.g. 300, 350, 400, 450 and 500^{0}C are taken with four exhaust mass flow rates typical of a moped at 30, 40, 50 and 65 km/hr as shown in Table 4.5. With these mass flow rates, inlet velocity to the converter is obtained through Fluent software at temperature of 300^{0}C. It is seen that velocity varies slightly in inlet to the converter

from 0.78 to 0.81 at mass flow rate equal to 1.5225 m/s. In the same way for mass flow rate equal to 2.349g/s, velocity varies from .98 to 1.1m/s. For different mass flow rates and inlet temperatures, the gas inlet velocities to the converter section are given in Table 4.7.

Figs. 4.50 and 4.51 shows CO and HC conversion at different inlet gas temperatures for different mass flow rates 1.5225 to 5.0g/s corresponding moped speed at 30 to 65Km/hr. At lower mass flow rate, i.e. at lower speed, inlet temperature is also lower. So at 300 and 350^{0}C inlet temperature and at 1.5225g/s mass flow rate (30Km/hr of vehicle speed), CO conversion is 23.5 and 39% respectively. HC conversion is only 3.3 and 14.5% respectively for the same condition. However at 450^{0}C inlet temperature, CO conversion is 67% and HC conversion is 56%. But in actual operating conditions, at lower mass flow rate i.e. at lower speed, inlet temperature 0f 450^{0}C may not be obtained. It is seen that conversion efficiency especially for HC at practical inlet temperature at different mass flow rates is quite low. Thus 12mm bed thickness is not suitable for practical purposes. Hence, bed thickness is increased to 15mm and 18mm. For 15mm bed thickness, CO and HC conversion, outlet temperature and pressure drop are shown in Figs. 4.54-4.57 respectively and for 18mm bed thickness, these are shown in Figs, 4.58-4.62. for 15mm bed thickness, at 30km speed, CO conversion is 33.5 and 55.1% while HC is 6.6 and 27.6% at inlet temperatures of 300 and 350^{0}C respectively. Corresponding outlet temperatures are 396 and 495^{0}C respectively. Increasing catalyst bed thickness to 15mm does not improve HC conversion to the desired label. This shows that there is not much improvement in conversion efficiency. So catalyst bed thickness is further increased to 18mm.

For 18mm catalyst bed thickness, CO and HC conversions, outlet temperature and pressure drop are shown in Figs. 4.58-4.62 respectively. It is seen that for 1.5225g/s mass flow rate and 300 and 350^0C inlet temperature, CO conversions are 44 and 68.2% and HC conversion is 11.9 and 44% respectively. Although, at higher inlet temperature (450^0C) and higher vehicle speed (65Km/hr), CO and HC conversion are significantly 53.9 and 42% compared to 17.3 and 3.8% at 300^0C inlet temperature.

It is found from the above discussion that conical converter even with 18mm catalyst bed thickness does not give significant CO and HC conversion especially at lower inlet temperature and even at lower vehicle speed. But on the other hand it uses a large amount of catalyst volume (192cm^3). It should be noted here that catalyst volume for 4-stroke engines used are generally equal to swept volume of the engine or lower. For the 2-stroke engines, catalyst volume are somewhat higher as higher HC and CO emissions are to be converted with adequate catalyst life. This moped is equipped with an engine of 75 cm^3 swept volume. Very high catalyst volume is not acceptable in practice, as the cost will be higher. Conversion efficiency, of equal volume of conical and cylindrical shaped converters are compared and discussed in next section.

4.7 Comparison of Conical and Cylindrical Catalytic Converter Having Equal Catalyst Volume:

Performance of conical converter with 12, 15 and 18mm catalyst bed thickness are compared with cylindrical catalytic converter of 117cm^3 catalyst volume (D_T = 50mm, L=60mm) which has the same catalyst volume as the 12mm conical converter at different inlet temperatures and exhaust mass flow rates is studied.

CO conversions are compared at different inlet temperatures in Figs. 4.63 -4.65 and HC conversion in Figs. 4.66-4.68. Both CO and HC conversions are significantly higher for the cylindrical converter than the conical ones at lower mass flow rate. For example, at 1.5225g/s mass flow rate, CO conversion in cylindrical converter is 78.2% while conical converters of 12mm, 15mm and 18mm catalyst bed thickness give only 23.5, 33.2 and 44.1% conversion respectively (Fig. 4.63). At higher inlet exhaust mass flow rate (5.0g/s), the difference in conversion between cylindrical and conical converter decreases. Cylindrical converter gives 15.5% conversion whereas conical converters give 10.2, 13.7 and 17.3% for 12mm, 15mm and 18mm catalyst bed thickness respectively. Conversion given by conical converter of 18mm catalyst bed thickness is only slightly higher than 12mm equivalent cylindrical catalytic converter at mass flow rate of 5.0g/s, in spite of catalyst volume of the former being 62%.

CO conversion at 400^0C inlet temperature and different exhaust mass flow rates is shown in Fig. 4.65. At lower mass flow rate (1.5225g/s), 100% CO conversion is obtained in cylindrical converter while conical converters give only 55.6 to 79.4%, highest being for 18mm catalyst bed thickness. At higher mass flow rate (5.0g/s) and 400^0C inlet temperature, CO conversion in cylindrical converter is 35.1% and in conical converter, conversion varies from 22.2-40.4% as catalyst bed thickness varies from 12 to 18mm. CO conversion for T_{in}=350^0C, in between conversions for 300 and 400^0C inlet temperature as expected (Fig. 4.64).

At T_{in}=300^0C and mass flow rate of 1.5225g/s, HC conversion is 84.1% for cylindrical converter (Fig. 4.66). For conical converters, 3.3, 6.6 and 11.8% HC conversions are observed. At higher mass flow rate (5.0g/s), HC conversion for all the

converter configurations are very low. For example, at 300^{0}C inlet temperature, cylindrical catalytic converter gives 1.6% conversion while conical converter with different catalyst bed thickness gives only 0.7, 1.3 and 2.0% conversions. At higher inlet temperature (400^{0}C) and lower mass flow rate (1.5225g/s), HC conversion reaches 100% in cylindrical converter and 33.8 to 71.4% for conical converter as bed thickness is increased. But for the same inlet temperature and at higher mass flow rate (5.0g/s), HC conversion in cylindrical converter is 26.6% and in conical converter is 9.17 to 22.1 %.

Outlet temperatures for cylindrical and conical converters are shown in Figs. 4.69-4.71. Fig. 4.69 shows that at low mass flow rate (1.5225g/s) and inlet temperature of 300^{0}C, outlet temperature for cylindrical converter is 823^{0}C and for conical converters are only 334to 467^{0}C. But at higher mass flow rate (5.0g/s) outlet temperatures for all converter configurations are only 354-362^{0}C. Fig. 4.71 shows outlet temperatures at 400^{0}C inlet temperature. It is seen that at lower mass flow rate (1.5225g/s), outlet temperature for cylindrical converter reaches to 1033^{0}C and for conical converters to 673and 875^{0}C. At the same inlet temperature but at higher mass flow rate (5.0g/s), outlet temperature in cylindrical converter is 604^{0}C and in conical converters varies from 500 to 601^{0}C.

Figs. 4.72-4.73 compares pressure drop of cylindrical and conical converters. At inlet temperature equal to 300^{0}C and lower mass flow rate (1.5225g/s), cylindrical converter gives 1.1KPa pressure drop whereas conical converter gives only 0.4 to 0.5KPa (Fig. 4.72). At higher mass flow rate (5.0g/s), pressure drop in cylindrical converter reaches as high as 5.0KPa but in conical converter it is much smaller (of the order of 1.0 to 1.4KPa). At inlet temperature (400^{0}C) and for the same mass flow rate, pressure drop

increases. But a higher increase in pressure drop is observed for cylindrical converter. For example, 2.4kPa pressure drop for 1.5225g/s and 7.4kPa for 5.0g/s mass flow rate is seen. The corresponding pressure drop for conical converters are only 0.5-0.8kPa and 1.3 to 1.9 kPa.

It is seen that cylindrical converter gives much higher converter rates compared to conical converter its main disadvantage is that but pressure drop is significantly high. So, further study is done on cylindrical converter with lower catalyst volume keeping the same diameter (50mm), this is discussed in next section.

4.8 Comparison of cylindrical converters with two different catalyst volumes:

Comparison on cylindrical converters with two different catalyst volumes (117 and 97cm^3) is studied. Diameter is kept constant and only length is reduced from 60mm to 50mm. Figs. 4.75-4.77 show comparison on CO and HC conversion, outlet temperature and pressure drop. At lower mass flow rate (1.5225g/s), and T_{in} = 400^{0}C, both converters give 100% conversion but at 300^{0}C, 98cm^3, converter give 60% CO conversion compared to 79% for 117cm^3 converter. At 5.0g/s mass flow rate and at 400^{0}C inlet temperature, corresponding CO conversions are 28 and 37% and at 300^{0}C, 12 and 16% respectively. HC conversion reaches 100% in both converters at 1.5225g/s and reduces by 8% at 5.0g/s mass flow rate. The outlet temperature is lowered by 50^{0}C for 98cm^3 at mass flow rate equal to 5.0g/s. Pressure drop reduces by about 1kPa in 98cm^3 compared to 117cm^3 cylindrical converter. It is seen that there is still significantly high pressure drop even when converter with smaller volume is used. Further geometry modifications need to be studied for reducing pressure drop in converter. One such

geometry could be a hollow cylinder with relatively small inlet diameter to maintain radial fluid flow for lower pressure drop and also smaller catalyst volume.

Table 4.1
List of parameters

S.No.	Item	Dim.	
1.	Length of the cylindrical catalyst bed , L	50.50	mm
2.	Internal Diameter of the catalyst bed, D_I	40.00	mm
3.	External diameter of the catalyst bed, D_O	42.50	mm
4.	Bulk volume of the catalyst bed	63.46	cm^3
5.	Weight of the catalyst pellets in the bed	47.97	g
6.	Number of pellets in random sample of 10 gm	420	--
7.	Approximate number of pellets in the catalyst bed	2015	--
8.	Approximate volume of single catalyst pellet	1.9658e-2	cm^3
9.	Net volume of the pellets in the catalyst bed	39.61	cm^3
10.	Void fraction of the catalyst bed, ϕ	0.375	
11.	Catalyst: Pt-Rh	--	--
12.	Catalyst support: Modified cordierite	--	--
13.	Pellet size	3.0-3.2	mm
14.	Bulk density	0.6	g/cm^3
15.	Pore: Macropores	--	--
16.	Pore size	2	μ

Table 4.2
Experimental data with inlet and outlet values of species and inlet mass flow rate at different loads of the genset engine.

Load	CO		HC		CO_2		O_2		Total $\dot{m}_{in}$ air + fuel
	Inlet	Outlet	Inlet	Outlet	Inlet	Outlet	Inlet	Outlet	
	% vol.		PPM C_3		% vol.		% vol.		g/s
Idle	4.38	3.82	5590	5410	10.28	11.18	4.37	3.64	1.128
100 W	3.97	3.28	4860	4590	10.77	11.68	3.78	3.23	1.362
200 W	3.78	2.47	4700	3920	11.07	12.74	3.74	2.45	1.367
300 W	3.96	2.15	5130	3950	10.56	13.06	3.93	2.25	1.458
400 W	3.69	1.78	5670	4050	10.50	13.93	4.30	1.66	1.512
500 W	3.36	1.35	6120	4040	10.30	14.09	4.72	1.80	1.582
600 W	3.53	1.30	6970	4430	9.91	14.16	5.18	1.74	1.750
700 W	3.175	0.74	7510	4370	9.61	14.40	5.65	1.62	1.943

Table 4.3

Experimental data of temperature along bed at different loads of the genset engine

Load	Temperature, ^{0}C			
	T_{in}	T_{17}	T_{34}	T_{out}
Idle	275	664	365	409
100W	290	376	477	517
200W	301	466	499	525
300W	327	509	530	543
400W	348	601	599	657
500W	363	725	756	772
600W	376	803	838	866
700W	382	824	846	866

where T_{17} and T_{34} are temperatures measured from 17mm and 34mm to the inlet of the converter.

Table 4.4

Computed results of heterogeneous and homogeneous models with experimental values using experimental catalytic converter inlet gas data.

Load	T_{in}	Heterogeneous Model			Homogeneous Model			Experimental Values		
		CO	HC	T_{out}	CO	HC	T_{out}	CO	HC	T_{out}
	(^{0}C)	(% conversion)		(^{0}C)	(% conversion)		(^{0}C)	(% conversion)		(^{0}C)
Idle	275	10.10	1.22	305	8.21	1.01	297	12.78	3.22	409
100W	290	24.22	3.65	374	15.76	1.81	338	17.38	5.56	517
200W	301	36.97	10.22	442	29.43	4.50	397	34.65	16.59	525
300W	327	52.41	33.31	590.8	44.55	16.61	514	45.70	23.00	543
400W	348	54.78	44.00	650	49.58	25.70	547.	51.76	28.57	657
500W	363	52.65	46.07	663	47.82	27.49	584.	59.67	33.98	772
600W	376	48.41	49.33	679	44.92	30.56	621.	63.17	36.44	855
700W	382	42.45	43.10	697	38.00	24.34	581	76.69	41.81	866

Table 4.5: Measured Exhaust Mass Flow Rate versus Vehicle Speed for a Moped (IOCL Ltd.)

S. No.	Vehicle speed (km/hr)	Exhaust mass flow rate (g/s)
1.	30	1.5225
2.	40	2.349
3.	50	3.5225
4.	65	5.0

Table 4.6: Composition of Inlet Gas used for Computation

CO (% vol.)	HC (PPM C_3)	CO_2 (% vol.)	O_2 (%vol.)	H_2O (%vol.)
3.96	5130	11.07	3.74	0.0

Table 4.7: Calculated Mean Exhaust Gas Velocity to Converter Section Using Fluent

S. No.	Exhaust Mass Flow Rate (g/s)	Inlet Gas Velocity (m/s)			
		T_{in}=300^{0}C	T_{in}=350^{0}C	T_{in}=400^{0}C	T_{in}=450^{0}C
1.	1.5225	0.80	0.87	0.94	1.00
2.	2.349	1.00	1.08	1.18	1.22
3.	3.5525	1.20	1.30	1.41	1.51
4.	5.000	1.70	1.85	2.00	2.15

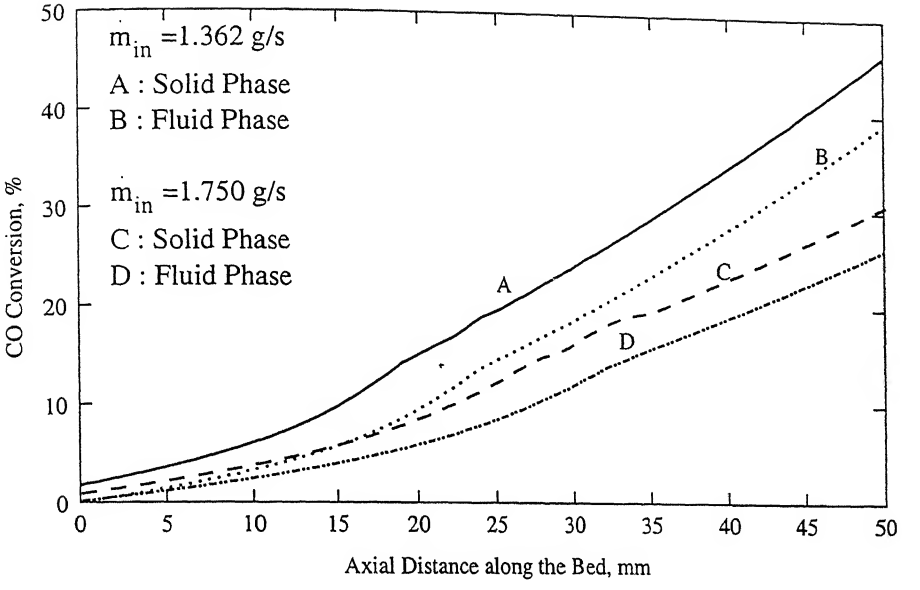

Figure 4.1: CO conversion efficiency along catalyst bed, adiabatic heterogeneous model, T_{in}= 300 °C

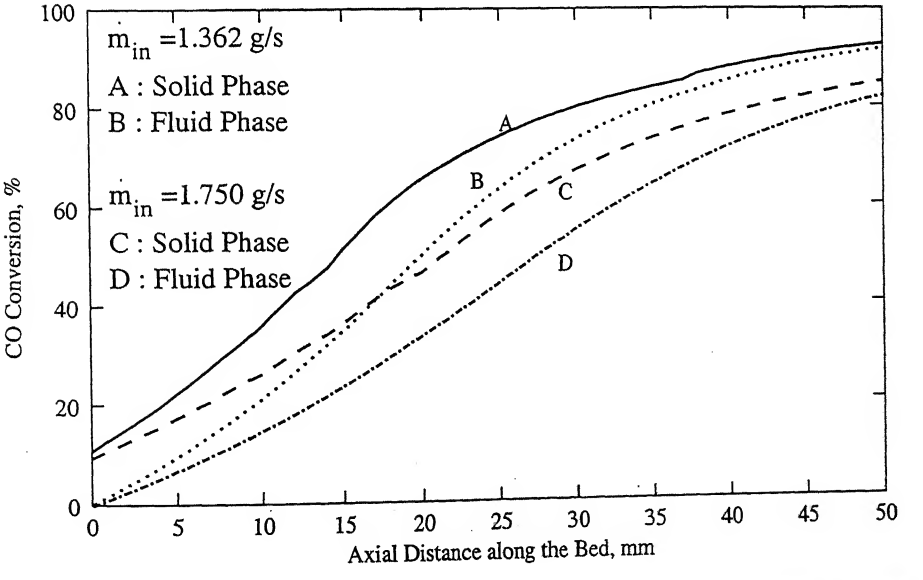

Figure 4.2: CO conversion efficiency along catalyst bed, adiabatic heterogeneous model, T_{in}= 450 °C

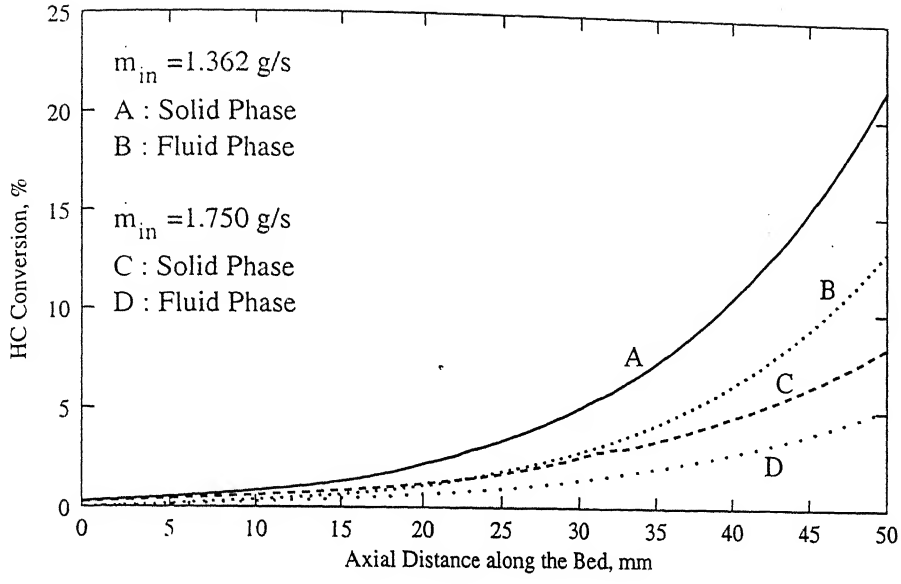

Figure 4.3: HC conversion efficiency along catalyst bed, adiabatic heterogeneous model, T_{in}= 300 °C

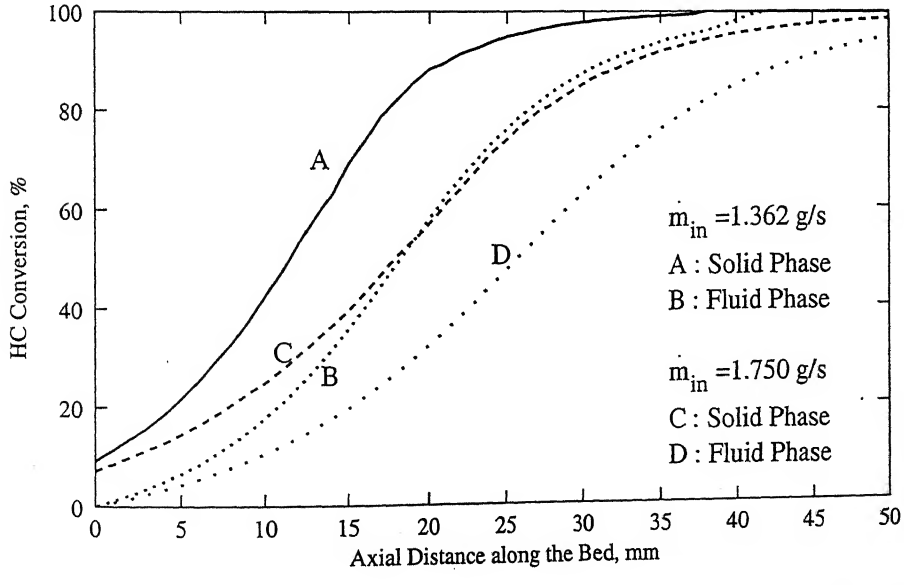

Figure 4.4: HC conversion efficiency along catalyst bed, adiabatic heterogeneous model, T_{in}= 450 °C

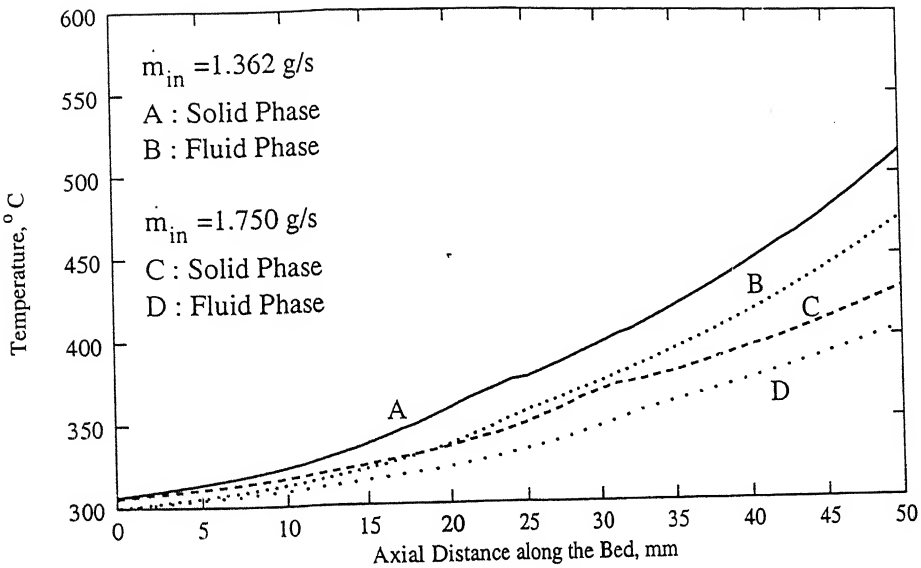

Figure 4.5: Solid and fluid phase temperatures along catalyst bed, adiabatic heterogeneous model, T_{in} = 300 °C

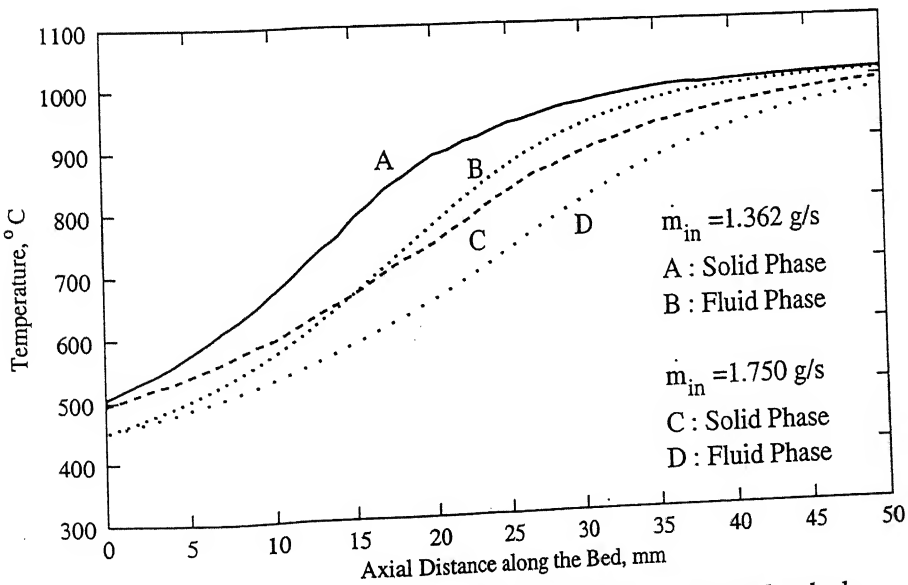

Figure 4.6: Solid and fluid phase temperatures along catalyst bed, adiabatic heterogeneous model, T_{in}= 450° C

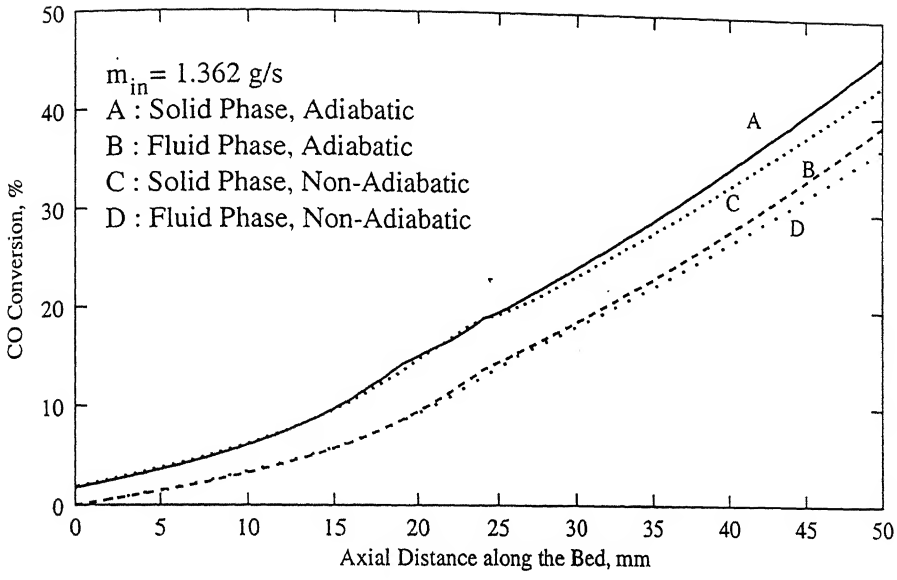

(a)

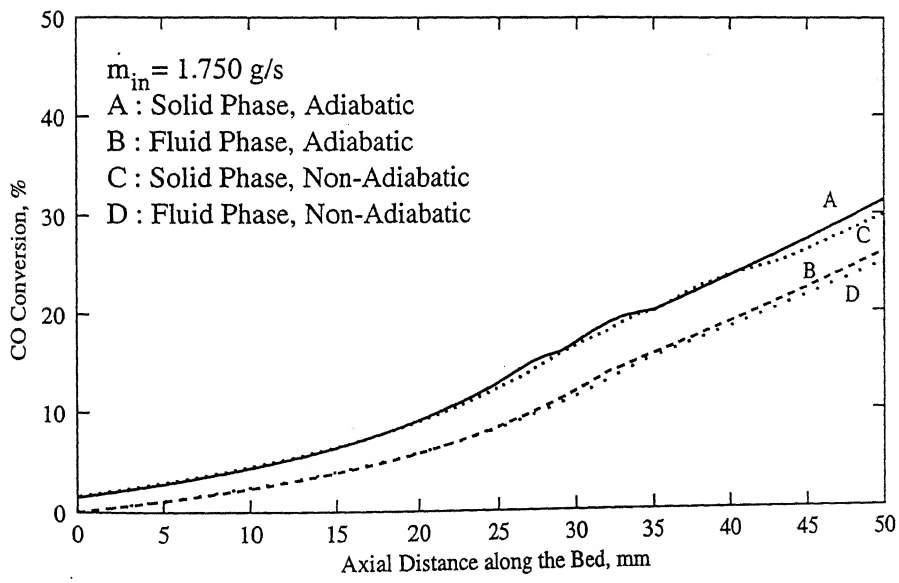

(b)

Figure 4.7: Comparison of adiabatic and non-adiabatic heterogeneous model (heat transfer to atmosphere from converter) on CO conversion, T_{in}=300 °C

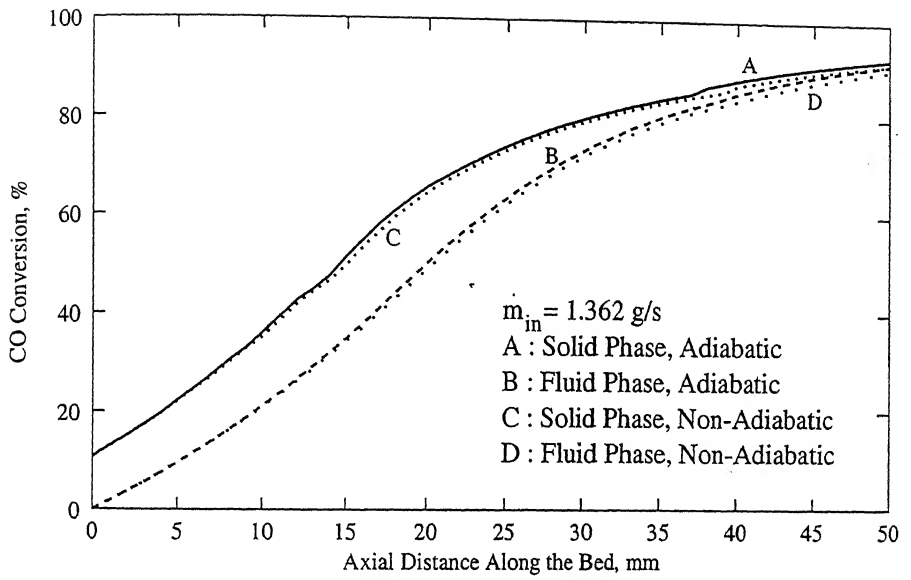

(a)

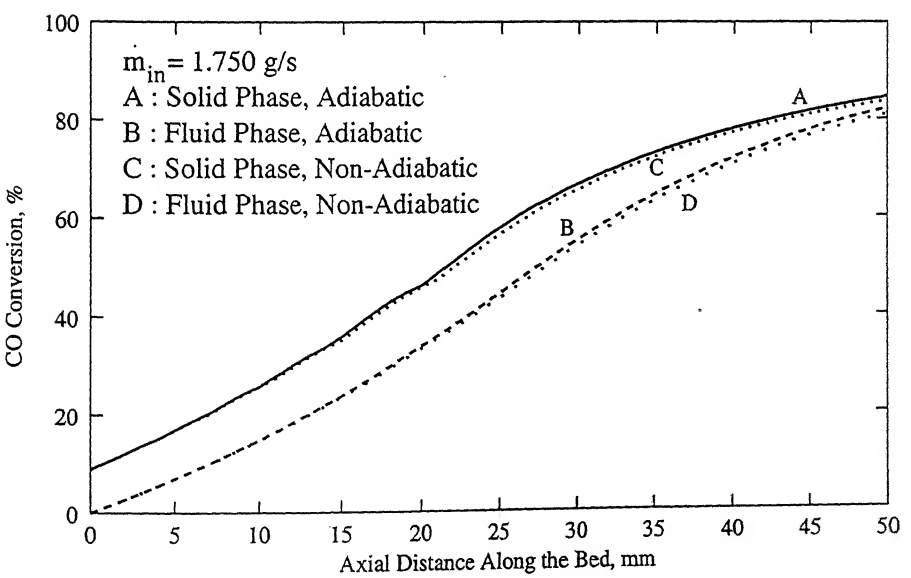

(b)

Figure 4.8: Comparison of adiabatic and non-adiabatic heterogeneous model (heat transfer to atmosphere from converter) on CO conversion, T_{in} =450 °C

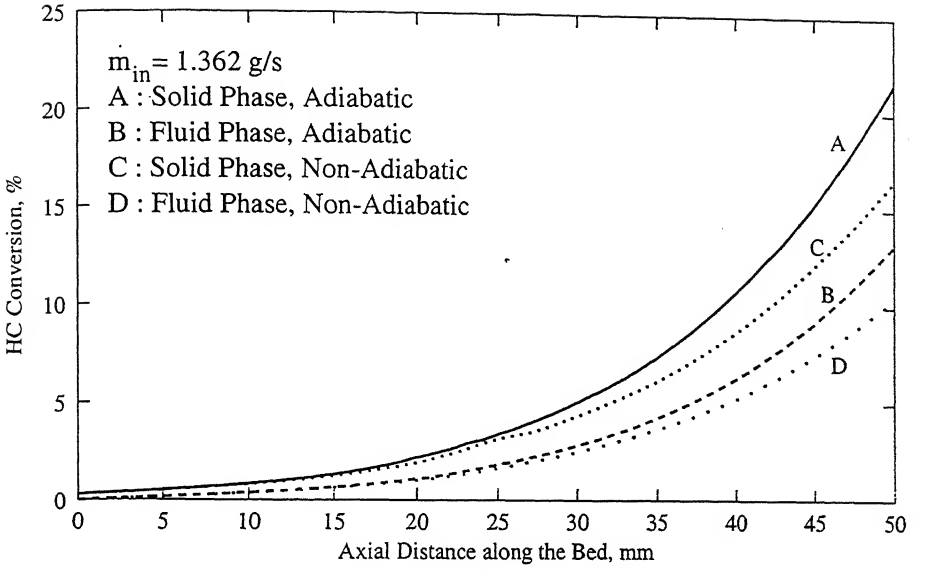

(a)

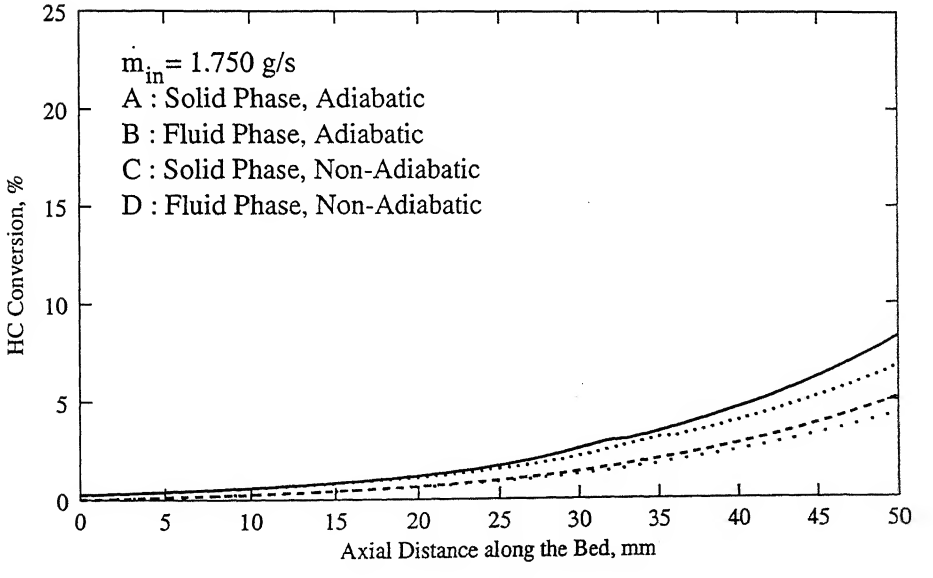

(b)

Figure 4.9: Comparison of adiabatic and non-adiabatic heterogeneous model (heat transfer to atmosphere from converter) on HC conversion, T_{in} =300 °C

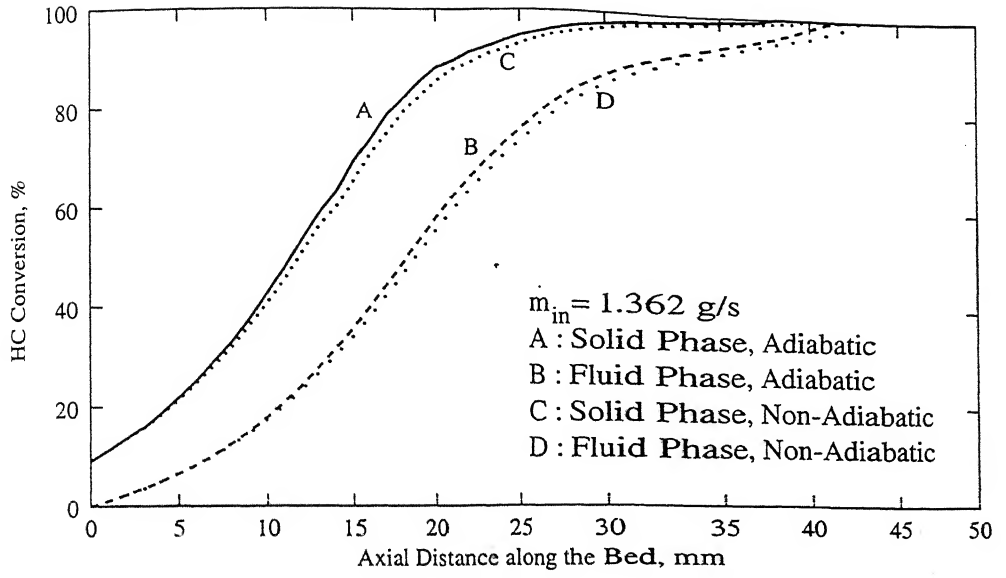

(a)

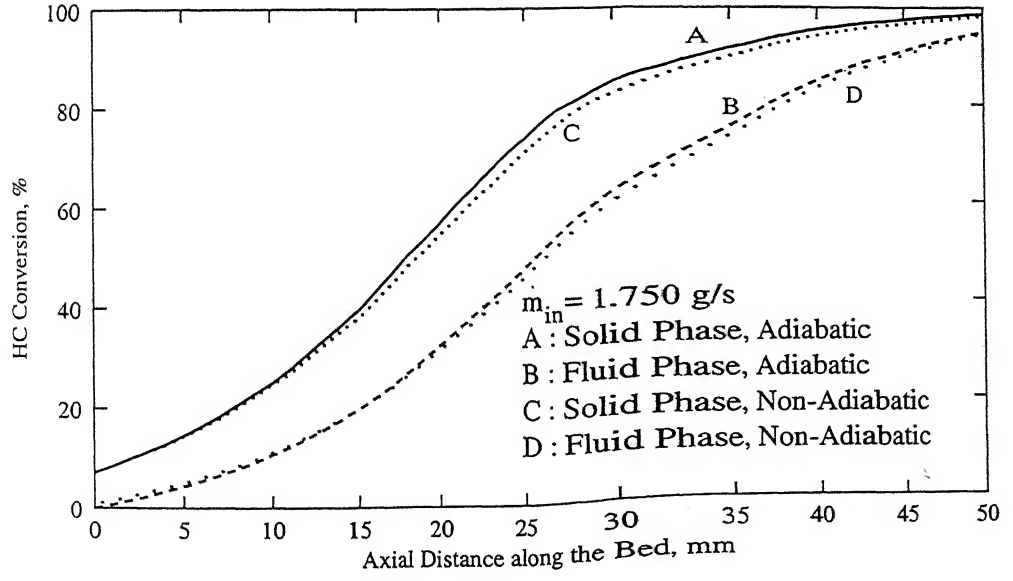

(b)

Figure 4.10: Comparison of adiabatic and non-adiabatic heterogeneous model (heat transfer to atmosphere from converter) on HC conversion, T_{in} =450 °C

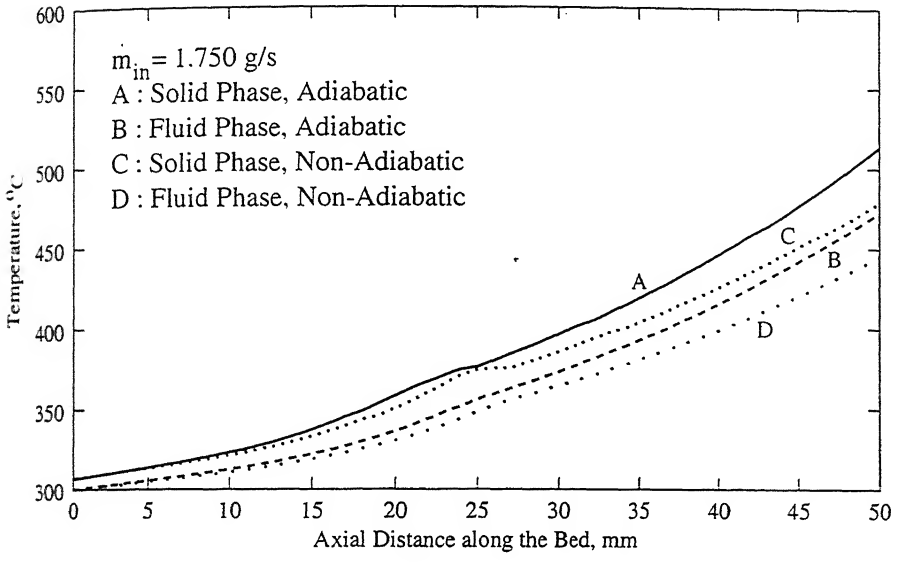

(a)

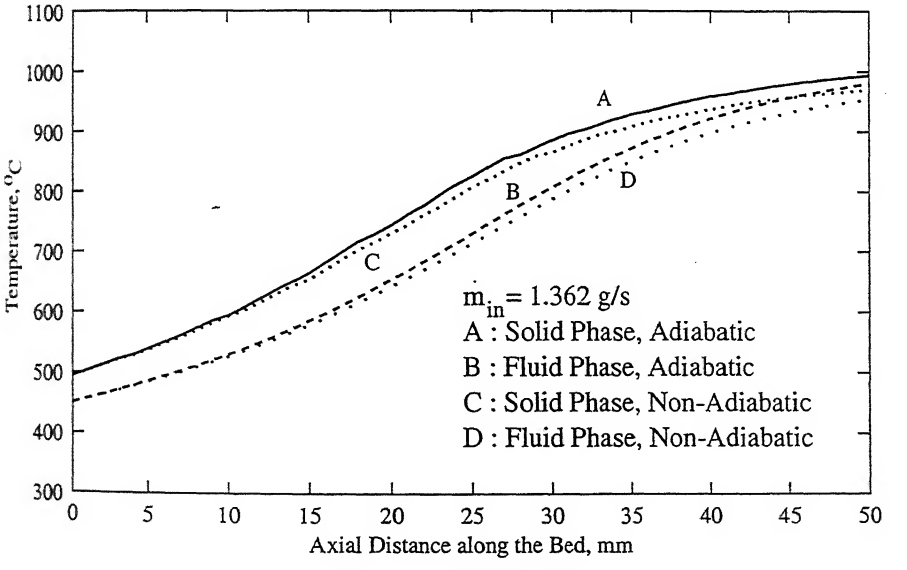

(b)

Figure 4.11: Comparison of adiabatic and non-adiabatic heterogeneous model (heat transfer to atmosphere from converter) on solid and fluid phase temperatures, $T_{in} = 300\ ^{o}C$

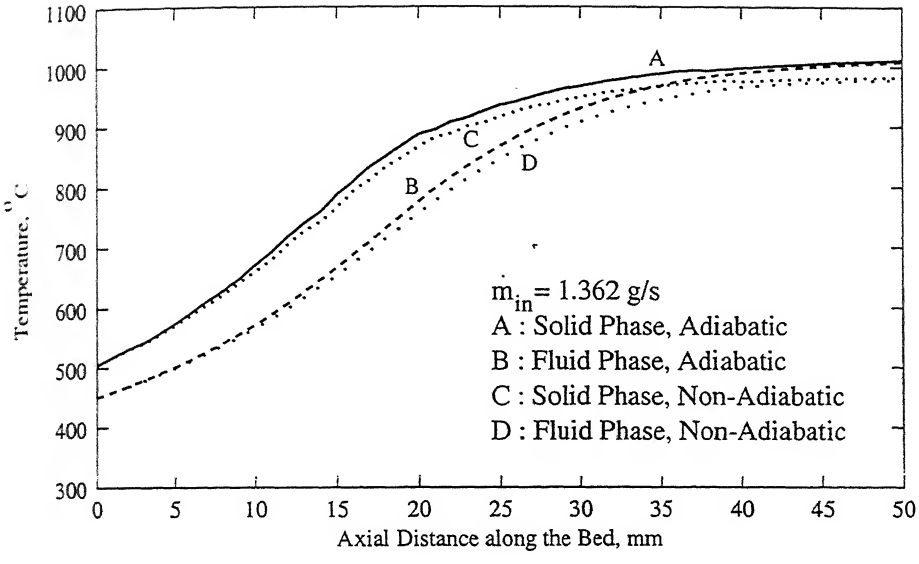

(a)

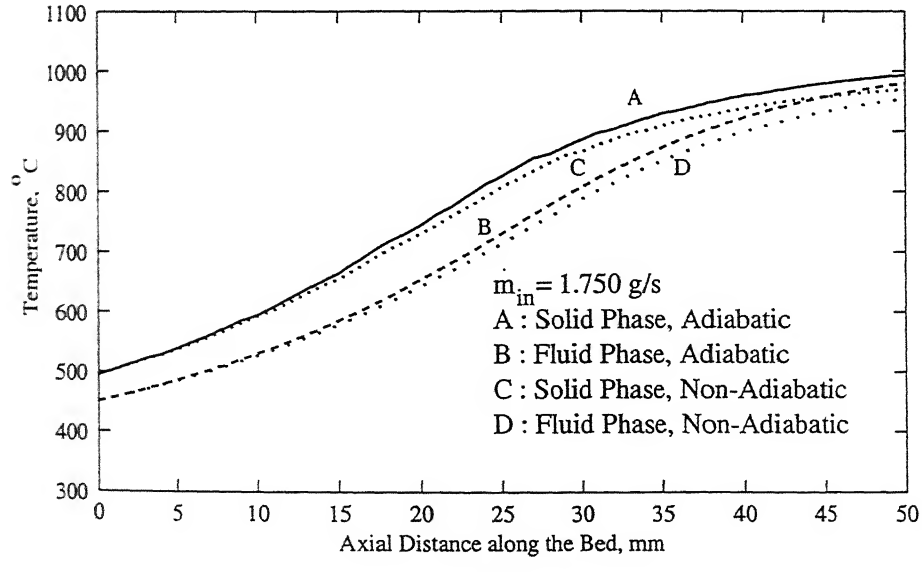

(b)

Figure 4.12: Comparison of adiabatic and non-adiabatic heterogeneous model (heat transfer to atmosphere from converter) on solid and fluid phase temperatures, T_{in} = 450 °C

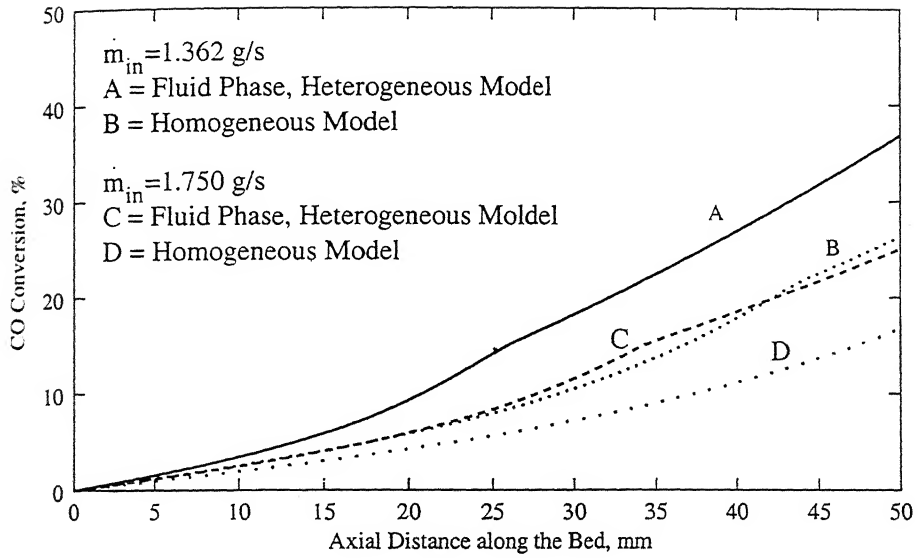

Figure 4.13: Comparison of CO conversion efficiency with non-adiabatic heterogeneous and homogneous models, T_{in} = 300°C

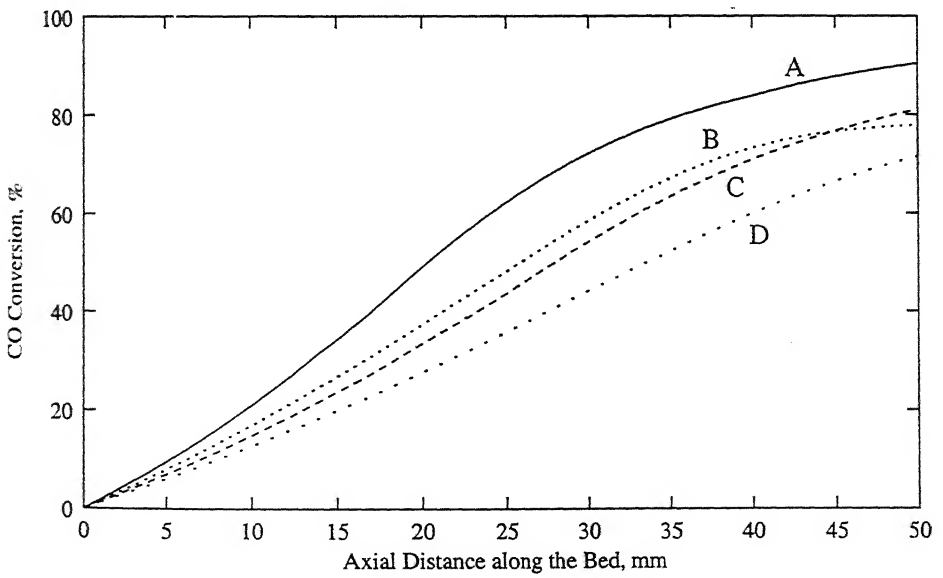

$\dot{m}_{in}$=1.362 g/s
A = Fluid Phase, Heterogeneous Model
B = Homogeneous Model

$\dot{m}_{in}$=1.750 g/s
C = Fluid Phase, Heterogeneous Moldel
D = Homogeneous Model

Figure 4.14 : Comparison of CO conversion efficiency with non-adiabatic heterogeneous and homogneous models, T_{in} = 450°C

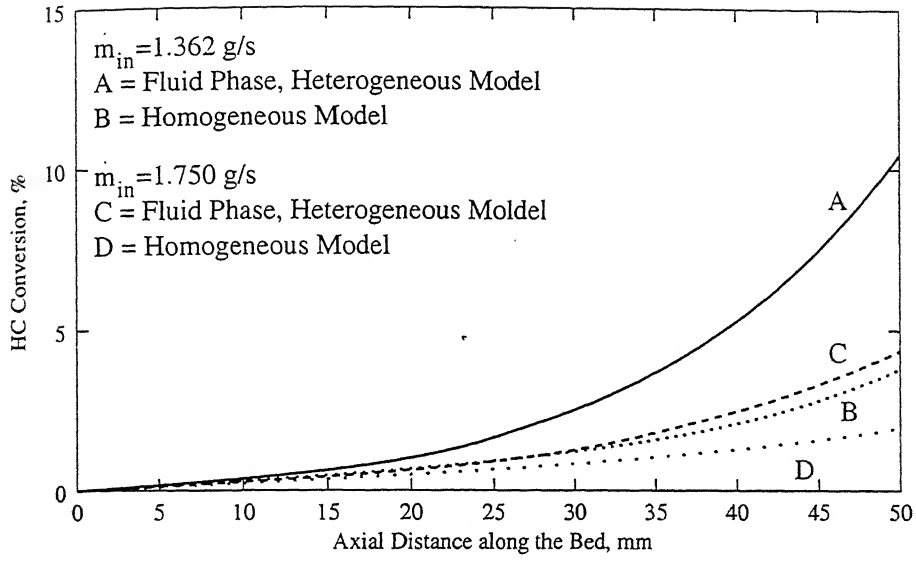

Figure 4.15: Comparison of HC conversion efficiency with non-adiabatic heterogeneous and homogneous models, T_{in} = 300°C

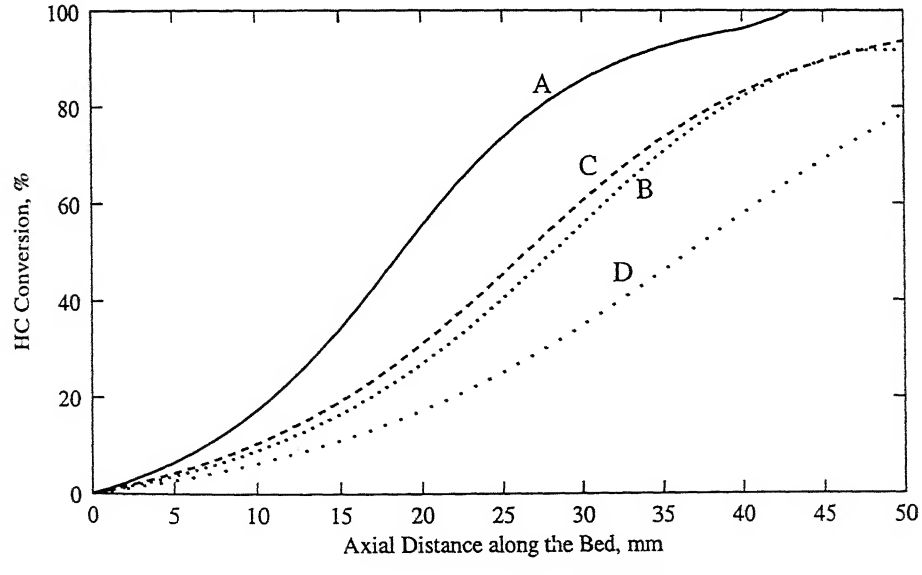

$\dot{m}_{in}$=1.362 g/s
A = Fluid Phase, Heterogeneous Model
B = Homogeneous Model

$\dot{m}_{in}$=1.750 g/s
C = Fluid Phase, Heterogeneous Moldel
D = Homogeneous Model

Figure 4.16: Comparison of HC conversion efficiency with non-adiabatic heterogeneous and homogneous models, T_{in} = 450°C

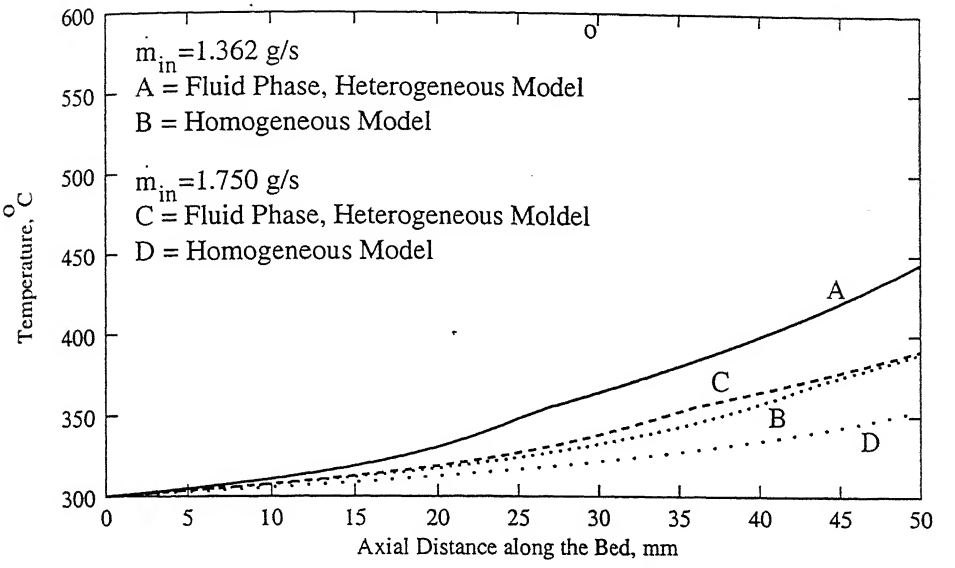

Figure 4.17: Comparison of solid and fluid phase temperatures with non-adiabatic heterogeneous and homogneous models, T_{in}= 300° C

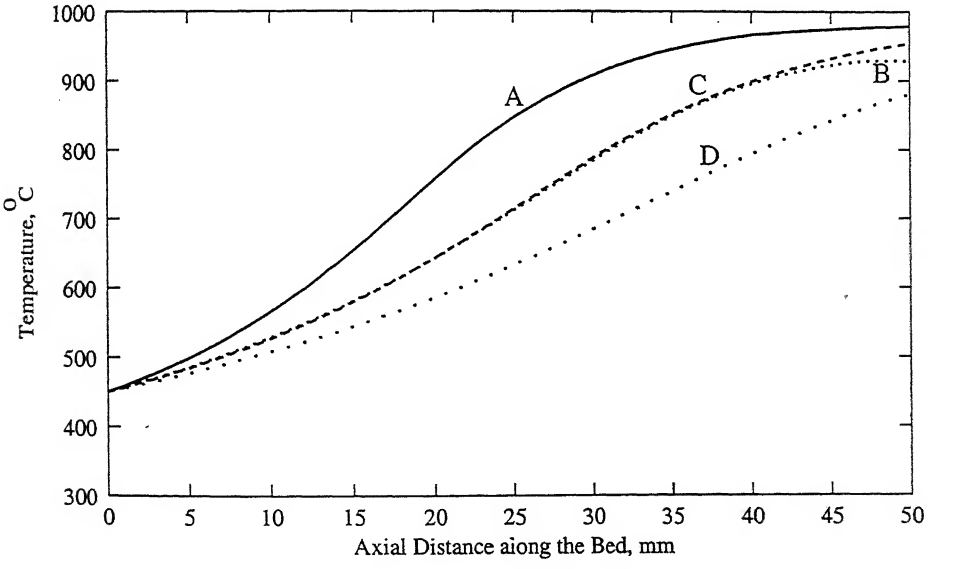

$\dot{m}_{in}$=1.362 g/s
A = Fluid Phase, Heterogeneous Model
B = Homogeneous Model

$\dot{m}_{in}$=1.750 g/s
C = Fluid Phase, Heterogeneous Moldel
D = Homogeneous Model

Figure 4.18: Comparison of solid and fluid phase temperatures with non-adiabatic heterogeneous and homogneous models, T_{in}= 450° C

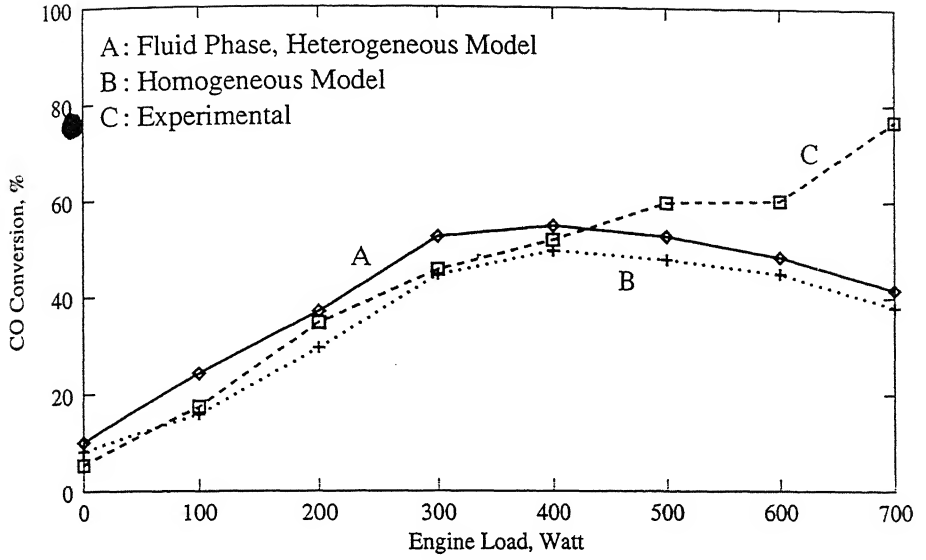

Figure 4.19: Comparison of CO conversion (fluid phase heterogeneous model, homogeneous model and experimental)

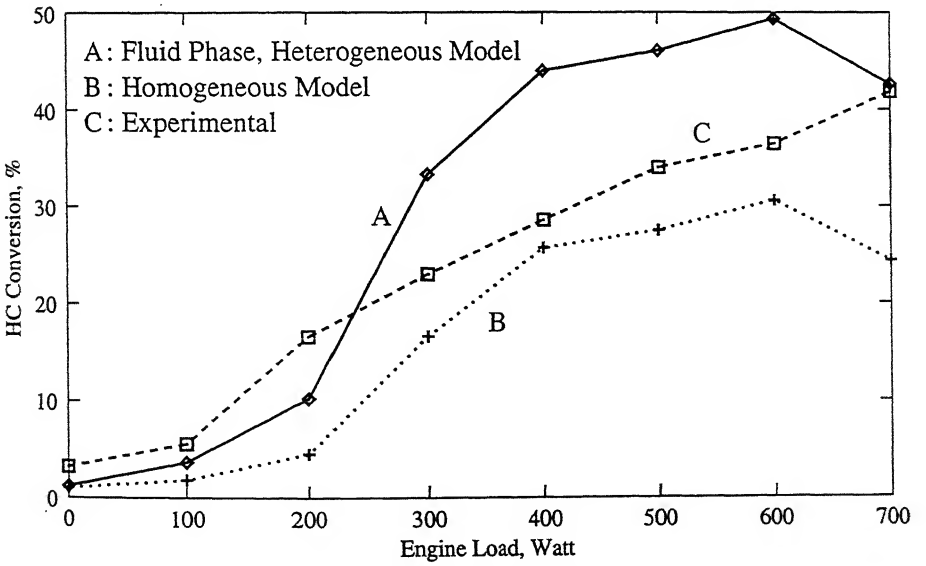

Figure 4.20: Comparison of HC conversion (fluid phase heterogeneous model, homogeneous model and experimental)

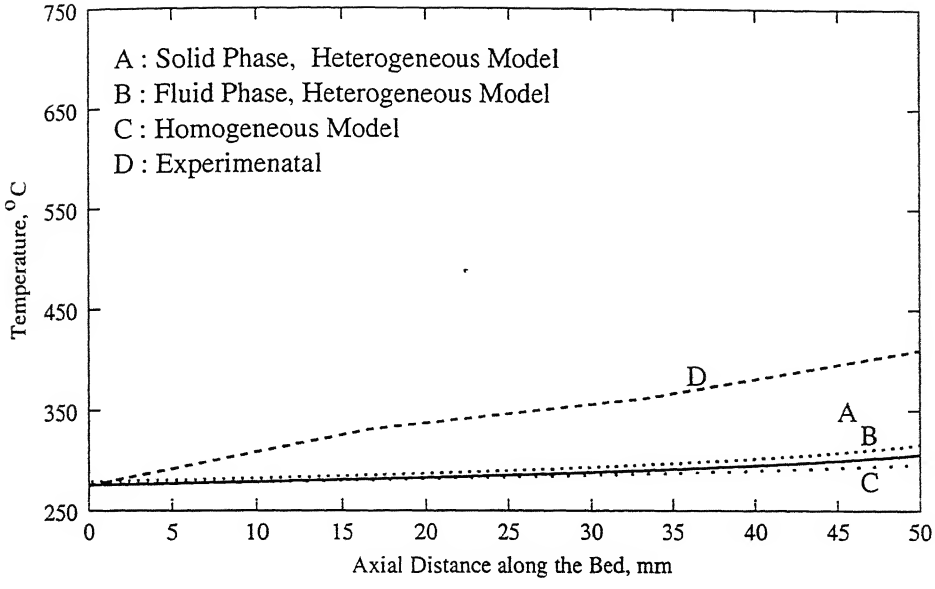

Figure 4.21: Comparison of predicted and experimental temperature at no load with non-adiabatic condition

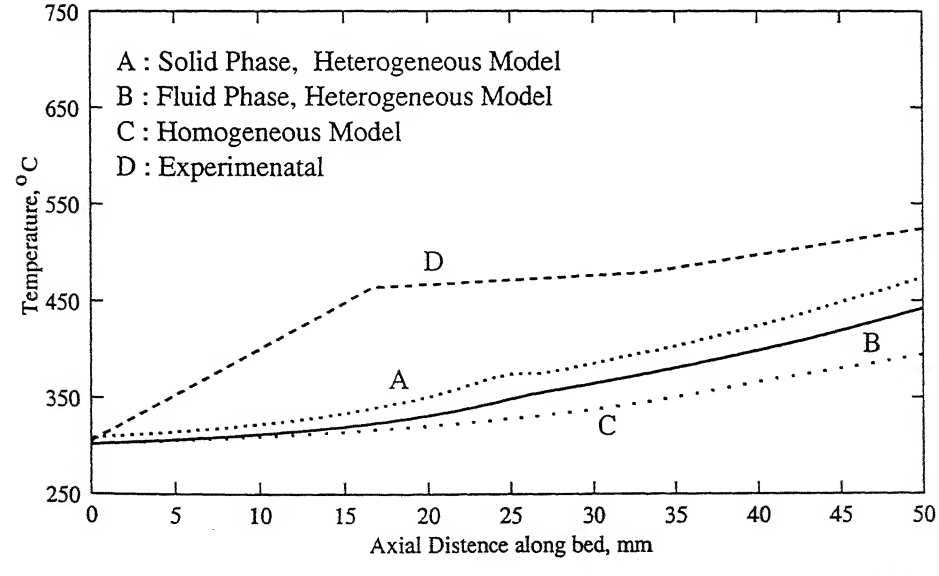

Figure 4.22: Comparison of predicted and experimental temperature at 200 W engine load with non-adiabatic condition

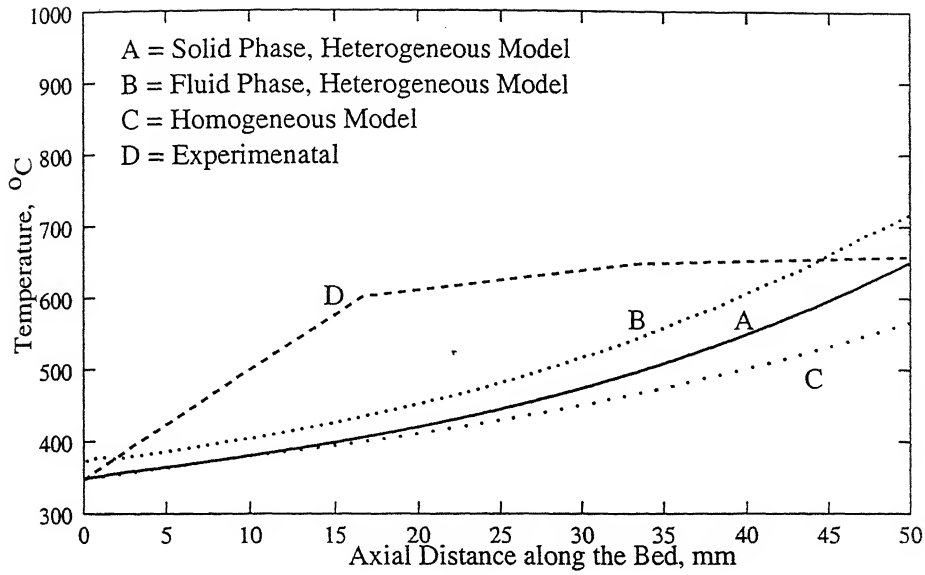

Figure 4.23: Comparison of predicted and experimental temperature at 400 W engine load with non-adiabatic condition

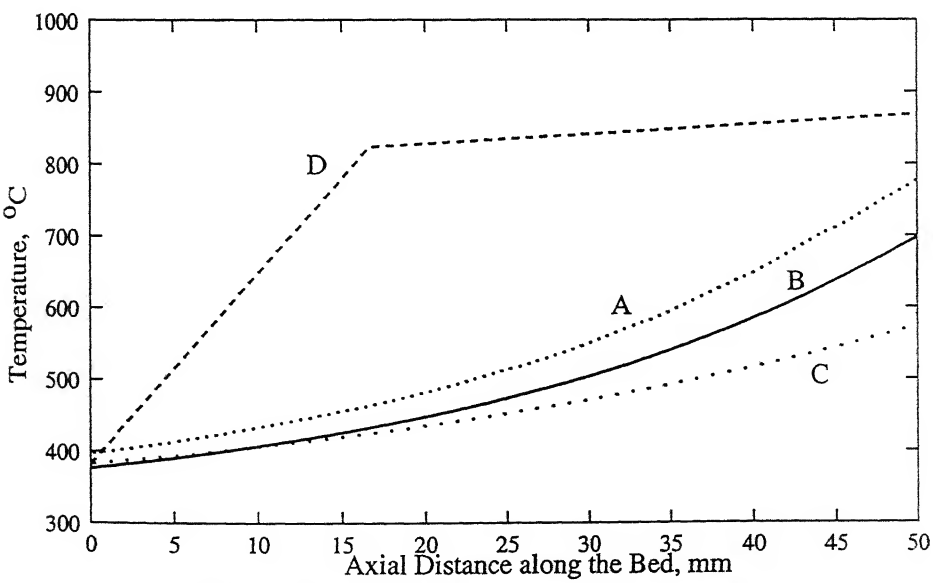

A = Solid Phase, Heterogeneous Model
B = Fluid Phase, Heterogeneous Model
C = Homogeneous Model
D = Experimenatal

Figure 4.24: Comparison of predicted and experimental temperature at 700 W engine load with non-adiabatic condition

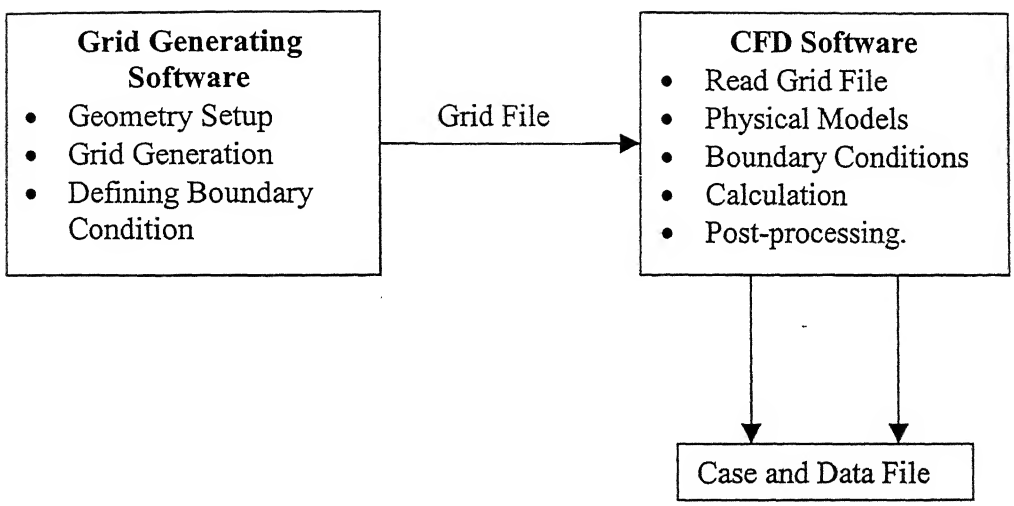

Figure. 4.25: Flow chart for solving problems using CFD software.

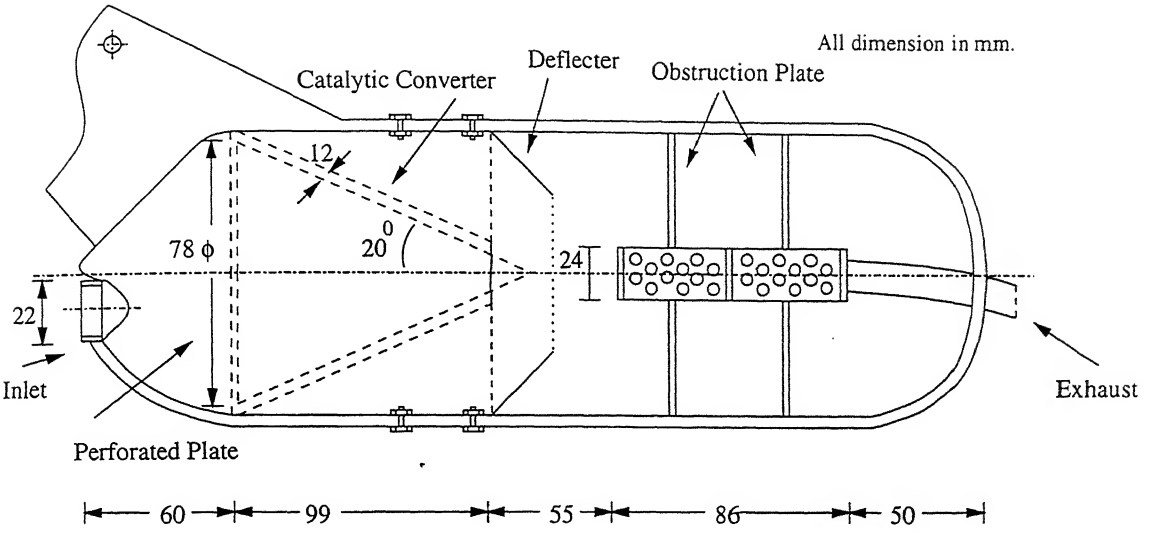

Figure 4.26 : Schematic of asymmetric exhaust muffler with apex of the conical converter towards downstream direction

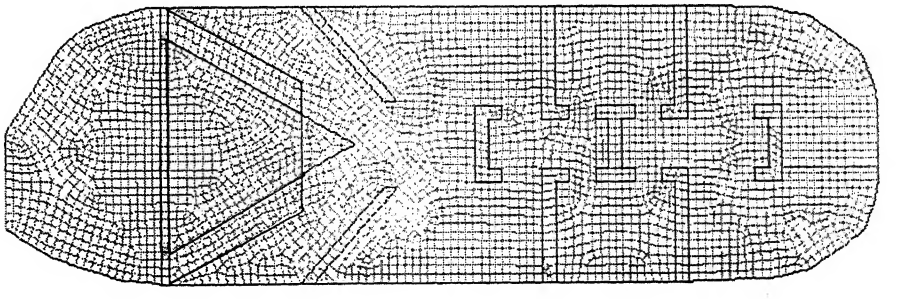

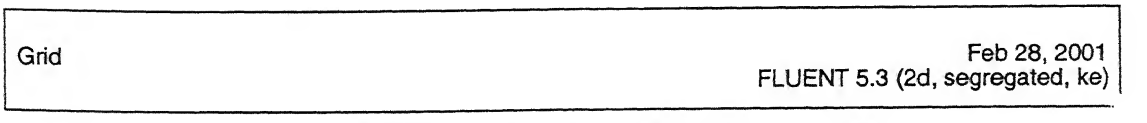

Figure 4.27: Grids of exhaust muffler with apex of the converter towards downstream direction

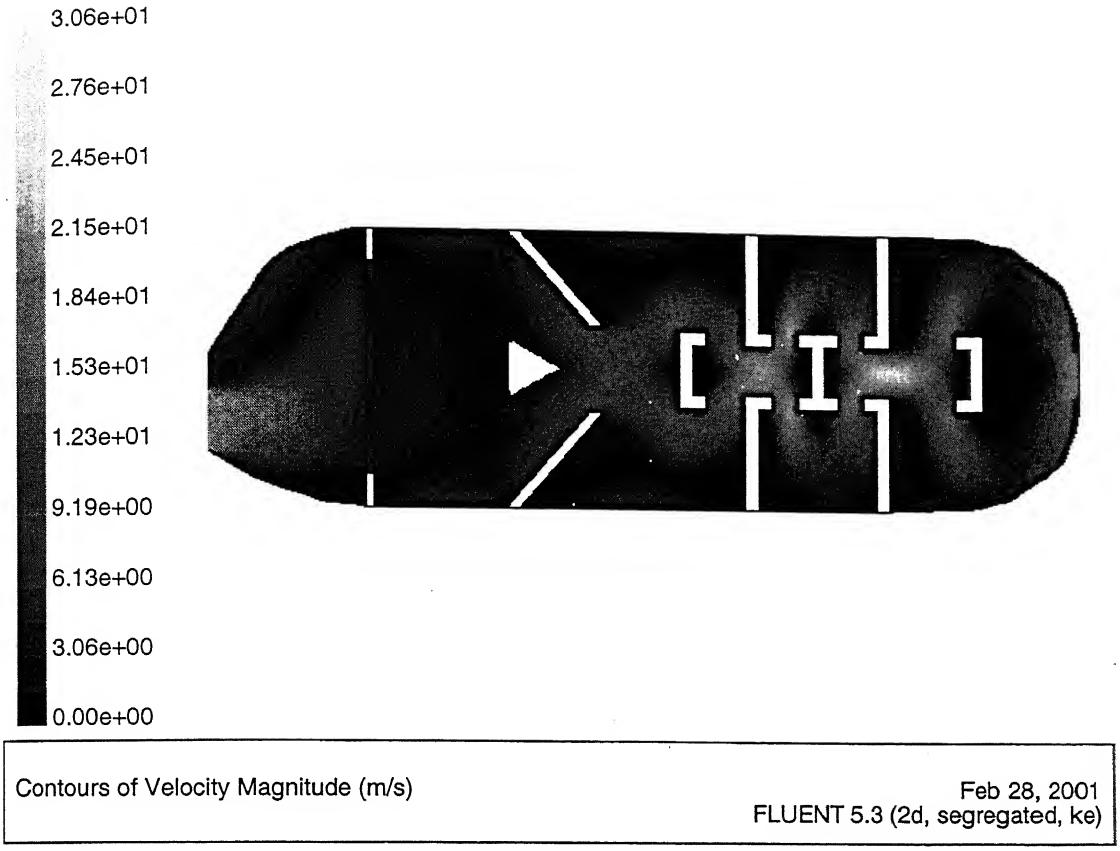

Figure 4.28: Velocity contours of exhaust muffler with apex of the converter towards downstream direction

Scale: 1mm = 0.5m/s

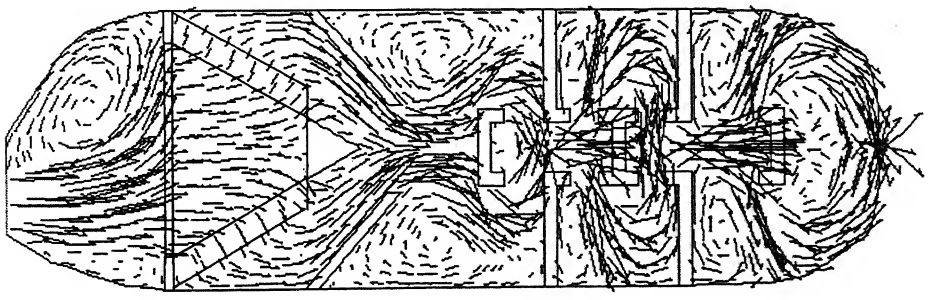

Figure 4.29: Velocity vectors of exhaust muffler with apex of the converter towards downstream direction

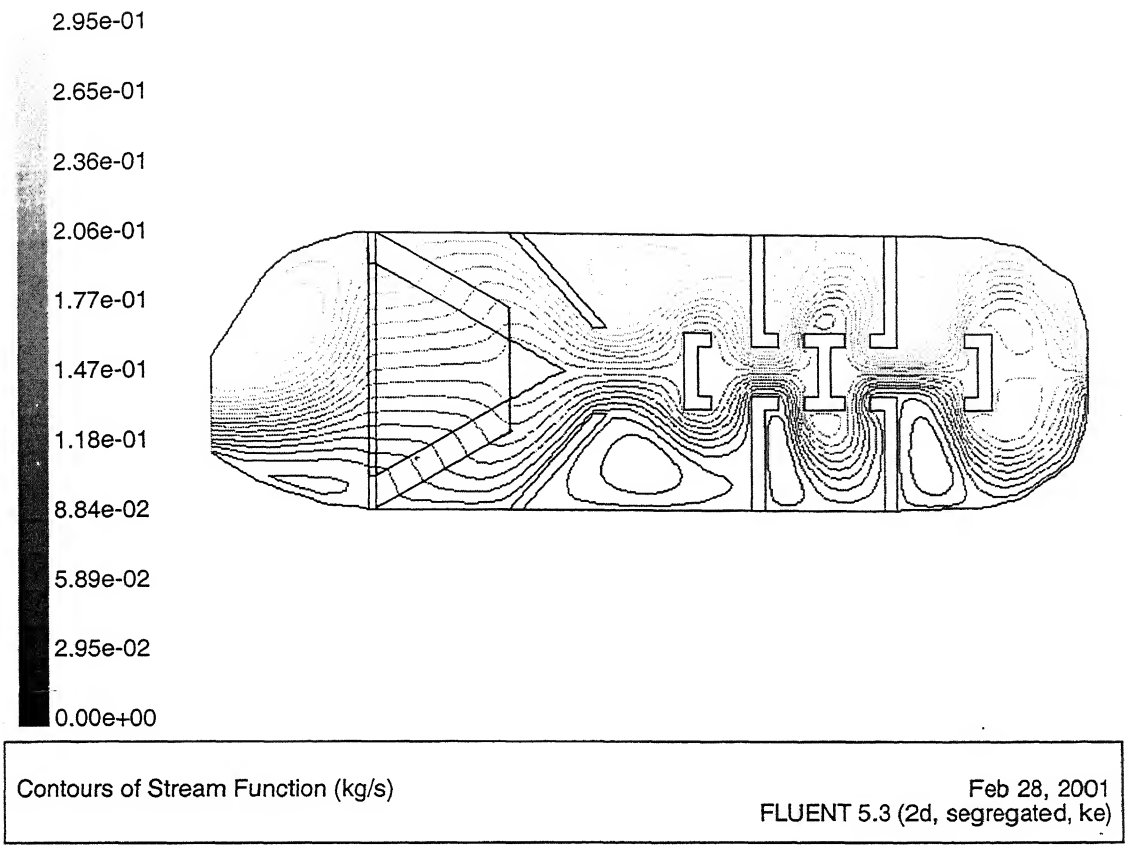

Figure 4.30: Stream function of exhaust muffler with apex of the converter towards downstream direction

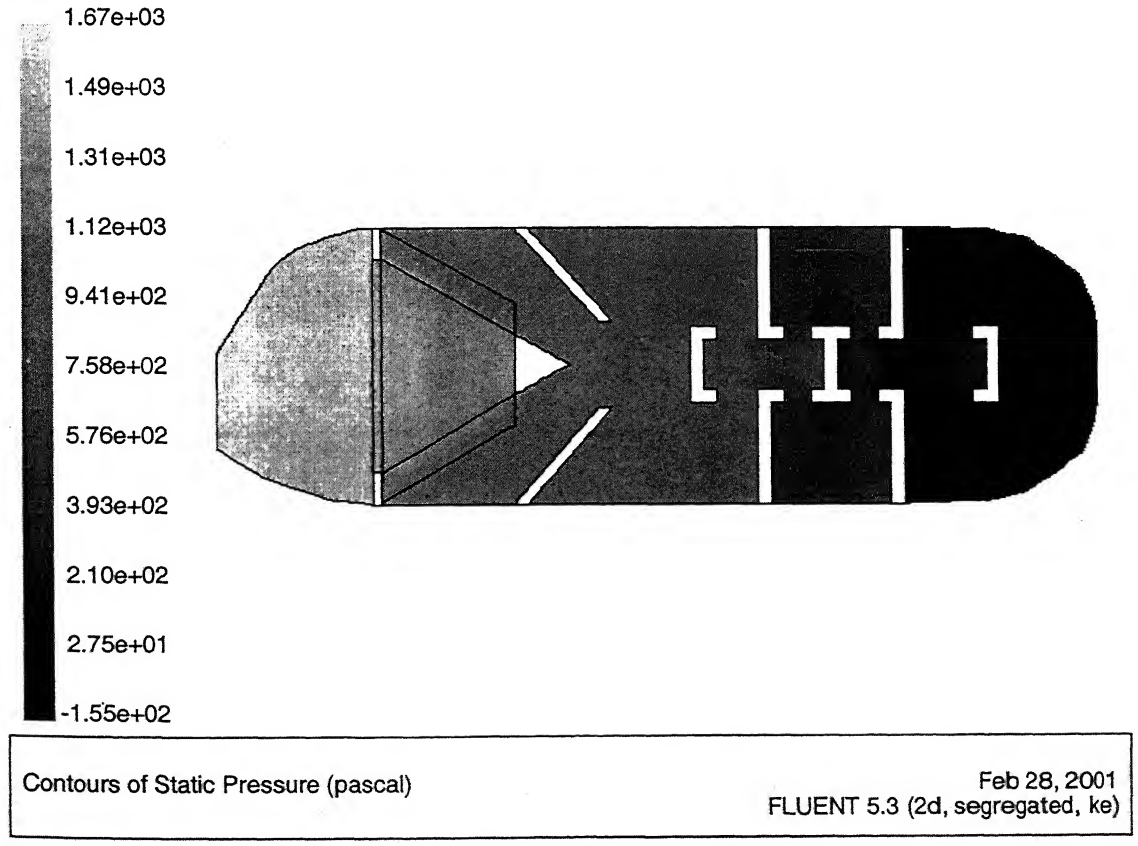

Figure 4.31: Pressure variation of exhaust muffler with apex of the converter towards downstream direction

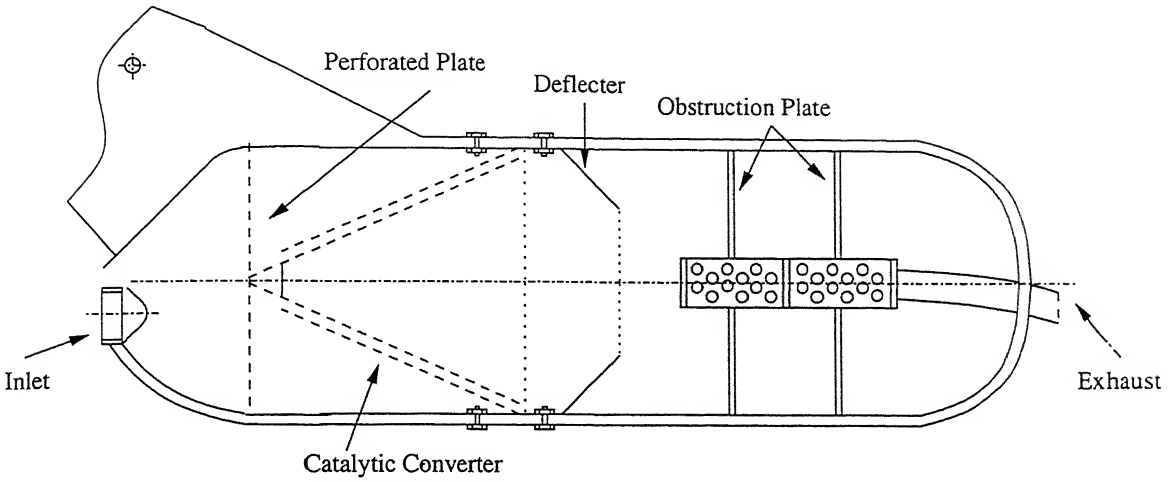

Figure 4.32: Schematic of the exhaust muffler with apex of the conical converter towards upstream direction

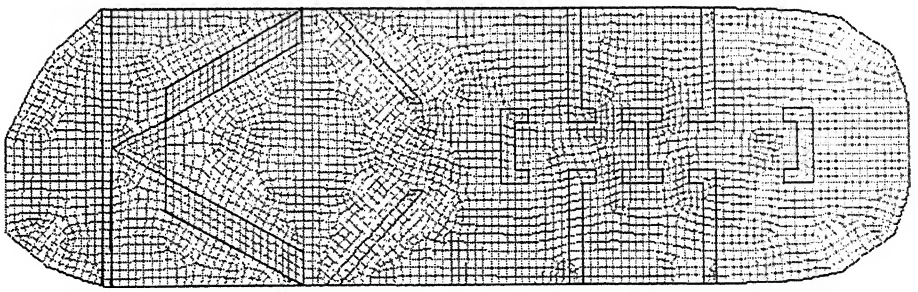

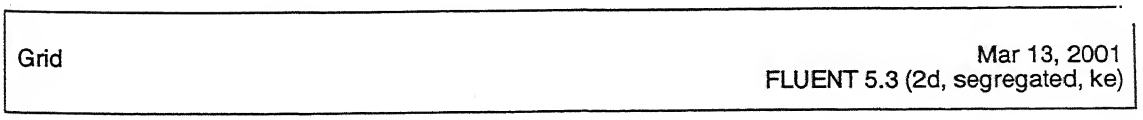

Figure 4.33: Grids of exhaust muffler with apex of the converter towards upstream direction

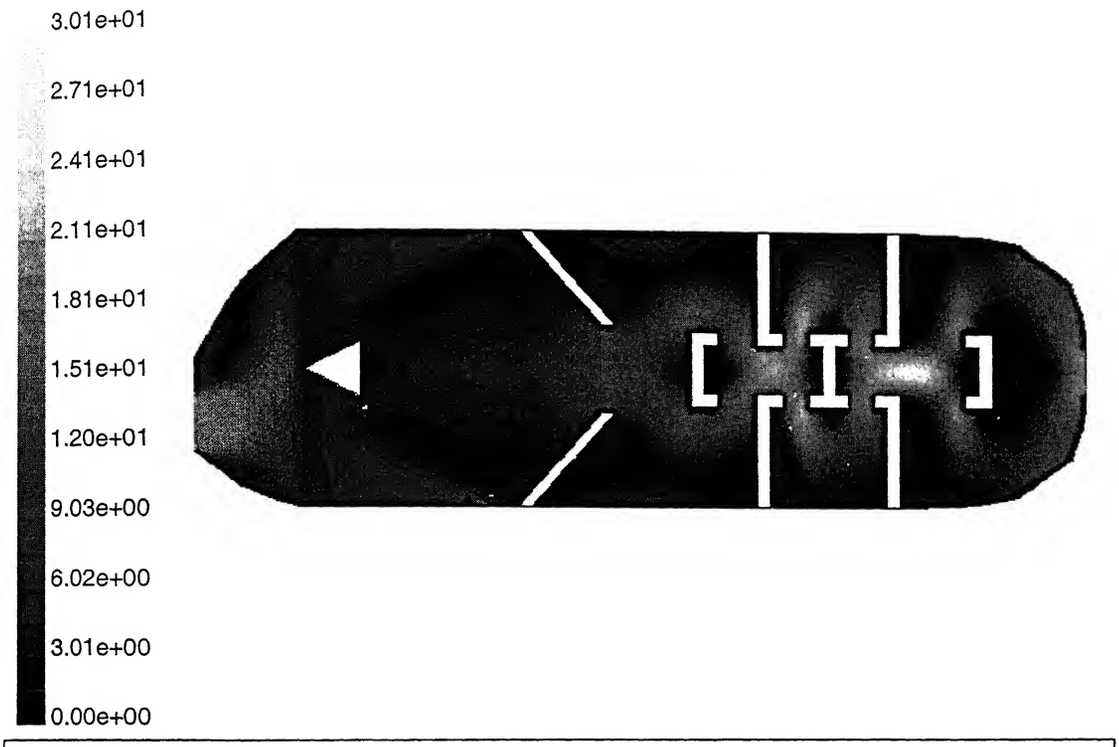

Figure 4.34: Velocity contours of exhaust muffler with apex of the converter towards upstream direction

Scale: 1mm = 0.5m/s

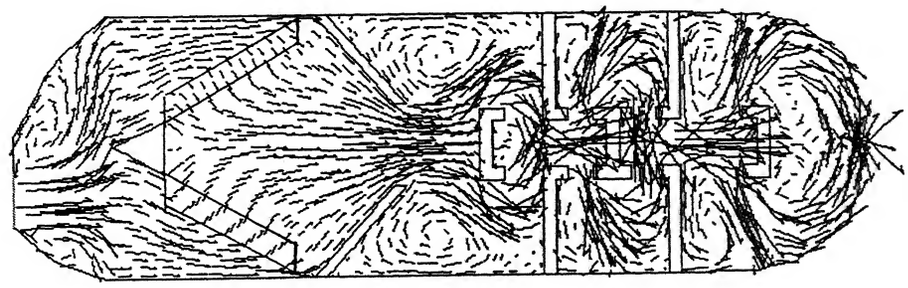

Figure 4.35: Velocity vectors of exhaust muffler with apex of the converter towards upstream direction

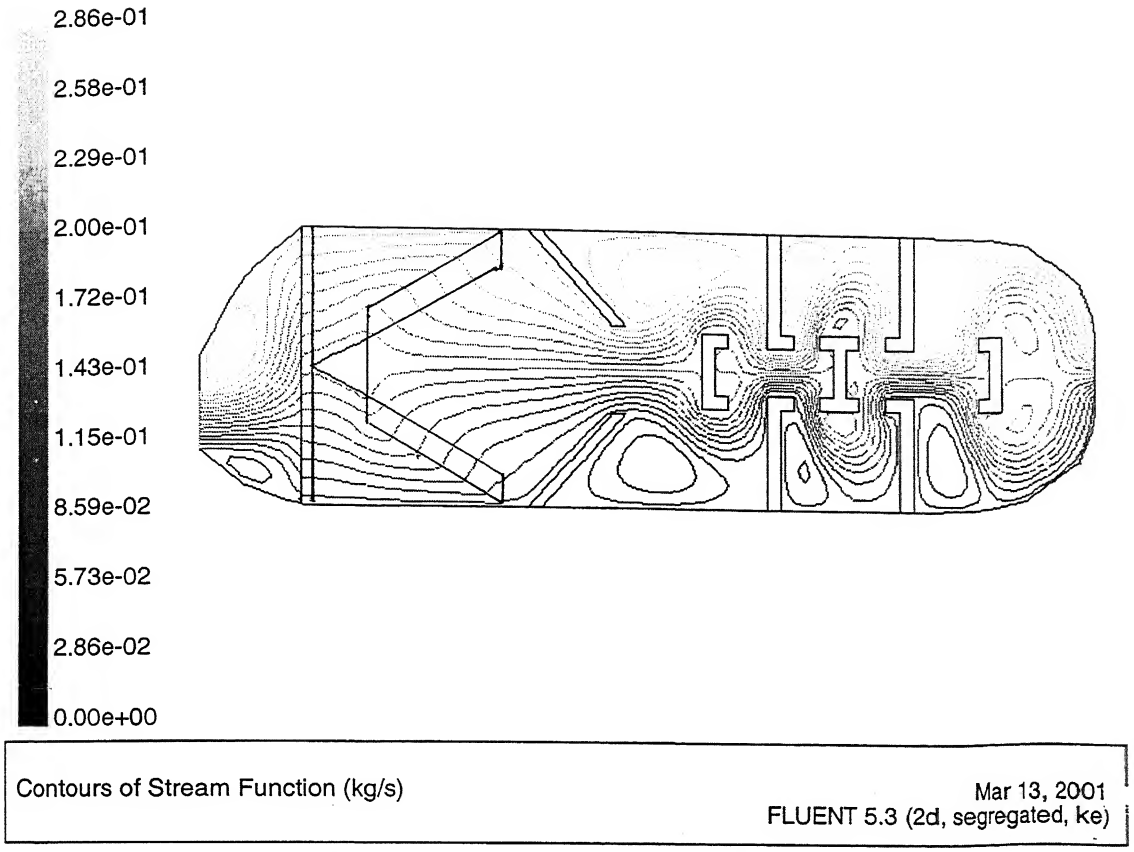

Figure 4.36: Stream function of exhaust muffler with apex of the converter towards upstream direction

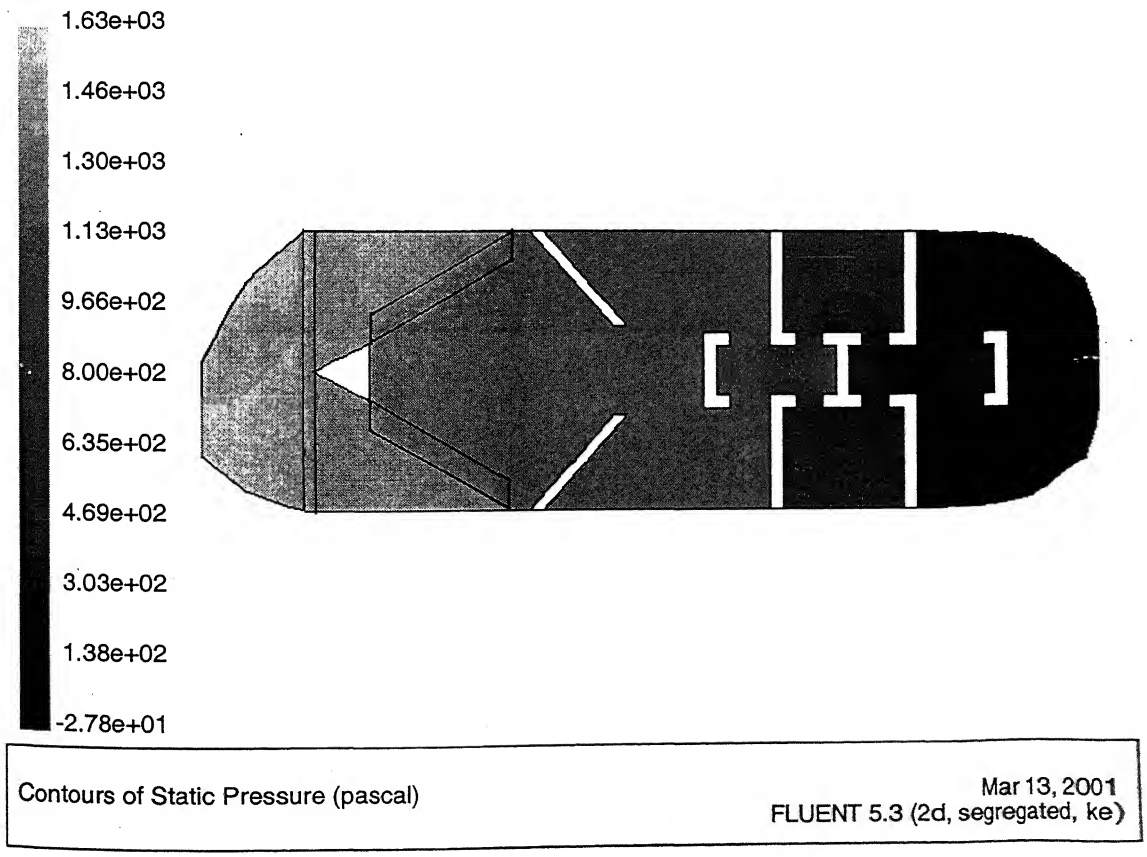

Figure 4.37: Pressure variation of exhaust muffler with apex of the converter towards upstream direction

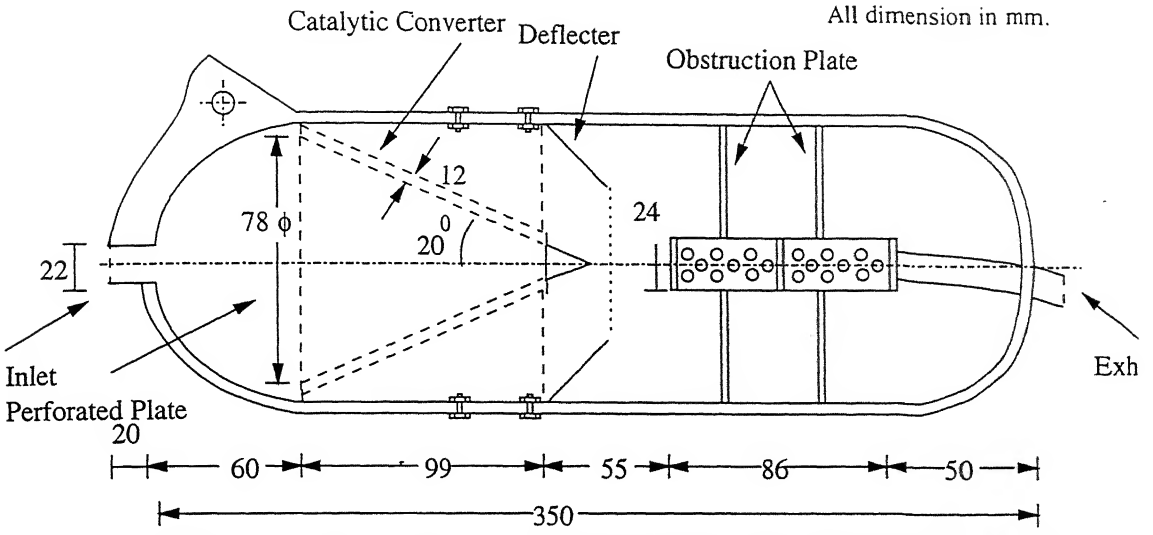

Figure 4.38: Schematic of symmetric exhaust muffler of with apex of the conical converter towards downstream direction

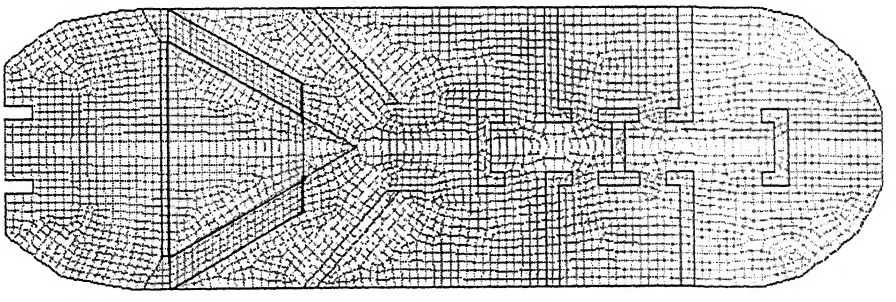

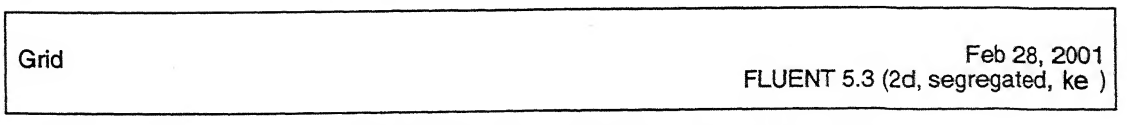

Figure 4.39: Grids of exhaust muffler with apex of the converter towards downstream direction

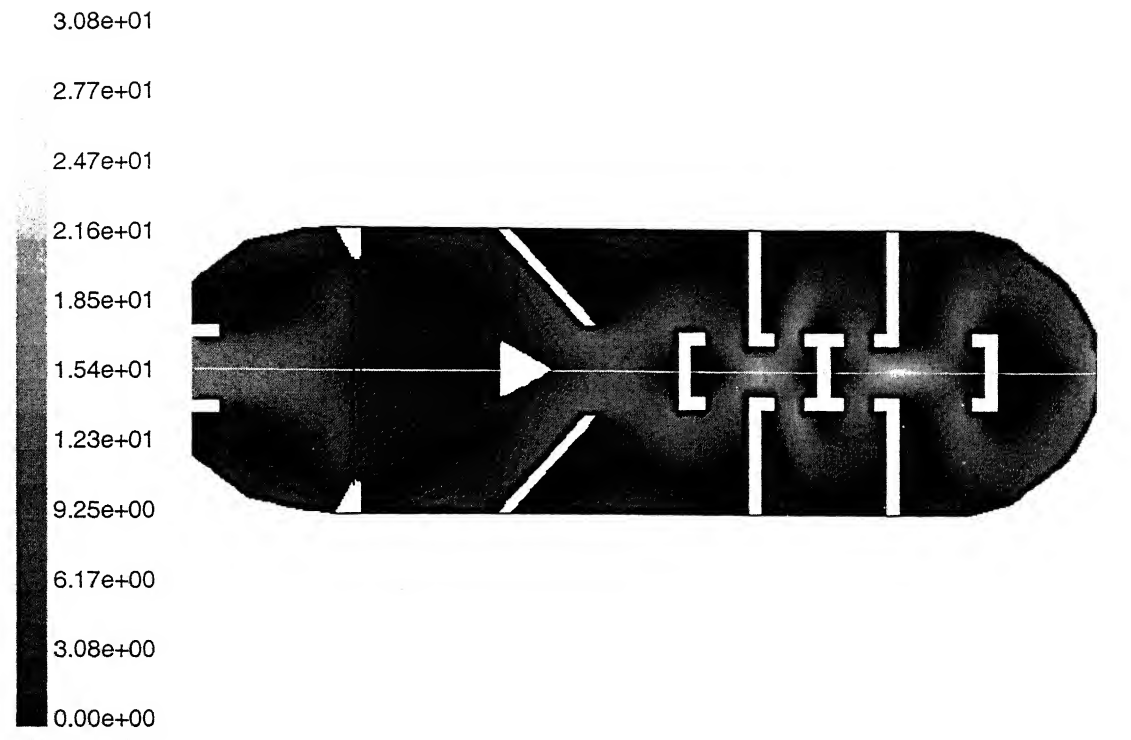

Figure 4.40: Velocity contours of exhaust muffler with apex of the converter towards downstream direction

Scale: 1mm = 0.5m/s

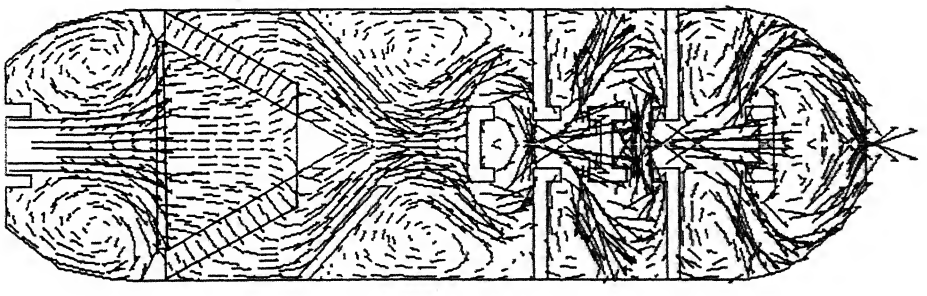

Figure 4.41: Velocity vectors of exhaust muffler with apex of the converter towards downstream direction

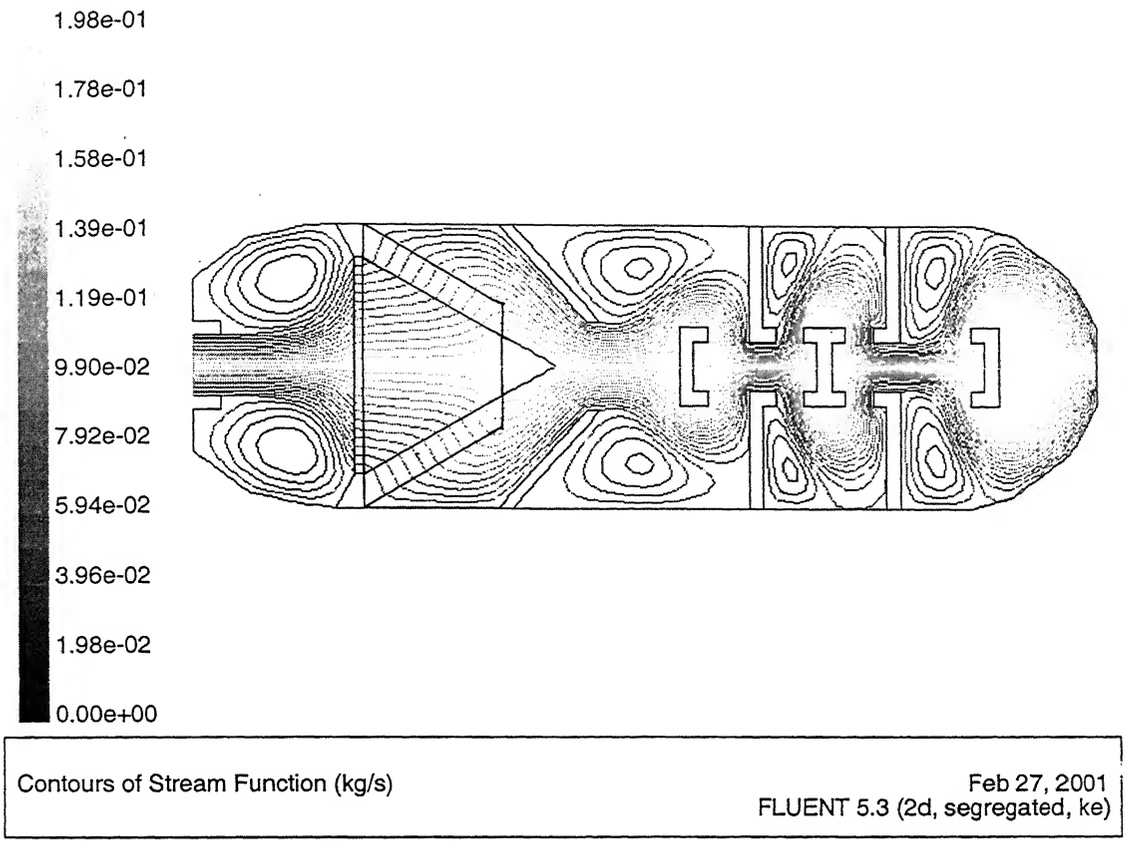

Figure 4.42: Stream function of exhaust muffler with apex of the converter towards downstream direction

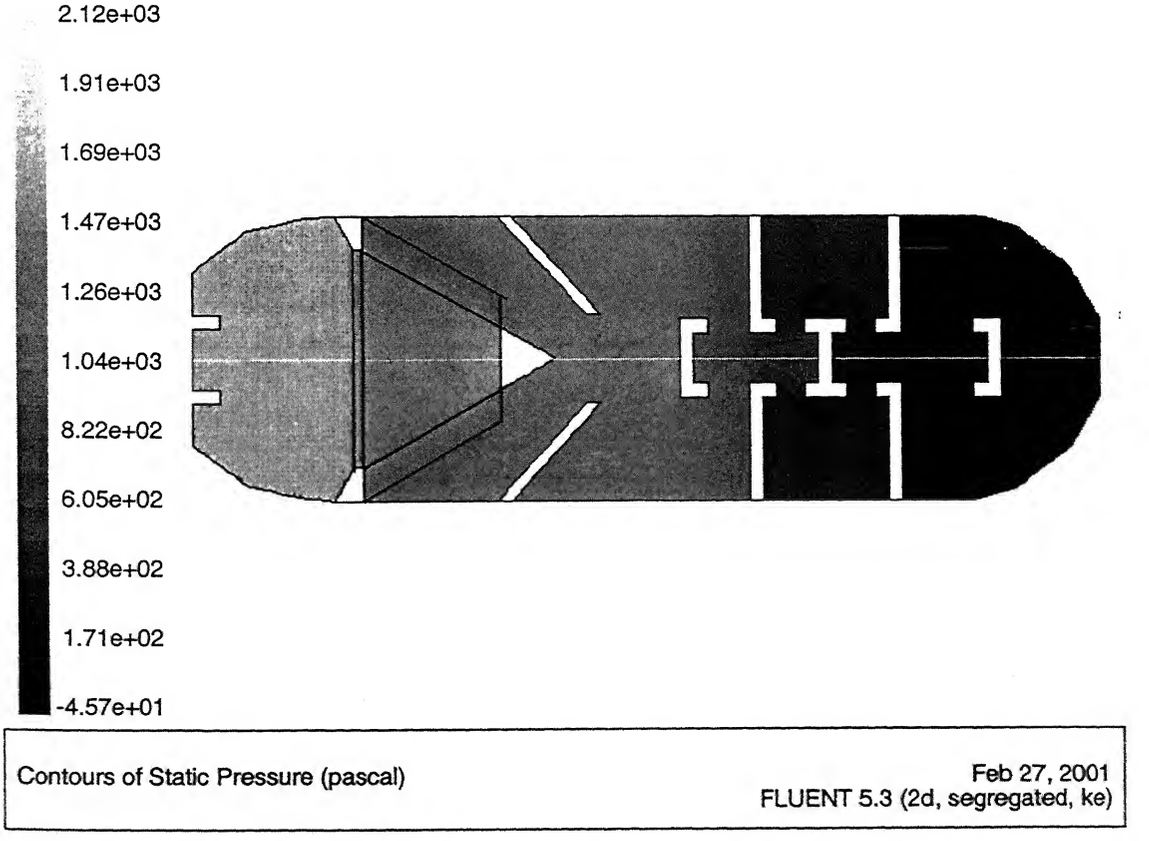

Figure 4.43: Pressure variation of exhaust muffler with apex of the converter towards downstream direction

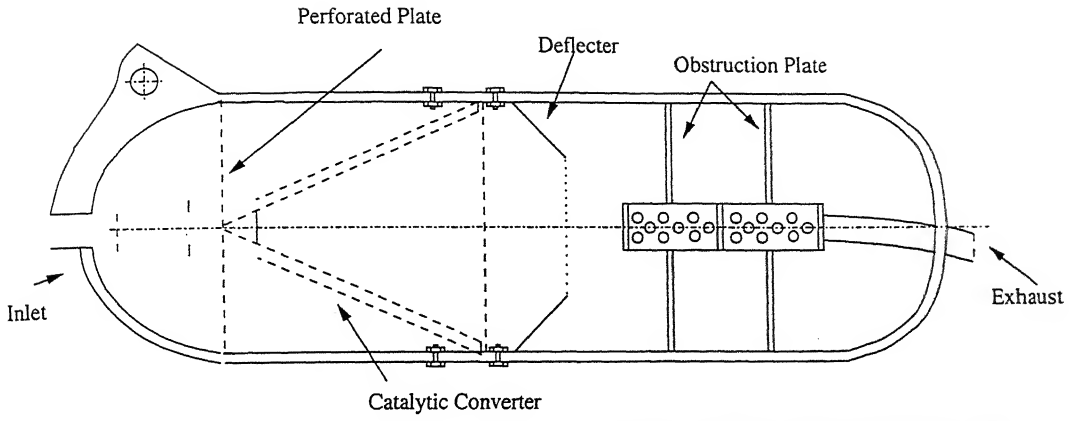

Figure 4.44 : Schematic of the symmetric exhaust muffler with apex of the conical converter towards upstream direction

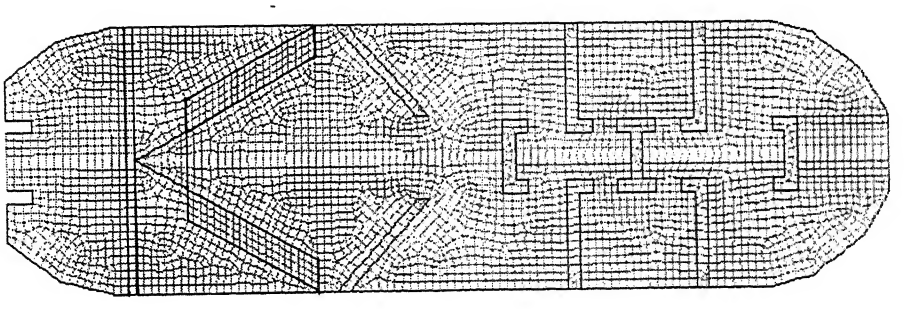

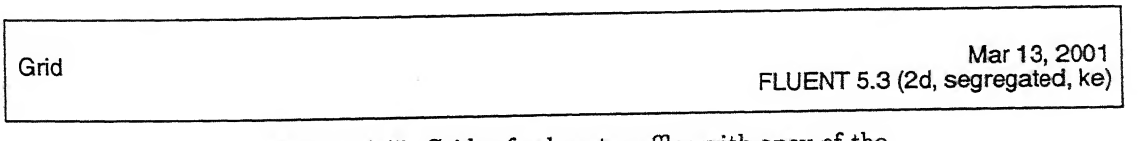

Figure 4.45: Grids of exhaust muffler with apex of the converter towards upstream direction

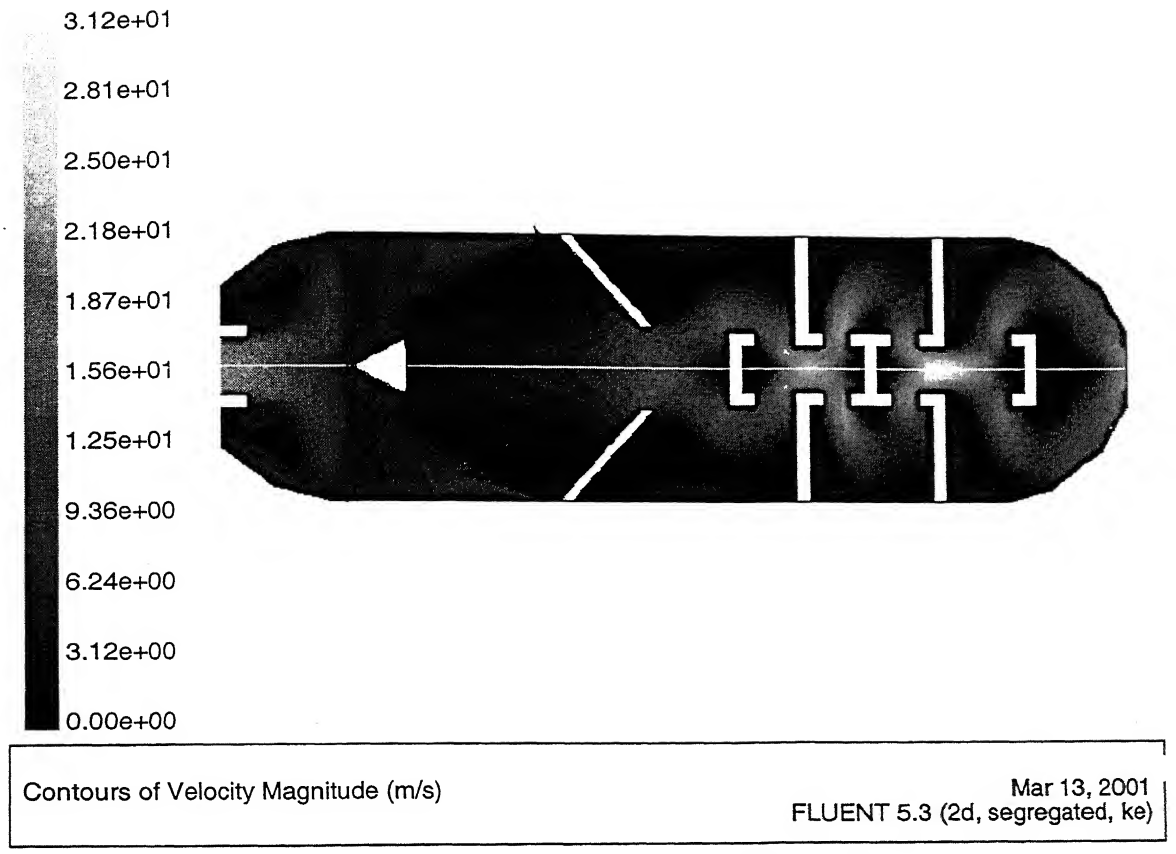

Figure 4.46: Velocity contours of exhaust muffler with apex of the converter towards upstream direction

Scale: 1mm = 0.5m/s

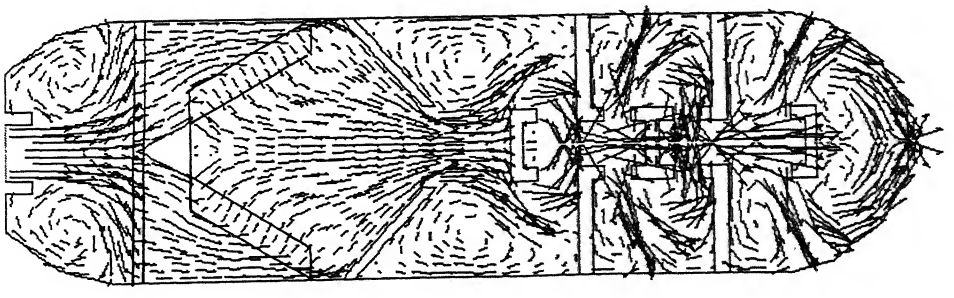

Figure 4.47: Velocity vectors of exhaust muffler with apex of the converter towards upstream direction

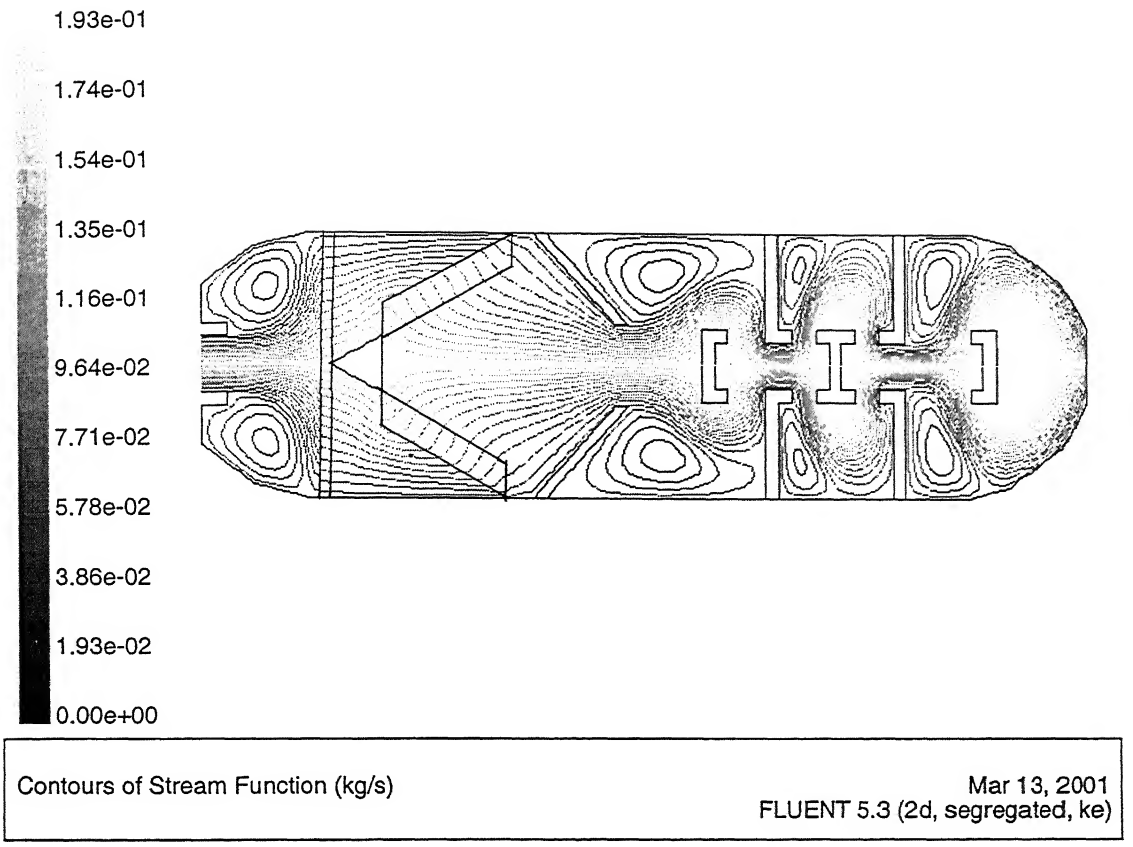

Figure 4.48: Stream function of exhaust muffler with apex of the converter towards upstream direction

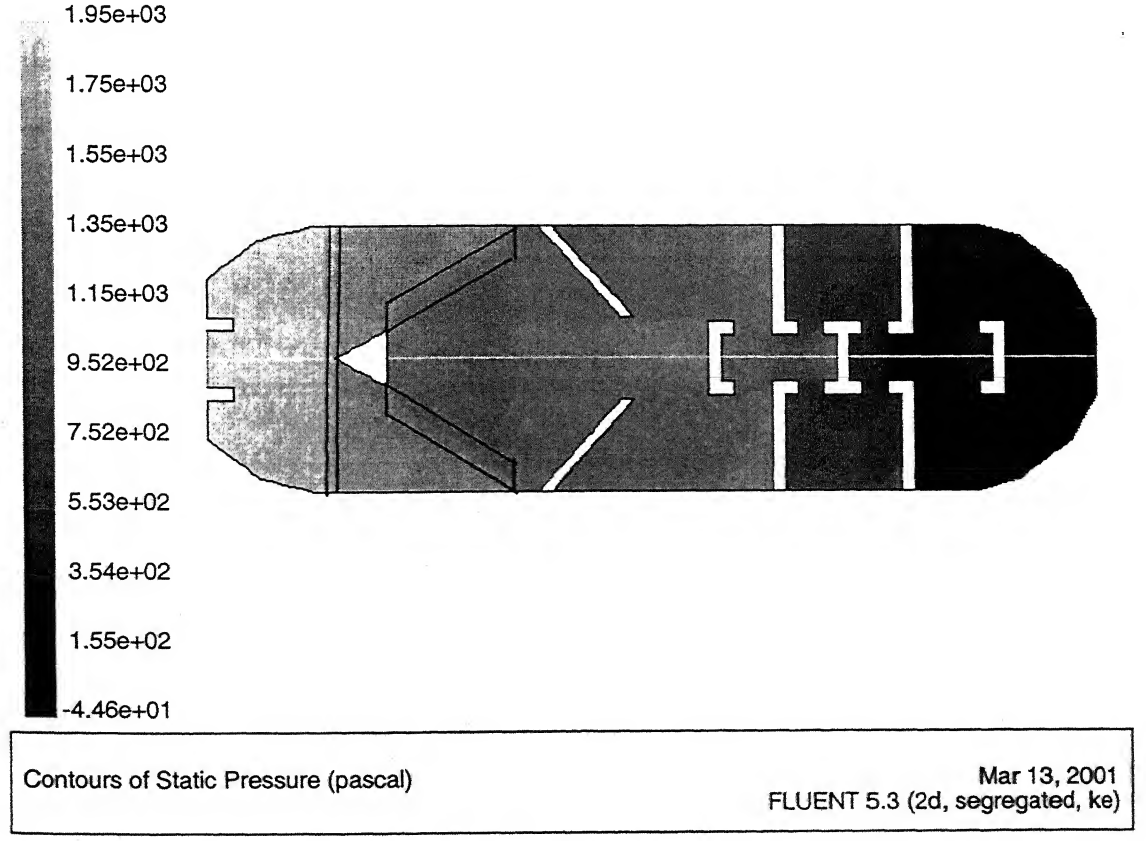

Figure 4.49: Pressure variation of exhaust muffler with apex of the converter towards upstream direction

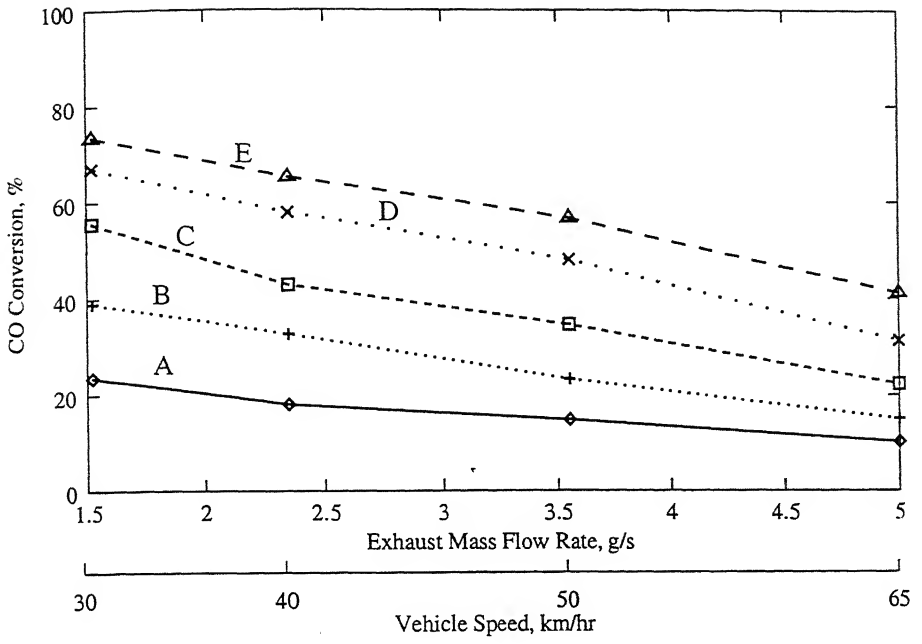

$A: T_{in} = 300\,^{\circ}C$ $D: T_{in} = 450\,^{\circ}C$
$B: T_{in} = 350\,^{\circ}C$ $E: T_{in} = 500\,^{\circ}C$
$C: T_{in} = 400\,^{\circ}C$

Figure 4.50: CO conversion efficiency with inlet temperature and exhaust mass flow rate, conical converter of 12 mm catalyst bed (catalyst vol.=117cm ^{3})

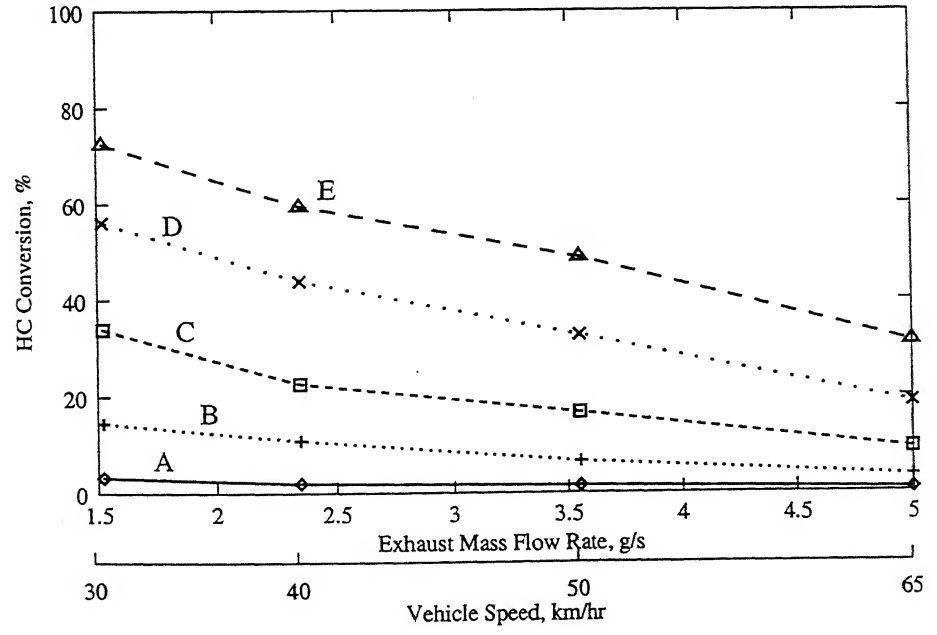

$A: T_{in} = 300\,^{\circ}C$ $D: T_{in} = 450\,^{\circ}C$
$B: T_{in} = 350\,^{\circ}C$ $E: T_{in} = 500\,^{\circ}C$
$C: T_{in} = 400\,^{\circ}C$

Figure 4.51: HC conversion efficiency with inlet temperature and exhaust mass flow rate, conical converter of 12 mm catalyst bed (catalyst vol.=117cm ^{3})

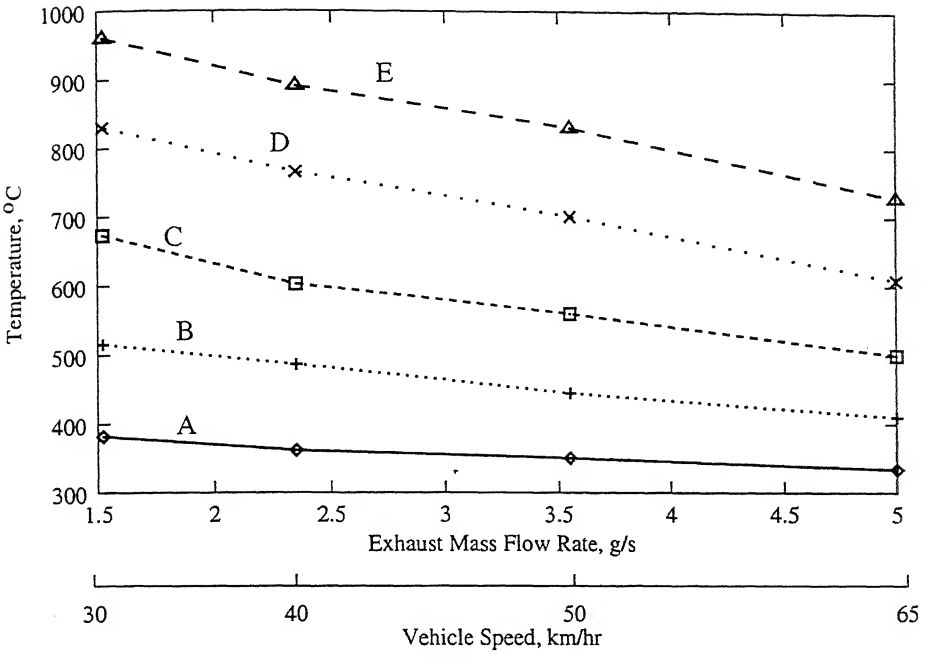

A: $T_{in} = 300\,^{\circ}C$ D: $T_{in} = 450\,^{\circ}C$
B: $T_{in} = 350\,^{\circ}C$ E: $T_{in} = 500\,^{\circ}C$
C: $T_{in} = 400\,^{\circ}C$

Figure 4.52: Converter outlet temperature with inlet temperature and exhaust mass flow rate, conical converter of 12 mm catalyst bed (catalyst vol.=117cm^3)

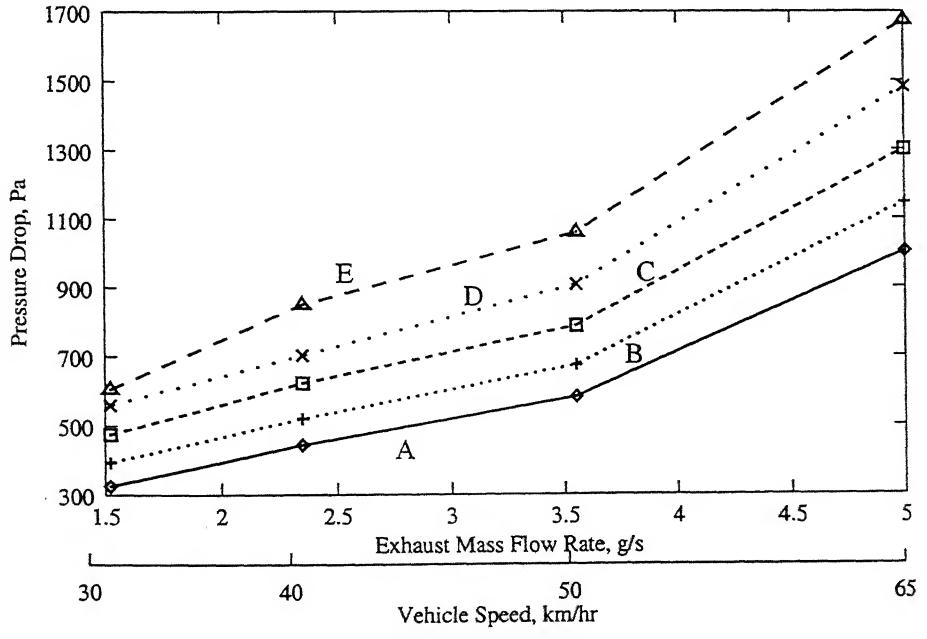

A: $T_{in} = 300\,^{\circ}C$ D: $T_{in} = 450\,^{\circ}C$
B: $T_{in} = 350\,^{\circ}C$ E: $T_{in} = 500\,^{\circ}C$
C: $T_{in} = 400\,^{\circ}C$

Figure 4.53: Pressure drop across bed with inlet temperature and exhaust mass flow rate, conical converter of 12 mm catalyst bed (catalyst vol.=117cm^3)

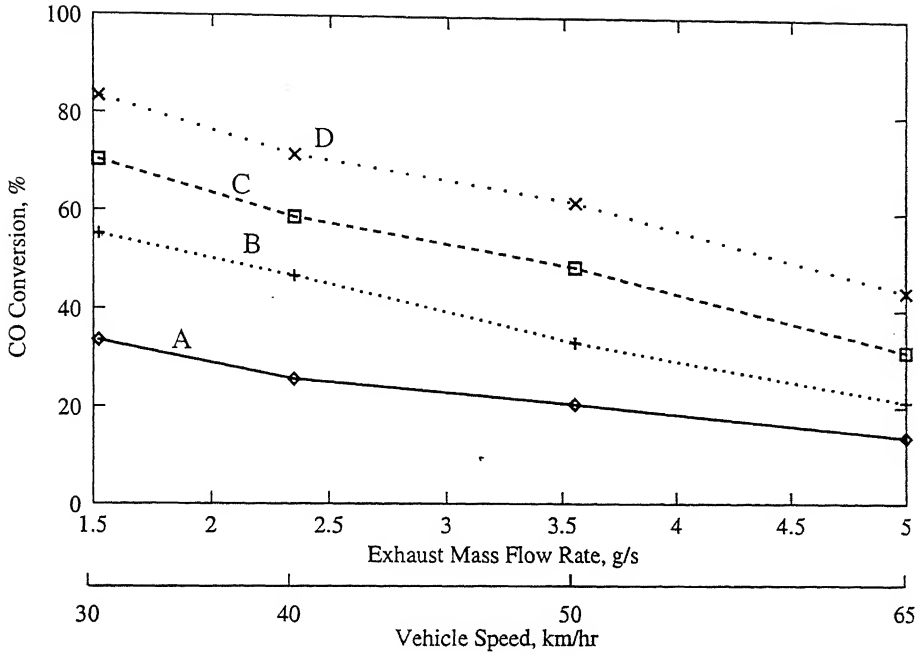

A: $T_{in} = 300\,^{\circ}C$ C: $T_{in} = 400\,^{\circ}C$
B: $T_{in} = 350\,^{\circ}C$ D: $T_{in} = 450\,^{\circ}C$

Figure 4.54: CO conversion efficiency with inlet temperature and exhaust mass flow rate, conical converter of 15 mm catalyst bed (catalyst vol.=153cm ^{3})

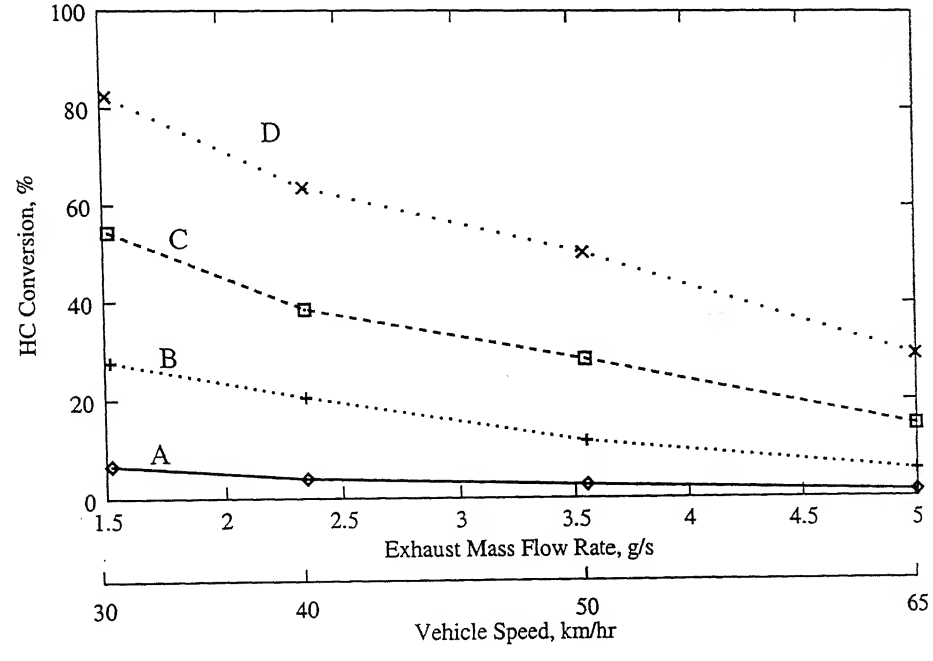

A: $T_{in} = 300\,^{\circ}C$ C: $T_{in} = 400\,^{\circ}C$
B: $T_{in} = 350\,^{\circ}C$ D: $T_{in} = 450\,^{\circ}C$

Figure 4.55: HC conversion efficiency with inlet temperature and exhaust mass flow rate, conical converter of 15 mm catalyst bed (catalyst vol.=153cm ^{3})

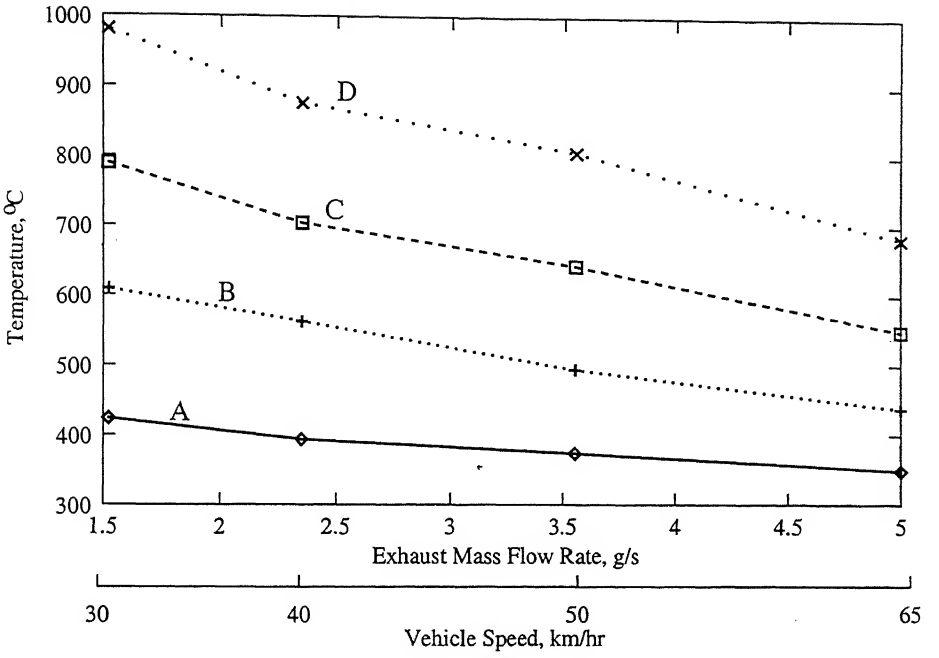

A : $T_{in} = 300\,^{\circ}C$ C : $T_{in} = 400\,^{\circ}C$
B : $T_{in} = 350\,^{\circ}C$ D : $T_{in} = 450\,^{\circ}C$

Figure 4.56: Converter outlet temperature with inlet temperature and exhaust mass flow rate, conical converter of 15 mm catalyst bed (catalyst vol.=153cm^3)

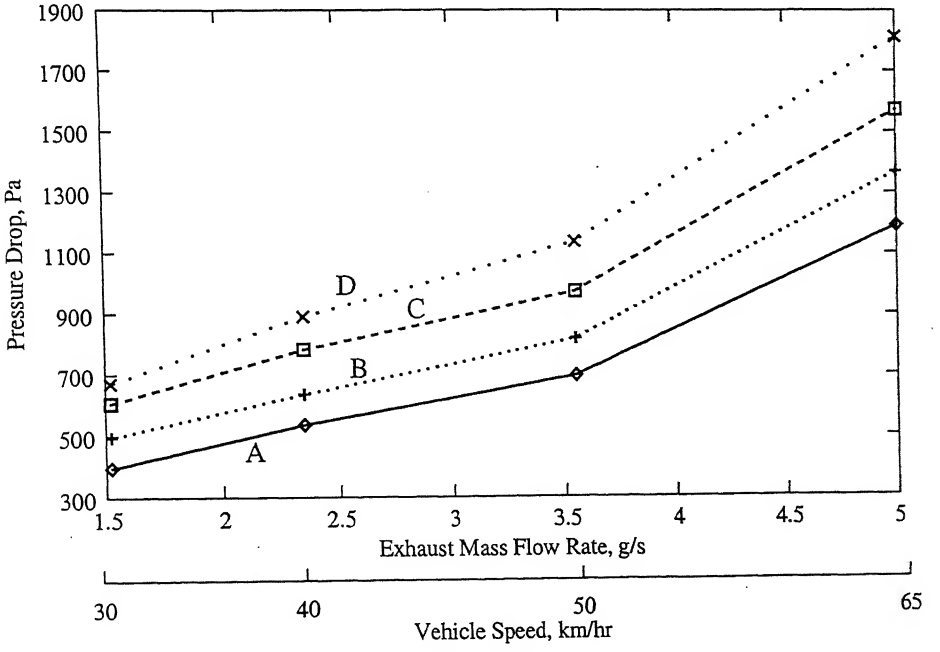

A : $T_{in} = 300\,^{\circ}C$ C : $T_{in} = 400\,^{\circ}C$
B : $T_{in} = 350\,^{\circ}C$ D : $T_{in} = 450\,^{\circ}C$

Figure 4.57: Pressure drop across bed with inlet temperature and exhaust mass flow rate, conical converter of 15 mm catalyst bed (catalyst vol.=153cm^3)

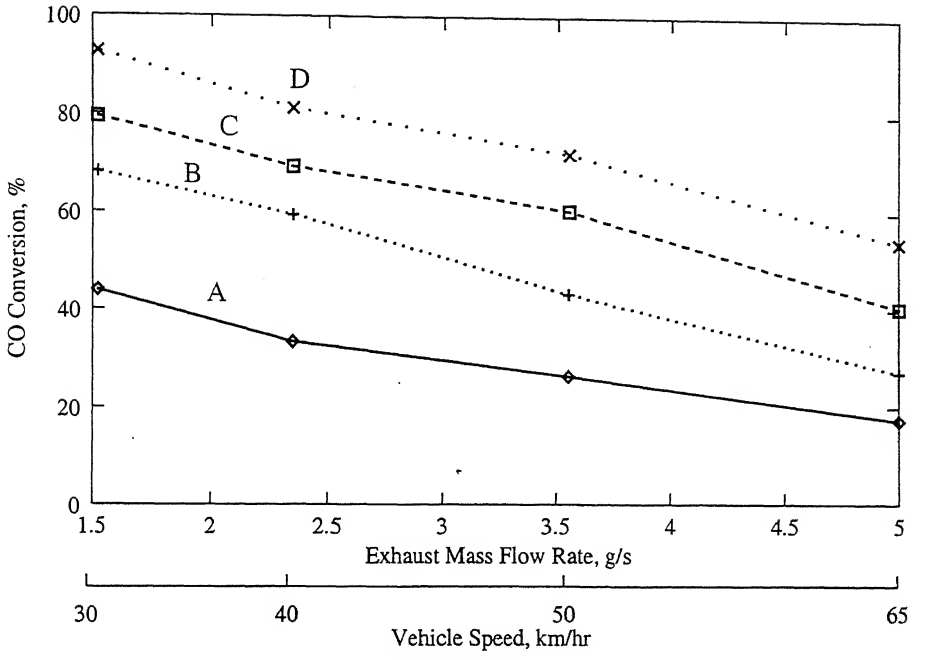

A: $T_{in} = 300\,^{\circ}C$ C: $T_{in} = 400\,^{\circ}C$

B: $T_{in} = 350\,^{\circ}C$ D: $T_{in} = 450\,^{\circ}C$

Figure 4.58: CO conversion efficiency with inlet temperature and exhaust mass flow rate, conical converter of 18 mm catalyst bed (catalyst vol.=192cm ^{3})

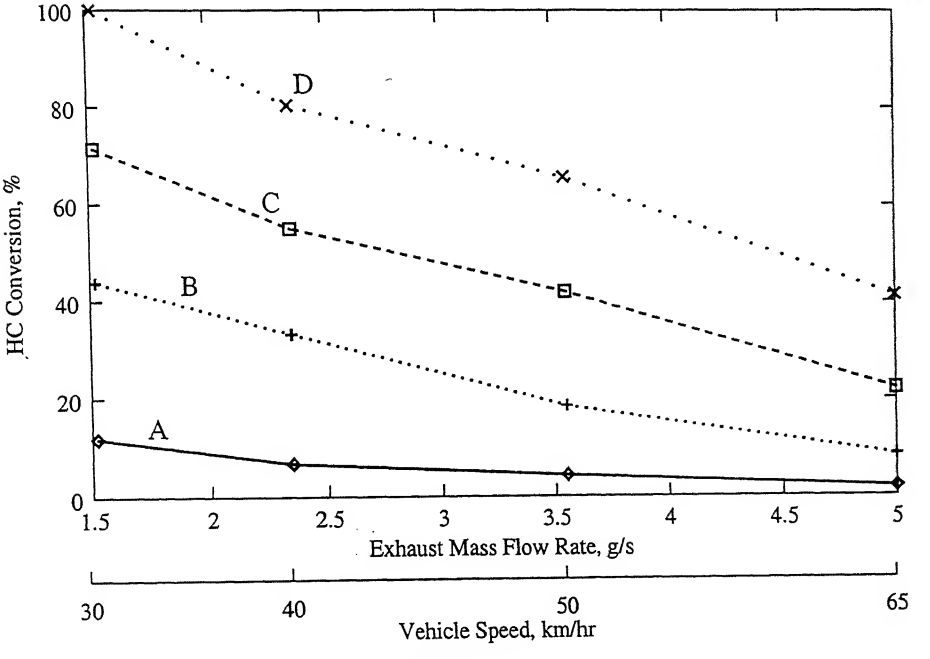

A: $T_{in} = 300\,^{\circ}C$ C: $T_{in} = 400\,^{\circ}C$

B: $T_{in} = 350\,^{\circ}C$ D: $T_{in} = 450\,^{\circ}C$

Figure 4.59: HC conversion efficiency with inlet temperature and exhaust mass flow rate, conical converter of 18 mm catalyst bed (catalyst vol.=192cm ^{3})

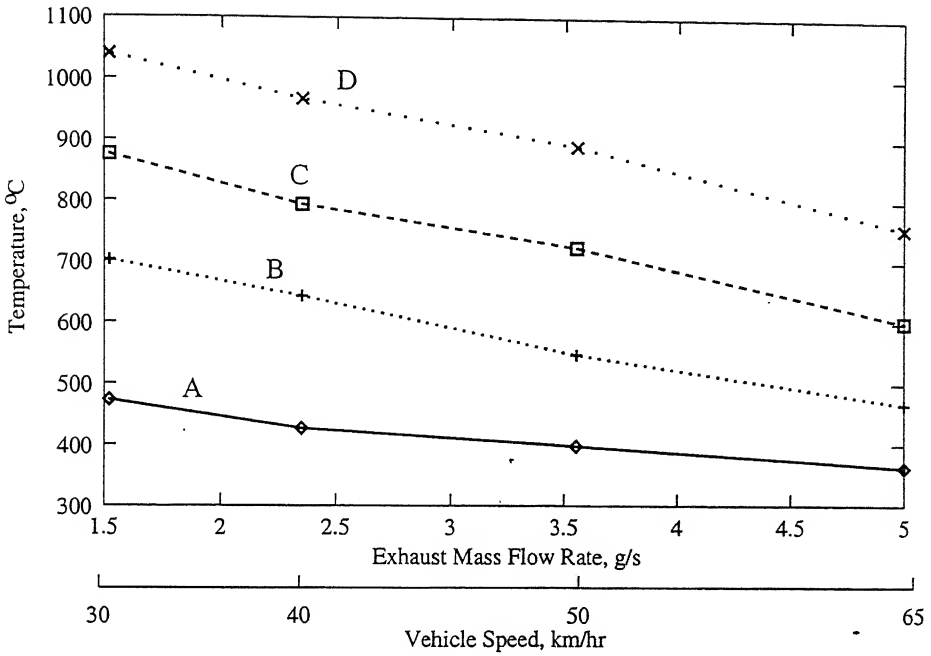

$A: T_{in} = 300\,^{\circ}C$ $C: T_{in} = 400\,^{\circ}C$

$B: T_{in} = 350\,^{\circ}C$ $D: T_{in} = 450\,^{\circ}C$

Figure 4.60: Converter outlet temperature with inlet temperature and exhaust mass flow rate, conical converter of 15 mm catalyst bed (catalyst vol.=153cm^3)

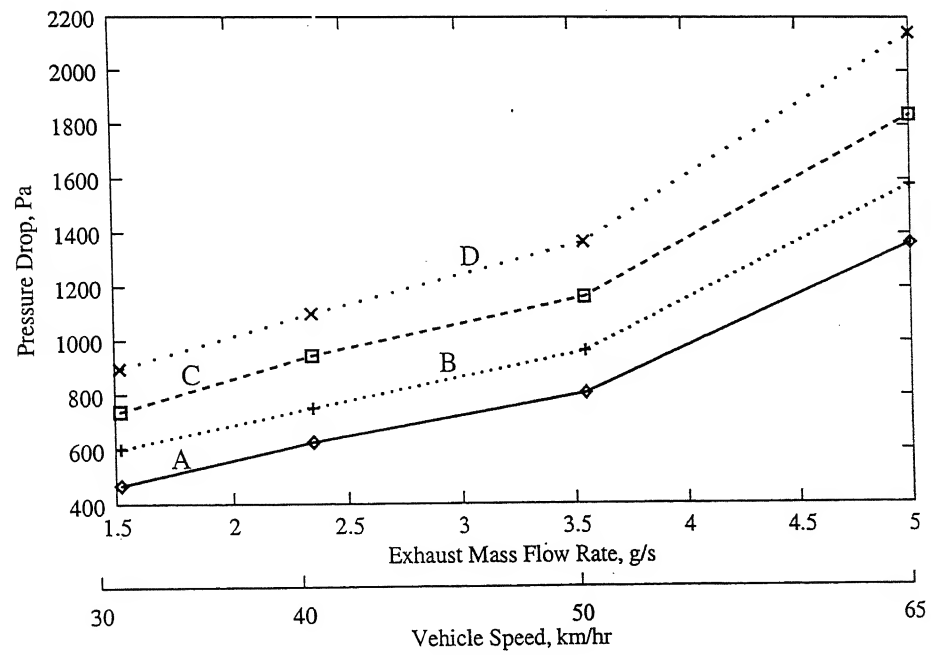

$A: T_{in} = 300\,^{\circ}C$ $C: T_{in} = 400\,^{\circ}C$

$B: T_{in} = 350\,^{\circ}C$ $D: T_{in} = 450\,^{\circ}C$

Figure 4.61: Pressure drop across bed with inlet temperature and exhaust mass flow rate, conical converter of 15 mm catalyst bed (catalyst vol.=153cm^3)

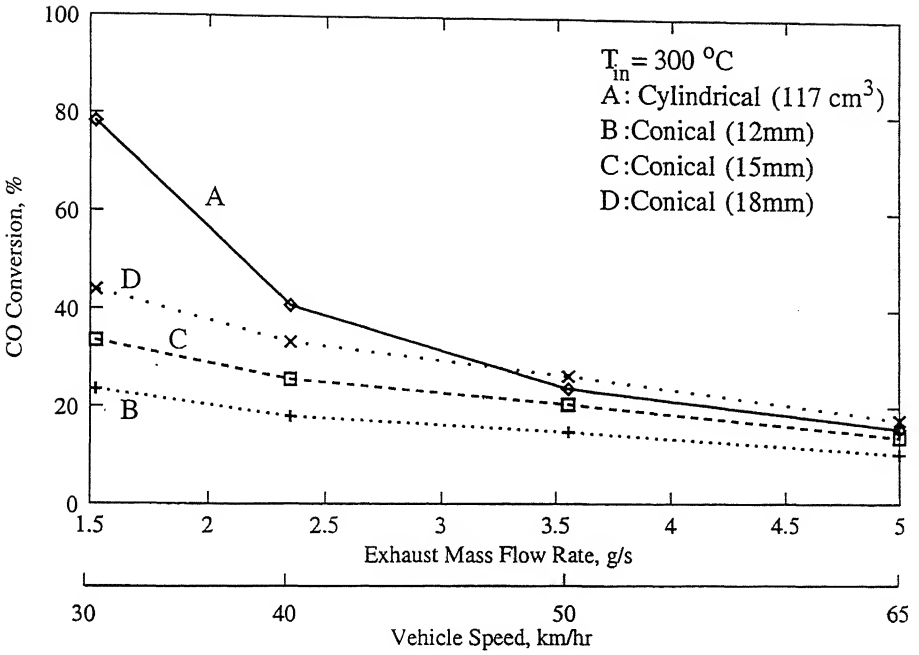

Figure 4.62: Comparison of cylindrical (117 cm^3) and conical converter of 12mm (117 cm^3), 15mm (153 cm^3) and 18mm (192 cm^3) on CO conversion, T_{in} = 300 °C

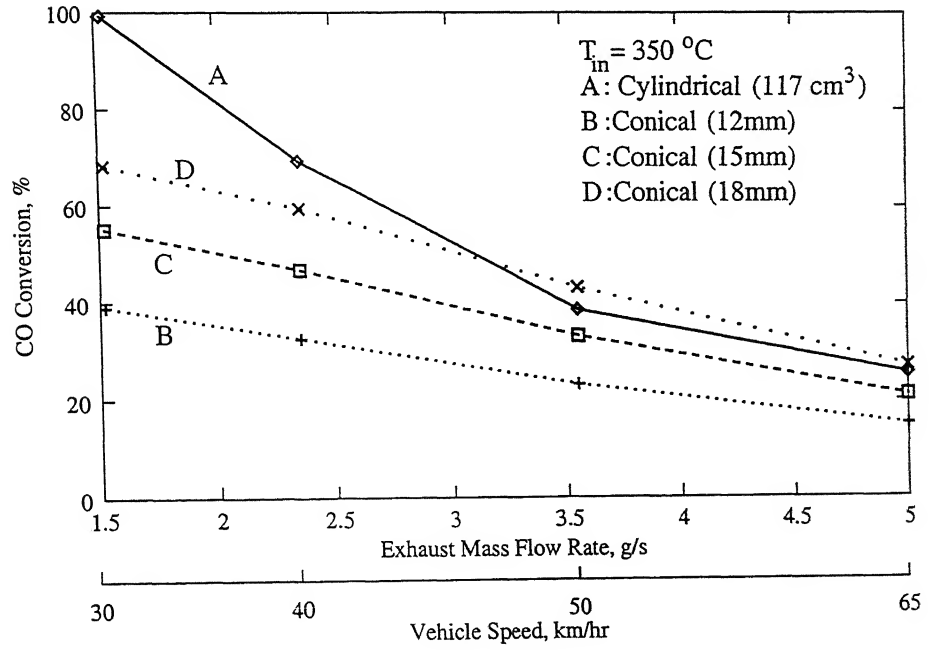

Figure 4.63 : Comparison of cylindrical (117 cm^3) and conical converter of 12mm (117 cm^3), 15mm (153 cm^3) and 18mm (192 cm^3) on CO conversion, T_{in} = 350 °C

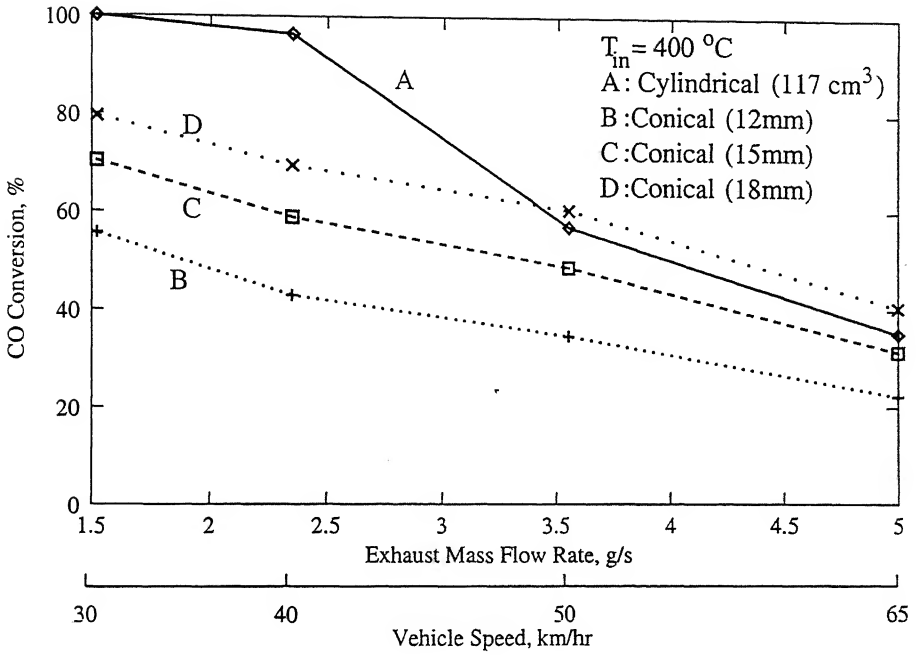

Figure 4.64: Comparison of cylindrical (117 cm^3) and conical converter of 12mm (117 cm^3), 15mm (153 cm^3) and 18mm (192 cm^3) on CO conversion, T_{in} = 400 °C

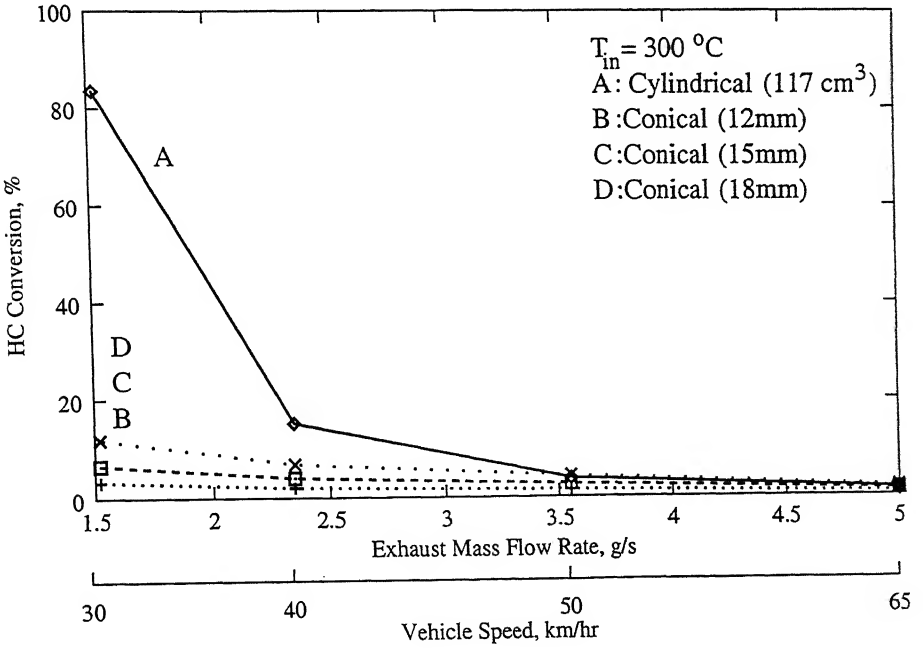

Figure 4.65 : Comparison of cylindrical (117 cm^3) and conical converter of 12mm (117 cm^3), 15mm (153 cm^3) and 18mm (192 cm^3) on HC conversion, T_{in} = 300 °C

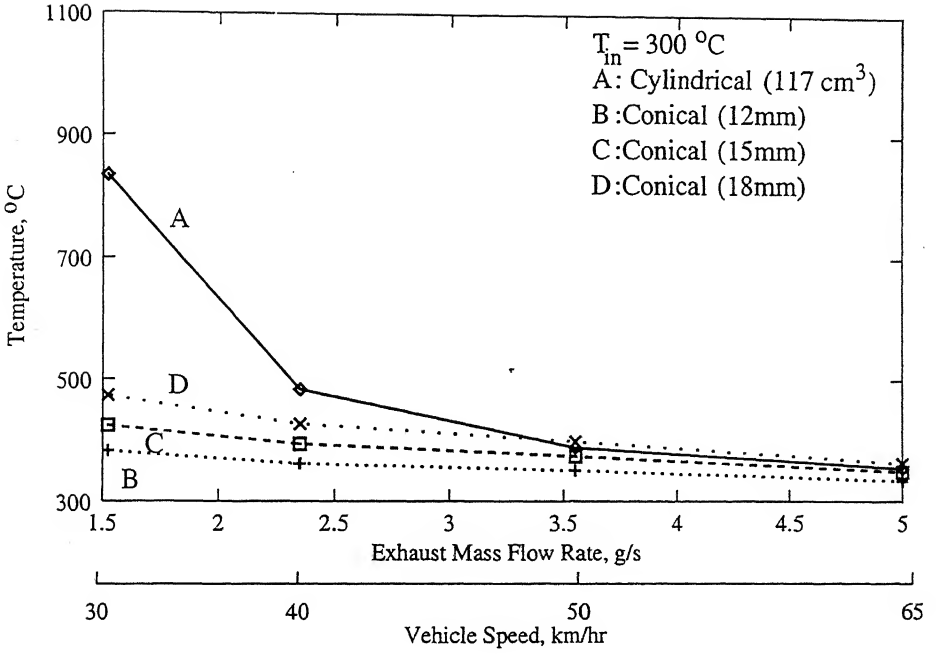

Figure 4.68: Comparison of cylindrical (117 cm^3) and conical converter of 12mm (117 cm^3), 15mm (153 cm^3) and 18mm (192 cm^3) on outlet temperature, T_{in}= 300° C

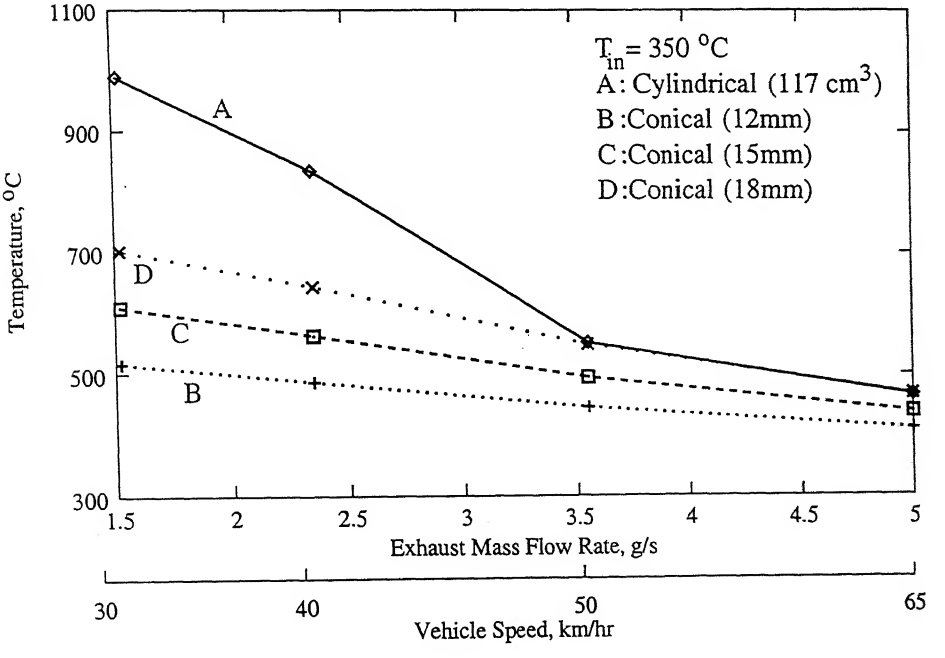

Figure 4.69: Comparison of cylindrical (117 cm^3) and conical converter of 12mm (117 cm^3), 15mm (153 cm^3) and 18mm (192 cm^3) on outlet temperature, T_{in}= 350° C

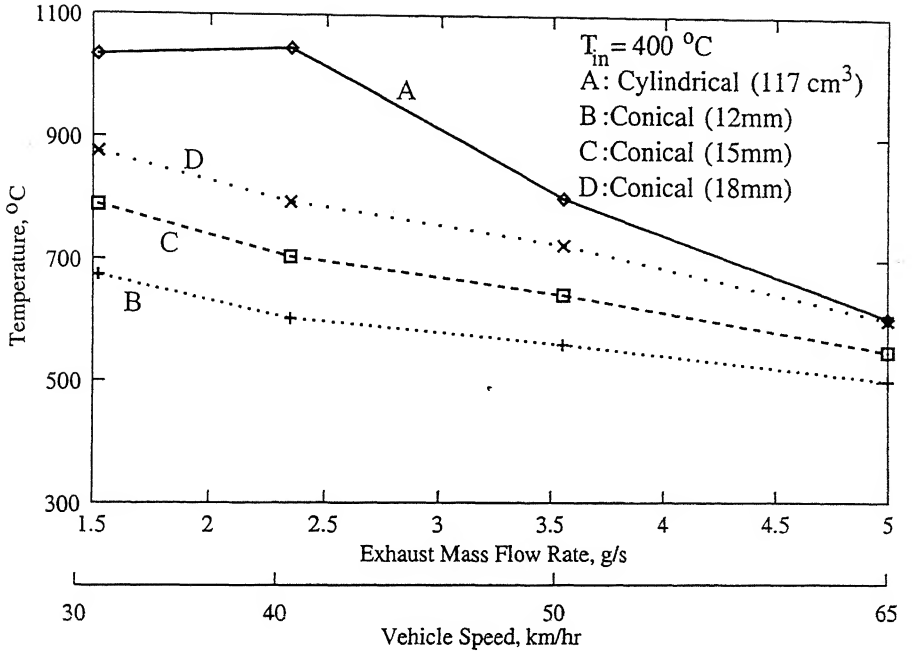

Figure 4.70 : Comparison of cylindrical (117 cm^3) and conical converter of 12mm (117 cm^3), 15mm (153 cm^3) and 18mm (192 cm^3) on outlet temperature, T_{in}= 400° C

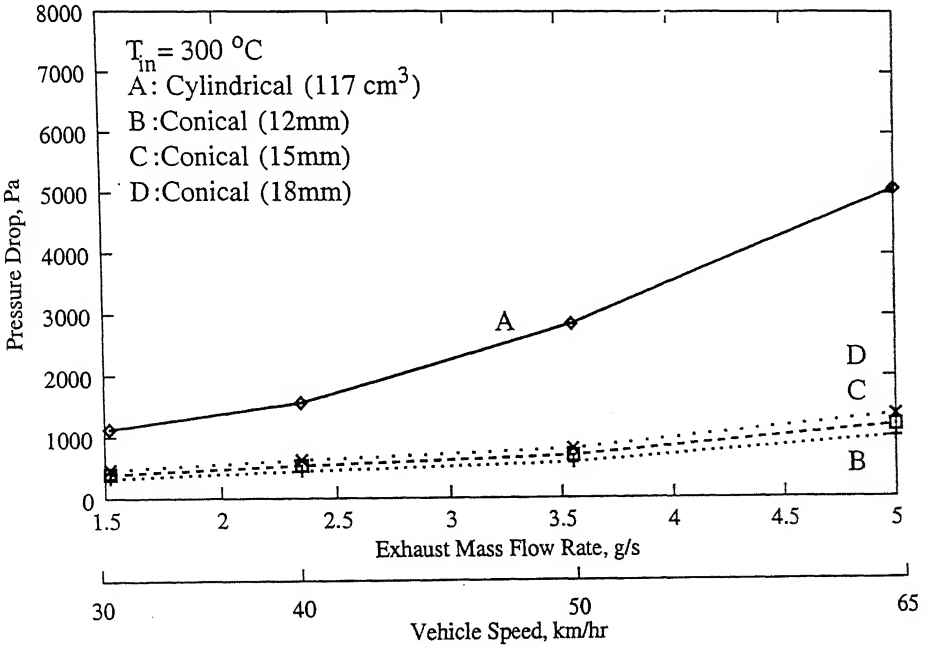

Figure 4.71: Comparison of cylindrical (117 cm^3) and conical converter of 12mm (117 cm^3), 15mm (153 cm^3) and 18mm (192 cm^3) on pressure drop, T_{in}= 300° C

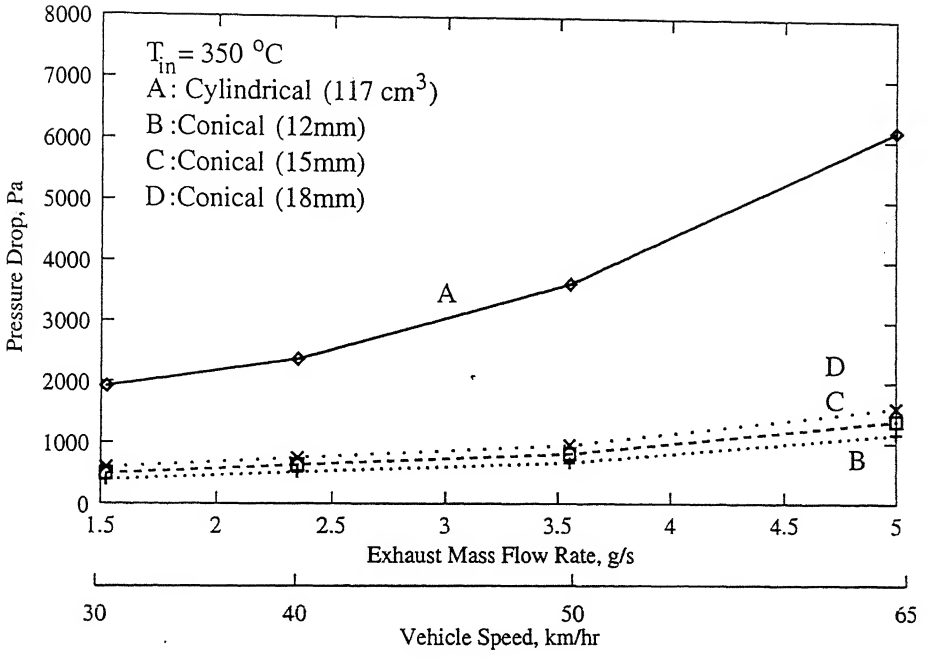

Figure 4.72: Comparison of cylindrical (117 cm^3) and conical converter of 12mm (117 cm^3), 15mm (153 cm^3) and 18mm (192 cm^3) on pressure drop, T_{in}= 350° C

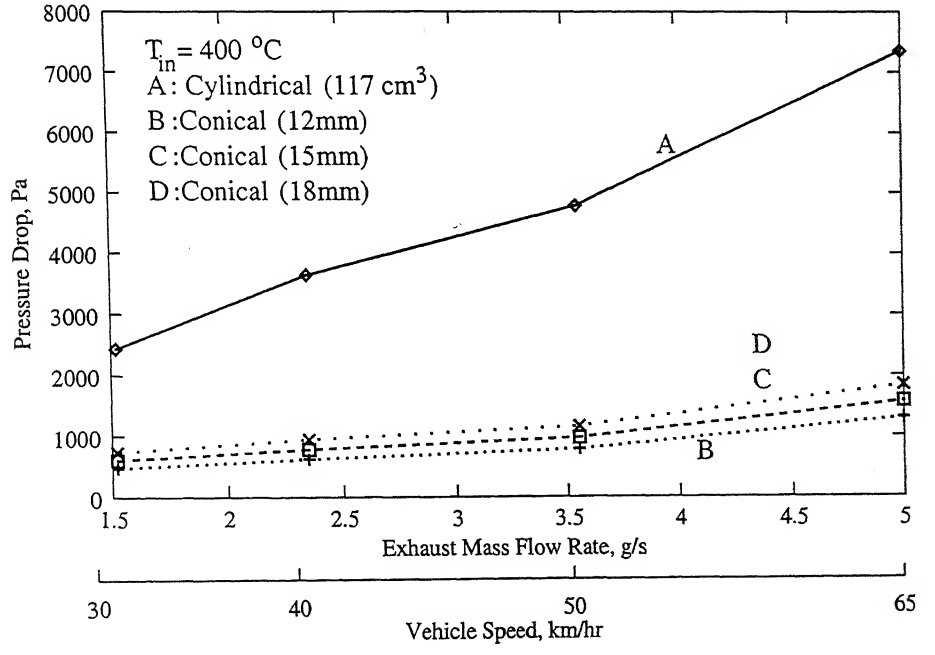

Figure 4.73: Comparison of cylindrical (117 cm^3) and conical converter of 12mm (117 cm^3), 15mm (153 cm^3) and 18mm (192 cm^3) on pressure drop, T_{in}= 400° C

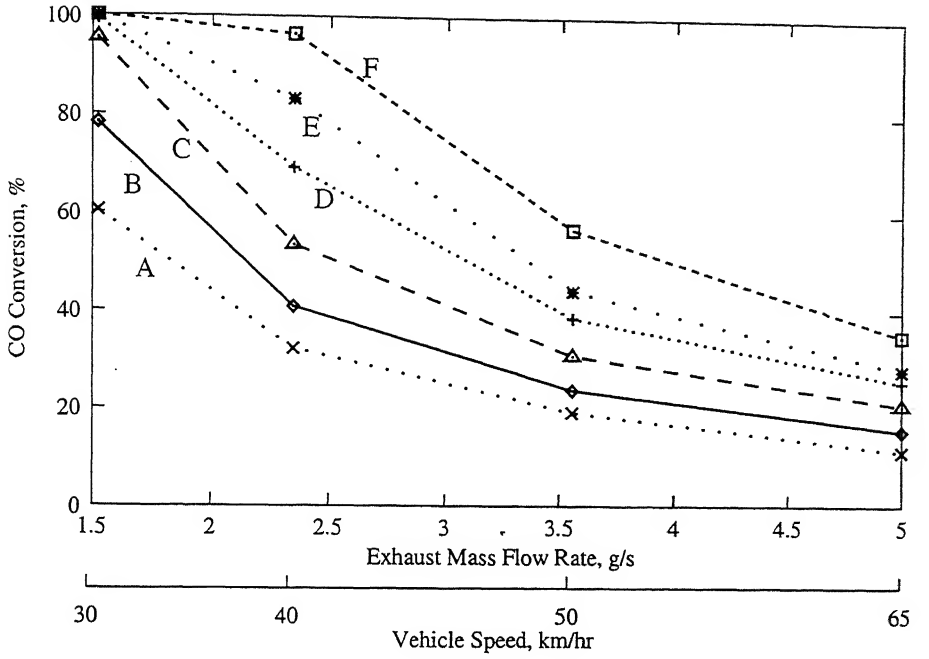

A: 50mm,50mm(98 cm^3), T_{in}= 300 °C
B: 50mm,60mm(117 cm^3), T_{in}= 300 °C
C: 50mm,50mm(98 cm^3), T_{in}= 350 °C
D: 50mm,60mm(117 cm^3), T_{in}= 350 °C
E: 50mm,50mm(98 cm^3), T_{in}=400 °C
F: 50mm,60mm(117 cm^3), T_{in}=400 °C

Figure 4.74: Comparison of cylindrical catalytic converters with two different catalyst volume (98 cm^3 and 117 cm^3) on CO conversion

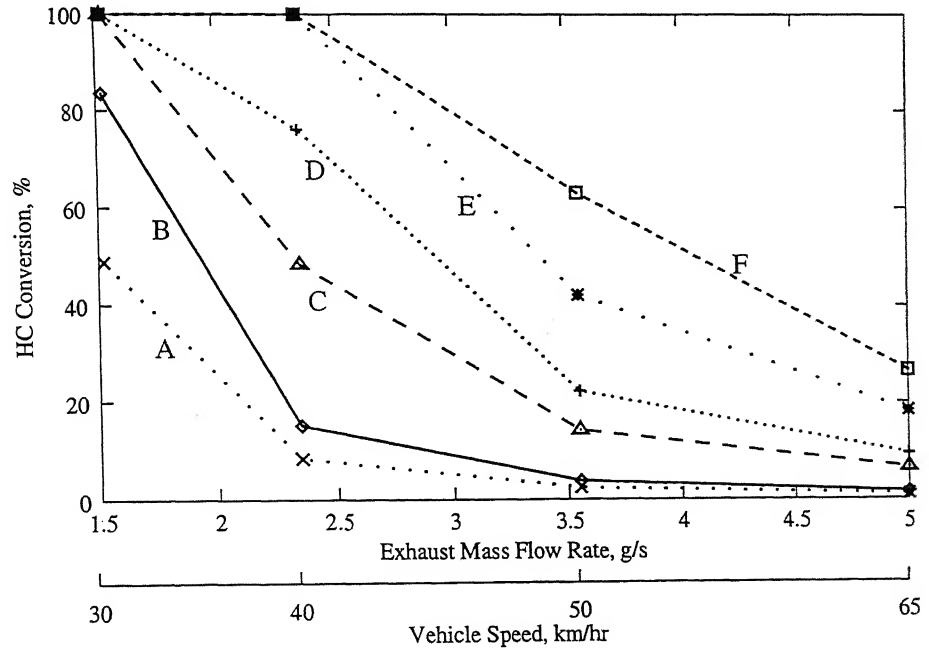

A: 50mm,50mm(98 cm^3), T_{in}= 300 °C
B: 50mm,60mm(117 cm^3), T_{in}= 300 °C
C: 50mm,50mm(98 cm^3), T_{in}= 350 °C
D: 50mm,60mm(117 cm^3), T_{in}= 350 °C
E: 50mm,50mm(98 cm^3), T_{in}=400 °C
F: 50mm,60mm(117 cm^3), T_{in}=400 °C

Figure 4.75 : Comparison of cylindrical catalytic converters with two different catalyst

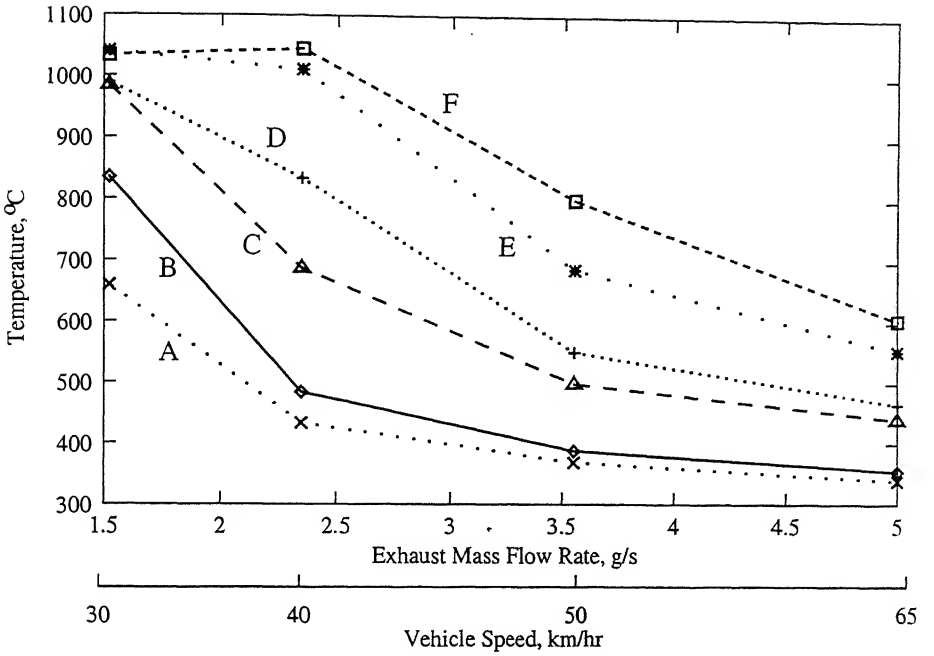

A: 50mm,50mm(98 cm^3), T_{in}= 300 °C
B: 50mm,60mm(117 cm^3), T_{in}= 300 °C
C: 50mm,50mm(98 cm^3), T_{in}= 350 °C
D: 50mm,60mm(117 cm^3), T_{in}= 350 °C
E: 50mm,50mm(98 cm^3), T_{in}=400 °C
F: 50mm,60mm(117 cm^3), T_{in}=400 °C

Figure 4.76: Comparison of cylindrical catalytic converters with two different catalyst volume (98 cm^3 and 117 cm^3) on outlet temperature

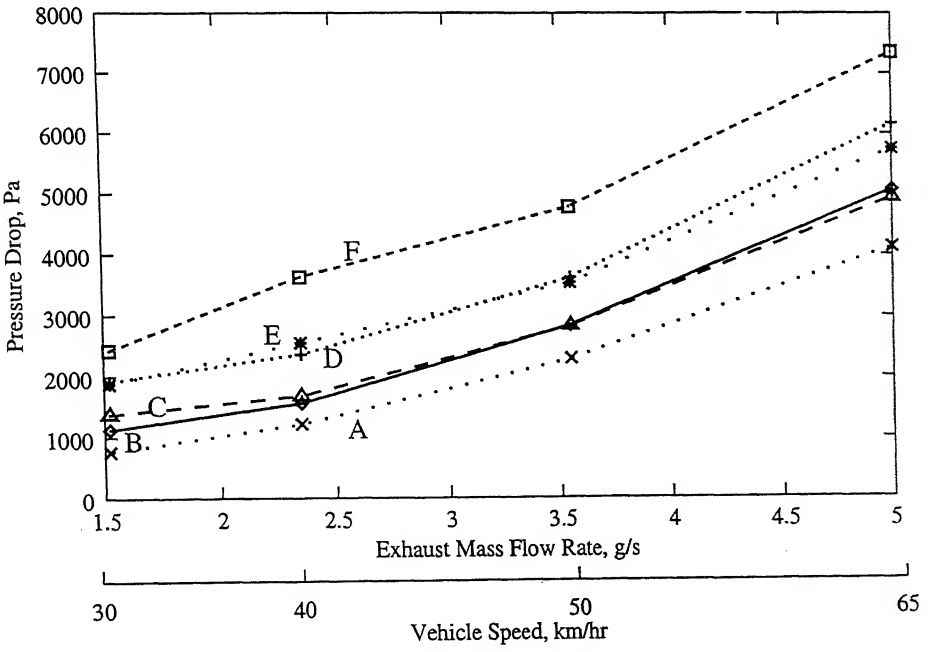

A: 50mm,50mm(98 cm^3), T_{in}= 300 °C
B: 50mm,60mm(117 cm^3), T_{in}= 300 °C
C: 50mm,50mm(98 cm^3), T_{in}= 350 °C
D: 50mm,60mm(117 cm^3), T_{in}= 350 °C
E: 50mm,50mm(98 cm^3), T_{in}=400 °C
F: 50mm,60mm(117 cm^3), T_{in}=400 °C

Figure 4.77: Comparison of cylindrical catalytic converters with two different catalyst volume (98 cm^3 and 117 cm^3) on pressure drop

CHAPTER 5

CONCLUSIONS

A one dimensional, plug flow, non-adiabatic, heterogeneous, steady state mathematical model has been developed for packed bed exhaust catalytic converters for SI engine application. Numerical scheme incorporating the simultaneous coupled solution of all the five basic governing equations of mole, momentum and energy balance has been presented. The model incorporates oxidation of propane, representing commercial gasoline and carbon monoxide (CO). Propane (HC) oxidation is taken as two step reaction, first to CO, which further oxidizes to carbon dioxide in the second step. Although the basic governing equations are developed from the theoretical aspect, the supporting expressions for intrinsic rate of reaction of propane and carbon monoxide that have been adapted from the literature, renders the overall model as semi-empirical. The predictions of developed model are compared with homogeneous model and experimental data.

Flow pattern in the muffler of a moped fitted with conical packed bed catalytic converter developed by M/s Indian Oil Corporation Limited, R&D Centre, Faridabad is studied using a CFD software. The catalytic converter model is applied to this conical shaped converter. Predictions of model for the conical catalytic converter are compared with cylindrical catalytic converter of equal catalyst volume.

The following conclusions can be drawn from the present study:

5.1 Numerical Modeling and Correlation with Experimental Data:

1. The semi-empirical approach for modeling integral catalytic converter is quite promising and computationally inexpensive. Due to non-availability of oxidation reaction rate data for commercial gasoline, which is a mixture of various hydrocarbons, use of propane is taken as the viable option.

2. Although the formulated problem requires the solution of non-linear coupled simultaneous differential equations, the Runge-Kutta algorithm coupled with non-linear, one dimensional diffusion equation solved by TDM Thomas algorithm did not have any convergence failure in the solution domain.

3. Predictions of heterogeneous model on CO conversion correlates well with experimental data for a 2-stroke, spark ignition engine generator set. The model, however, over predicts HC conversion rates. As regards, HC conversion rates of reaction for propane in differential (micro) reactors have been used. The reaction rates for typical gasoline in integral reactors could be different which may account for the differences observed between experimental and predicted values.

4. The model predictions on the bed temperature profile for low inlet gas temperature do not correlate well with experimental data. However, at higher exhaust

inlet temperature, temperature profile along the bed tends to come closer to the experimental trends. Because temperature-sampling probe is not exactly located at the converter outlet but in the mixing volume at the converter outlet, post catalytic reaction might have occurred showing higher CO conversion and gas temperatures.

5.2 Study of Flow Field in the Exhaust Muffler:

Study of flow in the exhaust muffler is done using Fluent 5.1 software. Following are the findings of the work.

It is found that asymmetric exhaust muffler having conical converter with apex towards upstream direction has less recirculation of flow though pressure drop is higher by 0.17kPa than converter with apex in downstream direction. It is also seen that symmetric muffler with both configurations does not give any improvement in flow field while pressure drop is almost same as in asymmetric muffler.

5.3 Performance of Conical Converter:

1. At first, conical converter with 12mm catalyst bed thickness is studied. But it is seen that this converter does not give significant conversion of CO and HC particularly at low inlet temperature.
2. Conical converter of 15mm and 18mm give significant improvement in conversion but employs relatively very large catalyst volumes.
3. Comparison of performance of conical converters of 12, 15 and 18mm bed thickness with cylindrical converter having catalyst volume equal to that of 12mm conical converter, show that cylindrical converter of aspect ratio of about one gives significantly higher conversion than conical converters, but has higher pressure drop in the range of 5.0 to 6.0kPa compared to about 1.0kPa for converter.

5.4 Scope for future work:

The following points are suggested as a scope of future work:

1. Axial conduction and radiation term should be incorporated. Such a model will then be able to predict more realistic axial temperature profile.

2. Experimental investigations should be carried out on integral type reactors to augment the available reaction rate data.

3. It is uncertain whether temperature measured is of pellet surface or of fluid. So a more detailed setup is needed for precise temperature measurement.

4. Further study should be done with different configurations of converter including monolith type to minimize the pressure drop while obtaining high conversion rates.

VI. Appendix A:

The Runge - Kutta Algorithm

We consider the two equations

$$\frac{dx}{dt} = f(t,x,y)$$
$$\frac{dy}{dt} = \phi(t,x,y)$$

with the initial conditions x = x_o and y = y_o, when t = t_o.

Assuming that $\Delta t = h$, $\Delta x = k$, and $\Delta y = l$, the fourth order Runge-Kutta method gives,

$$k_1 = h \cdot f(t_o, x_o, y_o);$$

$$l_1 = h \cdot \phi(t_o, x_o, y_o);$$

$$k_2 = h \cdot f(t_o + \tfrac{1}{2}h, x_o + \tfrac{1}{2}k_1, y_o + \tfrac{1}{2}l_1);$$

$$l_2 = h \cdot \phi(t_o + \tfrac{1}{2}h, x_o + \tfrac{1}{2}k_1, y_o + \tfrac{1}{2}l_1);$$

$$k_3 = h \cdot f(t_o + \tfrac{1}{2}h, x_o + \tfrac{1}{2}k_2, y_o + \tfrac{1}{2}l_2);$$

$$l_3 = h \cdot \phi(t_o + \tfrac{1}{2}h, x_o + \tfrac{1}{2}k_2, y_o + \tfrac{1}{2}l_2);$$

$$k_4 = h \cdot f(t_o + h, x_o + k_3, y_o + l_3);$$

$$l_4 = h \cdot \phi(t_o + h, x_o + k_3, y_o + l_3);$$

$$x_1 = x_o + \frac{1}{6}(k_1 + 2k_2 + 2k_3 + k_4)$$

$$y_1 = y_o + \frac{1}{6}(l_1 + 2l_2 + 2l_3 + l_4)$$

In a similar manner the method can be extended to a system of 'n' simultaneous equations.

Appendix B:

The Thomas Algorithm

Step 1: Transformation of the one-dimensional finite difference diffusion equation along with the proper boundary conditions to the following matrix form,

$$\begin{bmatrix} d_1 & a_1 & 0 & 0 & 0 & 0 & 0 \\ b_2 & d_2 & a_2 & 0 & 0 & 0 & 0 \\ 0 & b_3 & d_3 & a_3 & 0 & 0 & 0 \\ 0 & 0 & - & - & - & 0 & 0 \\ 0 & 0 & 0 & - & - & - & 0 \\ 0 & 0 & 0 & 0 & b_{n-1} & d_{n-1} & a_{n-1} \\ 0 & 0 & 0 & 0 & 0 & b_n & d_n \end{bmatrix} \bullet \begin{Bmatrix} C_1 \\ C_2 \\ C_3 \\ - \\ - \\ C_{n-1} \\ C_n \end{Bmatrix} = \begin{Bmatrix} r_1 \\ r_2 \\ r_3 \\ - \\ - \\ r_{n-1} \\ r_n \end{Bmatrix}$$

"Coefficients" "Variable" "Solution"

Step 2: Computation of all the coefficients $d_1,d_2,....d_n$, $a_1,a_2,....a_n$, $b_1,b_2,....b_n$, $r_1,r_2,....r_n$

Step 3: Forward substitution as follows,

For j = 2 to n, do:

$$d[j] = d[j] - \left(\frac{b[j]}{d[j-1]} \cdot a[j-1] \right)$$

$$r[j] = r[j] - \left(\frac{b[j]}{d[j-1]} \cdot r[j-1] \right)$$

Thus all the b_j are eliminated and we get an upper triangular matrix.

Step 4: Backward substitution as follows,

$$C[n] = \frac{r[n]}{d[n]}$$

For i = (n-1) to 1, step –1, do:

$$C[j] = \frac{(r[j] - a[j] * T[j+1])}{d[j]}$$

Thus by solving the above the entire solution C_i is obtained.

REFERENCES:

1. Aris R. *Introduction to the Analysis of Chemical Reactors.* Prentice Hall Inc., © 1965. Montreuil C.N., Williams S.C. and Adamczyk A., *Modeling Current Generation Catalytic Converters: Laboratory Experiments and Kinetic Parameter Optimization – Steady State Kinetics.* SAE Paper 920096, 1996.
2. Bear J., *Dynamics of Fluids in porous media*, American Elsevier, ©1972.
3. Baba N., Ohsawa K. and Sugiura S., *Numerical Approach for Improving the Conversion Characteristics of Exhaust Catalysts Under Warming-up Condition.* SAE paper 962076, 1996, **141-156.**
4. Babu P. R., Nagalingam B. and Mehta P. S., *Hydrocarbon Modeling for Two-Stroke SI Engine.* SAE Paper, 940403, 1994, **179-191.**
5. Beekman J.W. and Hegedus L.L. *Design of Power Plant Catalysts for Power Plant No_x Emission Control.* Ind. Eng. Chem. Res., Vol. 30(5), 1991, **969-978.**
6. Boehman A.L., Niksa S. and Moffat R.J., *A Comparison of Rate Laws for CO Oxidation over Pt on Alumina.* SAE paper 930252, 1993, **77-87.**
7. Cant N. W., Hicks P. C. and Lennon B. S., *Steady-State Oxidation of Carbon Monoxide over Supported Noble Metals with Particular Reference to Platinum.* Journal of Catalysis, Vol. 54, 1978, **372-383.**
8. De Wasch A.P. and Froment G.F., *Heat Transfer in Packed Beds.* Chemical Engineering Science, Vol. 27, 1972, **567-572.**

9. Dixon A.G. and Cresswell D.L., *Theoretical Prediction of Effective Heat Transfer Parameters in Packed Beds.* AIChE Journal, Vol. 25, No. 4, 1979, **663-676.**

10. Elnashaie S. S. E. H. and Elshishini, S. S., *Modeling, Simulation and Optimization of Industrial Fixed Bed Cata* Hayes R.E. and Kolaczkowski S.T., *Introduction to Catalytic Combustion.* Gordon and Breach Science Publishers, ©1997.

11. Ergun S., *Fluid Flow Through Packed Columns.* Chemical Engineering Progress, Vol. 48, No. 2, 1952, **89-94.**

12. Fuller E.N., Schettler P.D. and Giddings J.C. *A New Method for Prediction of Binary Gas-Phase Diffusion Coefficients*, Ind. and Engg. Chem, Vol. 58(5), 1966, **19-27.**

13. Harned J.L. *Analytical Evaluation of a Catalytic Converter System.* SAE paper 720520, 1972, **1781-1815.**

14. Hautman D.J., Dryer F.L. et.al. *A Multiple Step Overall Kinetic Mechanism for the Oxidation of Hydrocarbons.* Combustion Science and Technology, Vol. 25, 1981, **219-235.**

15. Heck R.H., Wei J. and Katzer J.R., *Mathematical Modeling of Monolith Catalysts*, AIChE Journal, Vol.22, No.3, 1976, **477-484.**

16. Hayes R.E. and Kolaczkowski S.T., *Introduction to Catalytic Combustion.* Gordon and Breach Science Publishers, ©1997.

17. Herkowitz M. and Kenney C.N., *CO Oxidation on Pt Supported Catalysts. Kinetics and Multiple Steady States.* The Canadian Journal of Chemical Engineering, Volume 61, 1983,**194-199.**

18. Heywood J.B., *Internal Combustion Engine Fundamentals.* McGraw-Hill Book Company, Automotive Technology Series, © 1988.

19. Hill. C.G., *Chemical Engineering Kinetics and Reactor Design.* Wiley, New York, © 1977.

20. Holman J.P. *Heat Transfer.* McGraw Hill © 1997.

21. Incropera F.P. and De Witt D.P., *Fundamentals of Heat and Mass Transfer.* John Wiley and Sons, © 1996.

22. Khandekar S., *Numerical Modeling of Packed Bed Catalytic Converter for Small Two-Stroke Petrol Engines and its Experimental Validation.* M. Tech. Thesis, IIT Kanpur, 2000.

23. Kuo J.C., Morgan C.R. and Lassen H.G., *Mathematical Modeling of CO and HC Catalytic Converter Systems.* SAE paper 710289, 1971, **1098-1122.**

24. McCarthy E., Zahradnik, J., Kuczynski, G.C. and Carbery, J.J., *Some Unique Aspects of CO Oxidation on Supported Pt*, Journal of Catalysis, Vol. 39, 1975,**29-35.**

25. Ministry of Environment & Forests, GOI notification No. G.S.R. 682(E), dated 05/10/1999, *Emission Regulations for SI Engine up to 19 kW for non-road application-System & Procedure for Compliance to Regulations,* 1999.

26. Montreuil C.N., Williams S.C. and Adamczyk A., *Modeling Current Generation Catalytic Converters: Laboratory Experiments and Kinetic Parameter Optimization – Steady State Kinetics.* SAE Paper 920096, 1996.

27. Nauman E.B., *Chemical Reactor Design,* John Wiley & Sons, © 1987.

28. Nicholas D.M., Shah Y.T. and Zlochower I.A., *Oxidation of an Automobile Exhaust Gas Mixture by Fiber Catalysts.* Ind. Eng. Chem., Prod. Res. Dev., Vol. 15, No. 1, 1976, **29-40.**

29. Oh S.H. and Cavendish, J.C., *Transients of Monolithic Catalytic Converters: Response to Step Changes in Feedstream Temperature as Related to Controlling Automobile Emissions.* Ind. Eng. Chem. Prod. Res. Dev., Vol. 21, No. 1, 1982, **29-37.**

30. Oh S.H. and Cavendish, J.C., *Mathematical Modeling of Catalytic Converter Lightoff: Part II: Model Verification by Engine-Dynamometer Experiments.* AIChE J Journal, Vol. 31, No. 6, 1985, **935-942.**

31. Oh. S.H., Cavendish, J.C. and Hegedus L.L., *Mathematical Modeling of Catalytic Converter Lightoff : Part III: Prediction of Vehicle Exhaust Emisions and Parametric Analysis.* AIChE Journal, Vol. 31, No. 6, 1985, **943-949.**

32. Pundir B.P., *Catalytic Converter as an Exhaust after Treatment Device,* unpublished report, 1999. O'Sullivan R.D., *Meeting the Indian 2000 Emission Standards for 2-stroke 2-wheelers,* SAE paper 990030, 1999, **325-330.**

33. Pundir B.P., Jain A.K. and Gogia D.K., *Vehicle Emissions and control Perspectives in India -- A state of the art report.* Ministry of Environment and Forests, GOI-Project No.:Q-16014/13/90/CPA, 1994.

34. Pundir B.P., *Vehicle Emission Control in India in Next Decade (A Proposed Plan of Vehicle Emission Standards)*, Central Pollution Control Board, GOI, 1999.

35. Reid R.C. Pravsnitz J.M. and Poling B.E., *The Properties of Gases and Liquids*, McGraw Hill, © 1987.

36. Sastry, S. S., *Introductory Methods of Numerical Analysis.* Prentice-Hall of India Private Limited, © 1998.

37. Satterfield C.N. and Sherwood T.K., *The role of Diffusion in Catalysis*, Addison-Wesley, © 1963.

38. `Scott Fogler H., *Elements of Chemical Reaction Engineering.* Prentice-Hall of India Private Limited, © 1992.

39. Skelland A.H.P., *Diffusional Mass Transfer*, Wiley, © 1974.

40. Springer G.S. and Patterson D.J., *Engine Emissions- Pollutant Formation and Measurement.* Plenum Press, © 1973.

41. Sun X., Assanis, D. and Brereton G., *Assessment of Alternative Strategies for Reducing Hydrocarbon and Carbon Monoxide Emissions from Small Two-Stroke Engines.* SAE Paper, 960743, 1996, **125-136.** .

42. Snyder P.W., Stover W.A. and Lassen H.G., *Status Report on HC/CO Oxidation Catalysts for Exhaust Emission Control.* SAE paper 720479, 1972, **1631-1641.**

43. Venkateswaran D., Raje N.R., et. al. *Cost-Effective Catalytic Converter Technology for Emission Control in 2-Stroke Engine Vehicles.* SAE paper 962475, 1995.

44. Voltz S.E., Morgan C.R., et. al. *Kinetic Study of Carbon Monoxide and Propylene Oxidation on Platinum Catalysts.* Ind. Eng. Chem. Prod. Res. Dev., Vol. 12, No. 4, 1973, **294-301.**

45. Wakao N. and Kaguei S., *Heat and Mass Transfer in Packed Beds.* Topics in Chemical Engineering Series, Gordon & Breach Science Publishers, © 1982.

46. Wanke S.E., *Oxidation of Propane over a Diesel Exhaust Catalyst.* Canadian Journal of Chemical Engineering, Vol. 51, 1973, **454-458.**

47. Westbrook C.K. and Pitz W.J.*A Comprehensive Chemical Kinetic Reaction Mechanism for Oxidation and Pyrolysis of Propane and Propene.* Combustion Science and Technology, Vol. 37, 1984, **117-152.**

48. Xiaobo S., Assanis D. and Brereton G., *Assessment of Alternative Strategies for Reducing Hydrocarbon and Carbon Monoxide Emissions from Small Two-Stroke Engines.* SAE paper 960743, 1996, **125-136**.

49. Yagi S. and Wakao N., *Heat and Mass Transfer from Wall to Fluid in Packed Beds.* AIChE Journal, Vol. 5, 1959, **79-88**.

50. Young L.C. and Finlayson B.A. *Mathematical Models of Monolith Catalytic Converter: Part I: Development of Model and Application of Orthogonal Collocation.* AIChE Journal, Vol. 22, No. 2, 1976, **331-341**.

51. Young L.C. and Finlayson B.A. *Mathematical Models of Monolith Catalytic Converter: Part II: Application to Automobile Exhaust.* AIChE Journal, Vol. 22, No. 2, 1976, **343-353**.

52. Zygourakis K. *Transient Operation of Monolith Catalytic Converters: A Two-Dimensional Reactor Model and the effects of Radially Non-uniform Flow Distributions.* Chemical Engg. Science, Vol. 44(9), 1989, **2075-2096**.